JAERI-M
84-026

EVALUATION REPORT ON CCTF CORE-II REFLOOD TESTS C2-AC1(RUN 51) AND C2-4(RUN 62)
—EFFECT OF INITIAL CLAD TEMPERATURE—

February 1984

Jun SUGIMOTO, Tadashi IGUCHI and Yoshio MURAO

日本原子力研究所
Japan Atomic Energy Research Institute

JAERI-Mレポートは，日本原子力研究所が不定期に公刊している研究報告書です。
入手の問合わせは，日本原子力研究所技術情報部情報資料課（〒319-11茨城県那珂郡東海村）あて，お申しこしください。なお，このほかに財団法人原子力弘済会資料センター（〒319-11 茨城県那珂郡東海村日本原子力研究所内）で複写による実費頒布をおこなっております。

JAERI-M reports are issued irregularly.
Inquiries about availability of the reports should be addressed to Information Section, Division of Technical Information, Japan Atomic Energy Research Institute, Tokai-mura, Naka-gun, Ibaraki-ken 319-11, Japan.

編集兼発行　日本原子力研究所
印　　刷　いばらき印刷㈱

JAERI-M 84-026

Evaluation Report on CCTF Core-II Reflood Tests C2-AC1 (Run 51) and C2-4 (Run 62)

- Effect of Initial Clad Temperature -

Jun SUGIMOTO, Tadashi IGUCHI and Yoshio MURAO

Department of Nuclear Safety Research,
Tokai Research Establishment, JAERI

(Received January 26, 1984)

A reflood test program has been conducted at Japan Atomic Energy Research Institute (JAERI) using large scale test facilities named Cylindrical Core Test Facility (CCTF) and Slab Core Test Facility (SCTF). The present report describes the effect of the initial clad temperature i.e., the initial stored energy on reflood phenomena observed in CCTF Core-II tests C2-AC1 and C2-4. The peak clad temperatures of tests C2-AC1 and C2-4 were 863 K and 1069 K, respectively at reflood initiation.

With higher initial clad temperature, obtained were lower water accumulation in the core and upper plenum, and higher loop mass flow rate in an early reflood transient due to larger heat release of the stored energy in the core. Core inlet flow conditions were only affected shortly after the reflood initiation, causing the suppressed flooding rate and the larger U-tube flow oscillation between the core and the downcomer. In the core, with higher initial clad temperature, slower quench front propagation and higher turnaround temperature were observed. Responses to a higher initial clad temperature were similar to those observed in CCTF Core-I and FLECHT tests. Thus, the lower temperature rise with higher initial clad temperature was experimentally confirmed. The importance of higher flooding rate at initial period was analytically shown for further decreasing the temperature rise.

The work was performed under contract with the Atomic Energy Bureau of Science and Technology Agency of Japan.

Keywords: PWR, LOCA, Reflooding, Initial Clad Temperature, CCTF, Heat Transfer, Two-Phase Flow, Temperature Dependence, Reactor Safety

JAERI－M 84－026

大型再冠水円筒第２次炉心試験Ｃ２－ＡＣ１（Run 51）およびＣ２－４（Run 62）評価報告書
―被覆管初期温度の影響―

日本原子力研究所東海研究所安全工学部
杉本　純・井口　正・村尾良夫

（1984年1月26日受理）

日本原子力研究所では，円筒炉心試験装置（CCTF）および平板炉心試験装置（SCTF）を用いた再冠水試験計画を実施している。本報告書は，円筒炉心第２次炉心試験Ｃ２－ＡＣ1およびC2－４で観測された，再冠水現象に及ぼす被覆管初期温度，すなわち初期蓄積熱の影響について述べている。試験Ｃ２－ＡＣ１およびＣ２－４の再冠水開始時における被覆管最高温度は，それぞれ863 Kおよび1069 Kであった。

再冠水初期においては，炉心からの蓄積熱の放出により，被覆管初期温度が高い程，炉心や上部プレナムへの蓄水は少く，またループ流量は増加した。炉心入口の条件は，再冠水開始直後の短期間のみ影響が見られ，被覆管初期温度が高いと炉心冠水量はやや押えられ，また炉心とダウンカマ間のＵ字管流体振動が大きくなった。炉心内では，被覆管初期温度の増加によりクエンチ点の進行は遅れ，ターンアラウンド温度は上昇した。被覆管初期温度の増加に対する応答は円筒炉心第１次炉心やFLECHT試験の結果と定性的に一致し，温度上昇量は減少することが実験的に確かめられた。また温度上昇量をさらに減少させるためには，初期の冠水量を増加させる必要のあることが解析的に示された。

本報告書は，電源開発促進対策特別会計法に基づき，科学技術庁からの受託によって行った研究の成果である。

Contents

目　　次

List of Tables

List of Figures

between CCTF Core-I and Core-II, and FLECHT tests

Fig. 3.27 Effect of initial and long-term flooding rates on calculated temperature responses

1. Introduction

The present report describes the effect of the initial clad temperature on the reflood phenomena observed in the Cylindrical Core Test Facility (CCTF) Core-II at Japan Atomic Energy Research Institute (JAERI).

The large scale reflood test program has been conducted at JAERI in order to demonstrate the effectiveness of the emergency core cooling (ECC) system, to verify the best-estimate analysis codes and to supply information for the improved thermo-hydrodynamic models during the reflood phase of a hypothetical loss-of-coolant accident (LOCA) of a PWR. For that purpose the CCTF and the Slab Core Test Facility (SCTF) have been constructed. The CCTF is a 1/20 scale integral test facility with a cylindrical core, 4-loop primary systems, and active steam generators. Whereas the SCTF is designed to simulate the two-dimensional flows in the core with an eight fuel bundles arranged in a slab geometry.

The clad temperature at reflood initiation much depends on the heat transfer in the preceding blowdown and refill phases in LOCA. In a safety analysis, for example, the initial clad temperature is conservatively evaluated at about 1140 K assuming the adiabatic heat-up during the refill phase. It is important, however, to experimentally investigate the effect of the initial clad temperature, and hence the initial stored energy on the reflood phenomena. This is because that the core cooling is sensitive to the core inlet mass flow rate which is controlled by the coupled feed-backs between the core and the system.

The FLECHT[1] experiment has shown that the higher initial clad temperature induces the higher peak clad temperature, the later quench time and the lower temperature rise under the constant forced-feed reflood condition. The series of the CCTF Core-I test[2][3] have revealed the similar trend in the core as FLECHT and have provided the detailed information about the system responses under the system feed-back condition as in an actual PWR.

In the CCTF Core-II test series, however, the vessel and core geometry were modified and the ECC flow condition was revised for the better simulation of the typical PWR-LOCA. Therefore, the effect of the initial clad temperature on the reflood phenomena needed to be generalized in a wider range of the test conditions. For that purpose, the test C2-AC1 (Run 51) was conducted with a fairly low initial clad

temperature compared with the base case test C2-4 (Run 62). The nominal peak clad temperatures of tests C2-AC1 and C2-4 are 863 K and 1069 K, respectively at the reflood initiation.

The test C2-4 is the repeated test of the base case test C2-SH1 (Run 53). Detailed analysis and the data evaluation of test C2-SH1 is reported in reference (4). The main results of test C2-AC1 are compiled in Appendix for the better understanding of the test results.

2. Test Description

2.1 Test Facility

The CCTF is an experimental test facility designed to reasonably simulate the flow conditions in the primary system of a PWR during the refill and reflood phases of a LOCA. The vertical dimensions and locations of the system components are kept as close as possible to those of reference 1000 MW PWRs with four primary loops. The reference reactors are the Trojan reactor in the USA and certain aspects of the Ohi reactor in Japan. The flow area of the system components are scaled down based on the core flow area scaling ratio of 1:21.4. The bird's-eye view and overall schematic diagram of the facility are shown in Figs. 2.1 and 2.2, respectively. The scaled dimensions of the components are given in Table 2.1.

The pressure vessel is a cylindrical type with the downcomer, the upper and lower plenums, and the core as shown in Fig. 2.3. The core consists of thirty-two 8×8 electrically heated rod bundles arranged in a cylindrical array. Each bundle simulates 15×15 array fuel assemblies including the unheated rods. The cross section of the pressure vessel and the configuration of the rods in the core are shown in Figs. 2.4 and 2.5, respectively.

The heater rod simulates 15×15 array type fuel in geometry and heat capacity. The heated length and the outer diameter of the heater rods are 3.66 m and 10.7 mm, respectively. The heating element is a herical nichrome coil with a 17 step chopped cosine axial power profile as shown in Fig. 2.6. The locations of the temperature measurement in the core are also shown in the figure.

The primary loop consists of three intact loops and a broken loop. Each loop consists of hot leg and cold leg pipings, a steam generator simulator with active secondary side, and a pump simulator. A 200% cold leg break is simulated for the broken cold leg. The broken cold leg is connected to two containment tanks. The inner diameter of the piping is scaled down in proportion to the core flow area scaling. The length of each piping section is almost the same as the corresponding section of the reference PWR. ECCS consists of an Acc and a LPCI. The injection points are located at each cold leg and at the lower plenum. The primary loop arrangement is shown in Figs. 2.7 and 2.8.

Approximately 1500 channels of data are recorded on a magnetic disk

or a magnetic tape, which include temperatures, pressures, differential pressures, liquid levels and mass flow rates. Measurement locations in the pressure vessel and the primary system are shown in Figs. 2.9 through 2.12.

2.2 Test Procedure

The test procedure was as follows: After establishing the initial conditions of the test, the electric power for preheaters was turned off and the lower plenum was filled with saturated water to a specified level (about 0.9m). When the water level in the lower plenum reached the specified level and the other initial conditions of the test stabilized, the electric power was applied to the heater rods in the core and the data recording was started. When a specified initial clad temperature of the heater rods was reached, direct injection of the Acc water into the lower plenum was initiated. The specified initial clad temperature for the initiation of coolant injection was predetermined by the interpolation between the initial clad temperature and the clad temperature assumed for the bottom of the core recovery time. The decay of the power input to the heater rods was scheduled to begin at the BOCREC time. The specified power decay was obtained by normalizing the decay curve of the ANS standard × 1.2 + ^{238}U capture decay at 30 seconds after scram.

At a predetermined time, the injection port was switched from the lower plenum to the three intact cold leg ECC ports. At a specified time after the initiation of Acc injection, the valves in Acc line and LPCI circulation line were closed and the valve in LPCI injection line was opened. These actions transferred the ECC water injection from Acc mode to LPCI mode.

The generated steam and the entrained water flowed through broken and intact loops to the containment tanks. The steam was then vented to the atmosphere to maintain the pressure in the containment tanks constant.

When all thermocouples on the surface of heater rods quenched and indicated temperatures close to the saturation temperature, the power supply to the heater rods was turned off. After that, the ECC water injection was terminated and data recording was ended, terminating the test.

2.3 Test conditions

Table 2.3 summarizes the comparison of the major initial and boundary test conditions between test C2-AC1 and C2-4. The initial clad temperature is defined as the measured maximum temperature at the rod surface in the core. It is realized at the midplane in the central high power region where the local power is the highest. The initial clad temperature of test C2-AC1 was 863 K, while that of test C2-4 was 1069 K.

Except for the initial clad temperature, other test conditions were almost the same, however, the followings were slightly different between the two tests: The total power and hence the average linear power was about 0.9% higher in test C2-AC1 than test C2-4. Secondary, the radial distribution of test C2-AC1 was more skewed than test C2-4 as shown in Table 2.3.

The ECC flow rates shown in Table 2.3 were about 30% higher than those of CCTF Core-I base case test[2]. This revision was made in consideration of the more realistic situation in the reflood phase of PWR-LOCA.

Table 2.4 gives the comparison of the chronology of events between two tests. The required heat-up time until the reflood initiation was longer with the higher initial clad temperature, because the clad temperatures at the initiation of the power supply were set to the saturation temperature in both tests. The evaluated initial stored energy of test C2-4 was about 60% higher than that of test C2-AC1.

Table 2.1 CCTF Component scaled dimensions

Component		PWR	JAERI	Ratio
Pressure vessel				
Vessel inside diameter	(mm)	4394 (173")	1084	
Vessel thickness	(mm)	216 (8 1/2")	90	
Core barrel outside diameter	(mm)	3874	961	
Core barrel inside diameter	(mm)	3760	929	
Thermal shield outside diameter	(mm)	4170		
Thermal shield inside diameter	(mm)	4030		
Downcomer length	(mm)	4849	4849	1/1
Downcomer gap	(mm)	114.3	61.5	
Downcomer flow area	(m^2)	4.23	0.197	1/21.44
Lower plenum volume	(m^3)	29.6	1.38	1/21.44
Upper plenum volume	(m^3)	43.6	2.76	1/15.8
Fuel (heater rod) assembly				
Number of bundles	(—)	193	32	
Rod array	(—)	15×15	8×8	
Rod heated length	(mm)	3660	3660	1/1
Rod pitch	(mm)	14.3	14.3	1/1
Fuel rod outside diameter	(mm)	10.72	10.7	1/1
Thimble tube diameter	(mm)	13.87	13.8	1/1
Instrument tube diameter	(mm)	13.87	13.8	1/1
Number of heater rods	(—)	39372	1824	1/21.58
Number of non-heated rods	(—)	4053	244	1/18.09
Core flow area	(m^2)	5.29	0.25	1/21.2
Core fluid volume	(m^3)	17.95	0.915	1/19.6
Primary loop				
Hot leg inside diameter	(mm)	736.6 (29")	155.2	1/4.75
Hot leg flow area	(m^2)	0.426	0.019	1/22.54
Hot leg length	(mm)	3940	3940	1/1
Pump suction inside diameter	(mm)	787.4 (31")	155.2	1/5.07
Pump suction flow area	(m^2)	0.487	0.019	1/25.77
Pump suction length	(mm)	9750	7950	1/1

Table 2.1 (cont'd)

Component		PWR	JAERI	Ratio
Cold leg inside diameter	(mm)	698.5 (27.5")	155.2	1/4.50
Cold leg flow area	(m^2)	0.383	0.019	1/20.26
Cold leg length	(mm)	5600	5600	1/1
Steam generator simulator				
Number of tubes/loop	(—)	3388	158	1/21.44
Tube length (average)	(m)	20.5	15.2	1/1.35
Tube outside diameter	(mm)	22.225 (0.875")	25.4	
Tube inside diameter	(mm)	19.7 (0.05")	19.6	1/1
Tube wall thickness	(mm)	1.27	2.9	
Heat transfer area/loop	(m^3)	4784 (51500 ft^2)	192	1/24.92
Tube flow area/loop	(m^2)	1.03	0.048	1/21.44
Inlet plenum volume/loop	(m^3)	4.25	0.198	1/21.44
Outlet plenum volume/loop	(m^3)	4.25	0.198	1/21.44
Primary side volume/loop	(m^3)	30.50 (1077 ft^3)	1.2	1/25.4
Secondary side volume/loop	(m^3)	157.33 (5556 ft^3)	2.5	1/62.9
Containment tank 1	(m^3)		30	
Containment tank 2	(m^3)		50	
Storage tank	(m^3)		25	
Acc. tank	(m^3)		5	
Saturated water tank	(m^3)		3.5	

Table 2.2 Component elevations of Cylindrical Core Test Facility

COMPONENT		PWR	CCTF	DISCREPANCY
BOTTOM OF HEATED REGION IN CORE	(mm)	0	0	0
TOP OF HEATED REGION IN CORE	(mm)	3660	3660	0
TOP OF DOWNCOMER	(mm)	4849	4849	0
BOTTOM OF DOWNCOMER	(mm)	0	0	0
CENTERLINE OF COLD LEG	(mm)	5198	4927	-271
BOTTOM OF COLD LEG (INSIDE)	(mm)	4849	4849	0
CENTERLINE OF LOOP SEAL LOWER END	(mm)	2056	2047	- 9
BOTTOM OF LOOP SEAL LOWER END	(mm)	1662	1959	+297
CENTER OF HOT LEG	(mm)	5198	4927	-271
BOTTOM OF HOT LEG (INSIDE)	(mm)	4830	4849	+ 19
BOTTOM OF UPPER CORE PLATE	(mm)	3957	3957	0
TOP OF LOWER CORE PLATE	(mm)	- 108	- 50	+ 58
BOTTOM OF TUBE SHEET OF STEAM GENERATOR SIMULATOR	(mm)	7308	7307	- 1
LOWER END OF STEAM GENERATOR SIMULATOR PLENUM	(mm)	5713	5712	- 1
TOP OF TUBES OF STEAM GENERATOR SIMULATOR (avg)	(mm)	17952.7	14820	

Table 2.3 Comparison of initial and boundary condition

Item	Test C2-AC1	Test C2-4
Total power (MW)	9.26	9.34
Averaged linear power (kW/m)	1.39	1.40
Radial power distribution (A:B:C)	1.50:1.14:0.77	1.36:1.20:0.76
Containment pressure (MPa)	0.20	0.20
SG secondary side pressure (MPa)	5.2	5.2
Downcomer wall temperature (K)	470	471
Primary piping wall temperature (K)	393	393
SG secondary side temperature (K)	538	539
Peak clad temperature (K)		
at ECC initiation	801	995
at reflood initiation	863	1069
Lower plenum filled water temperature (K)	393	394
ECC water temperature (K)	308	308
Lower plenum water level (m)	0.9	0.8
SG secondary side water level (m)	7.6	7.4
Accumulator injection rate (m^3/s)		
into lower plenum	0.10	0.11
into cold legs	0.085	0.090
LPCI injection rate (m^3/s)	0.011	0.011

Table 2.4 Comparison of chronology of events

(unit: s)

	Test C2-AC1	Test C2-4
Test initiated (Heater rod power on) (Data recording initiated)	0	0
Accumulator injection initiated	45.0	86.0
Power decay initiated (Bottom of core recovery)	53.5	95.0
Accumulator injection switched from lower plenum to cold legs	58.5	99.0
Accumulator injection ended and LPCI initiated	69.0	110.0
All heater rods quenched	613.0	652.0
LPCI ended	966.0	1005.0
Test ended	993.0	1035.0

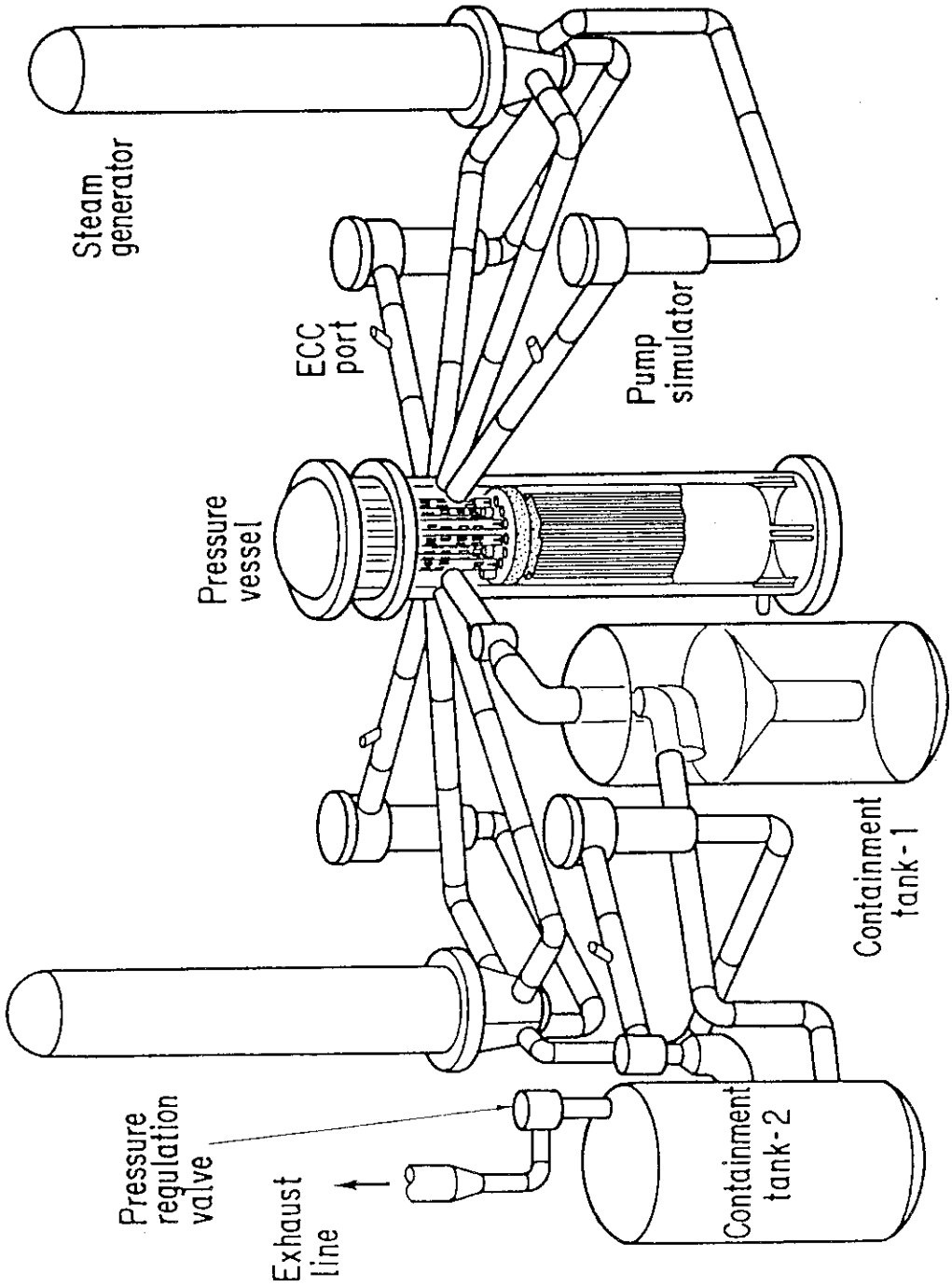

Fig. 2.1 Bird's-eye view of CCTF

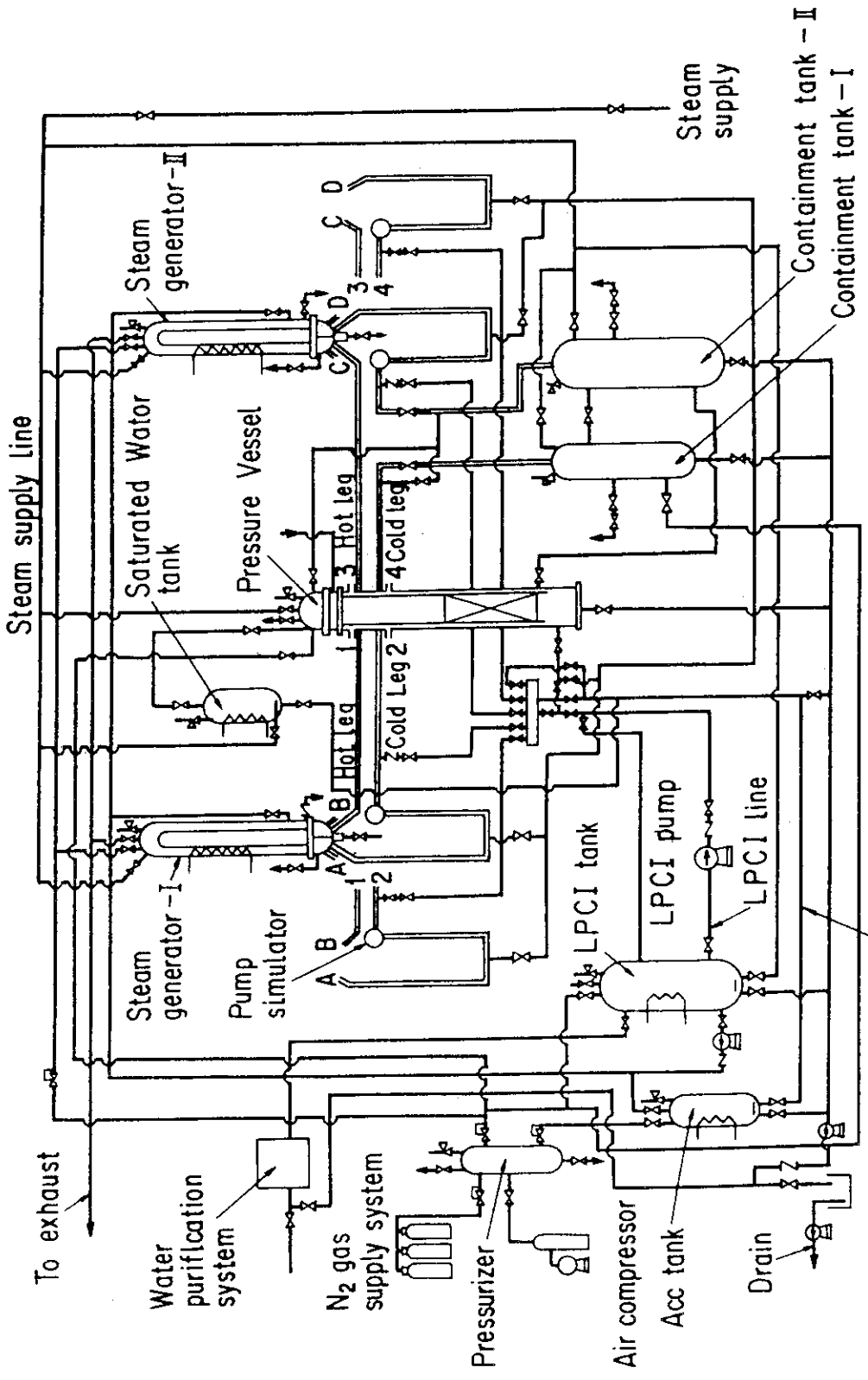

Fig. 2.2 Schematic diagram of CCTF

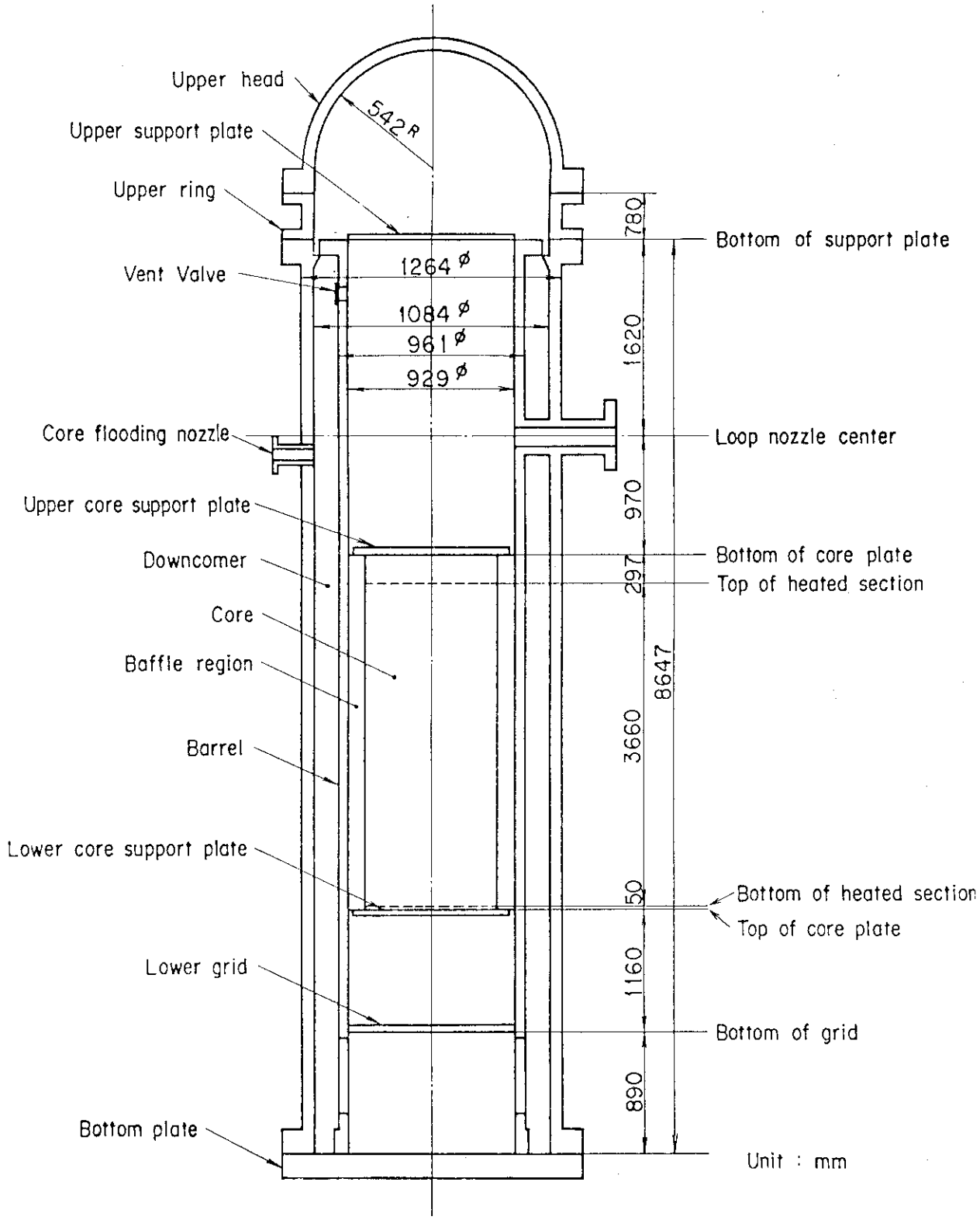

Fig. 2.3 Dimensions of pressure vessel

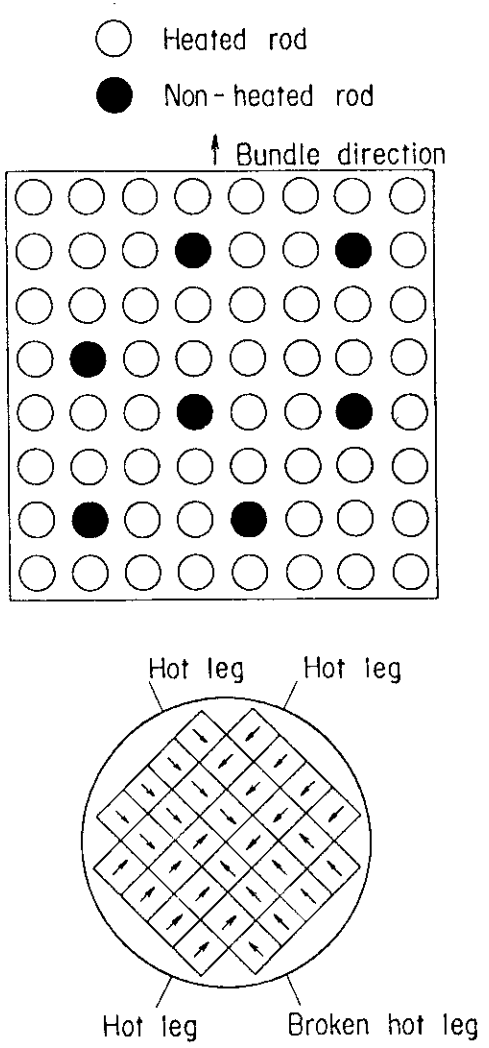

Fig. 2.4 Cross section of pressure vessel

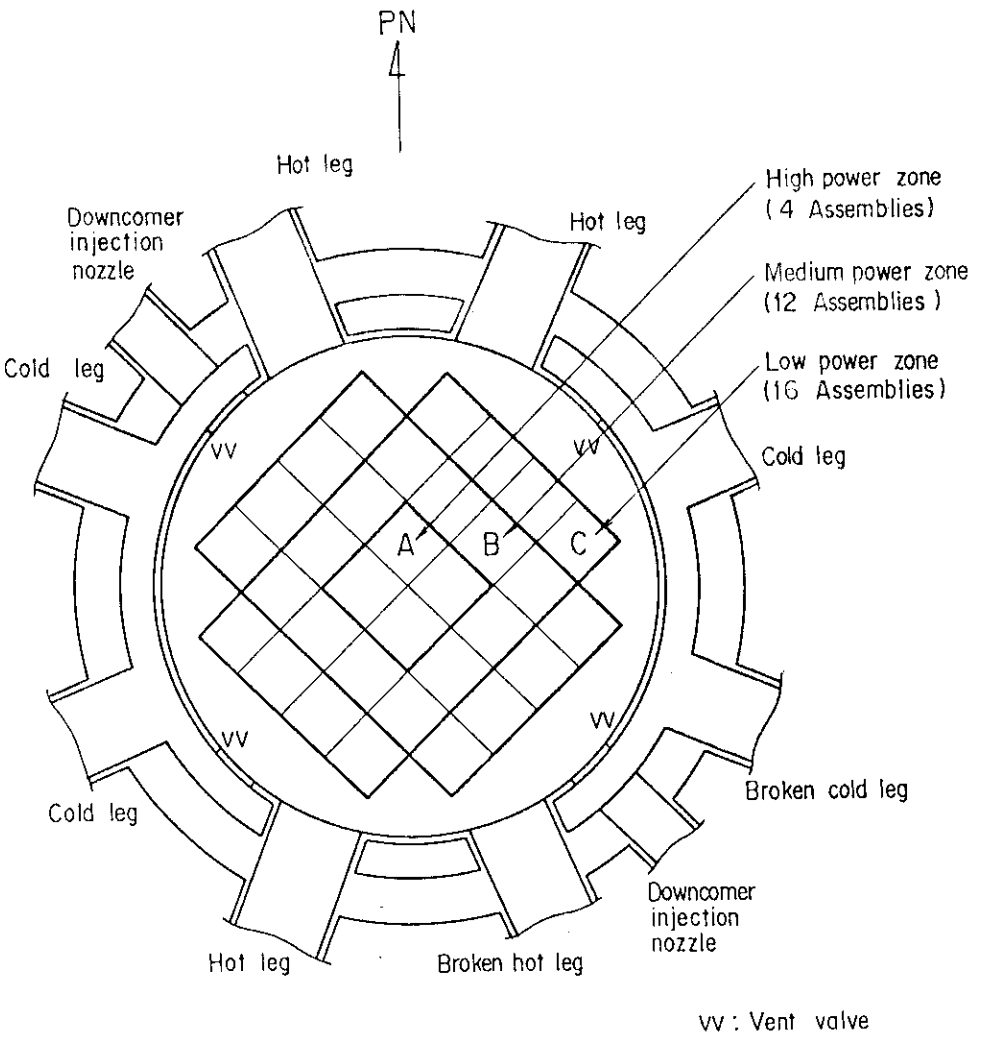

Fig. 2.5 Configuration of rods in core

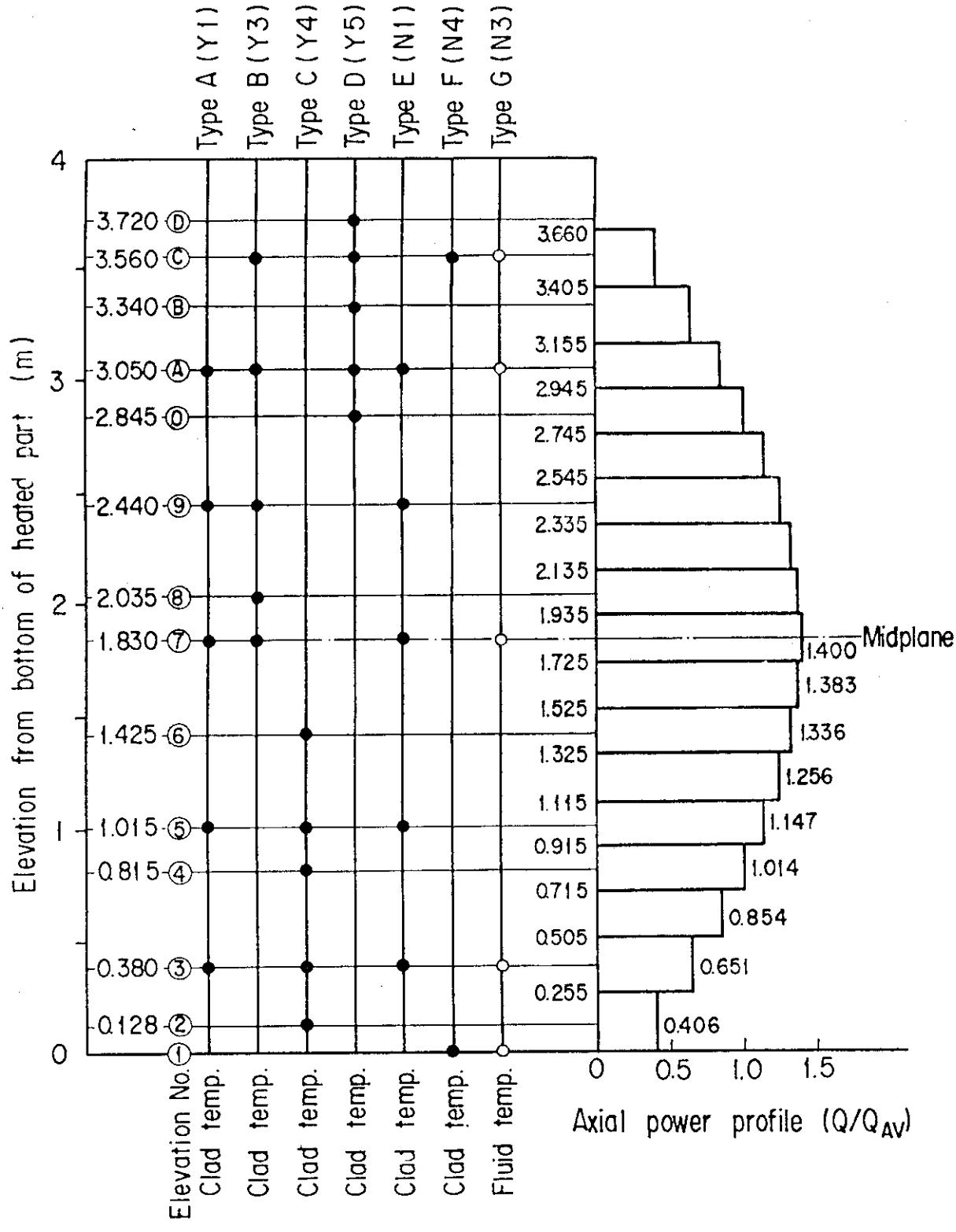

Fig. 2.6 Power profile and thermocouple elevations of heater rods

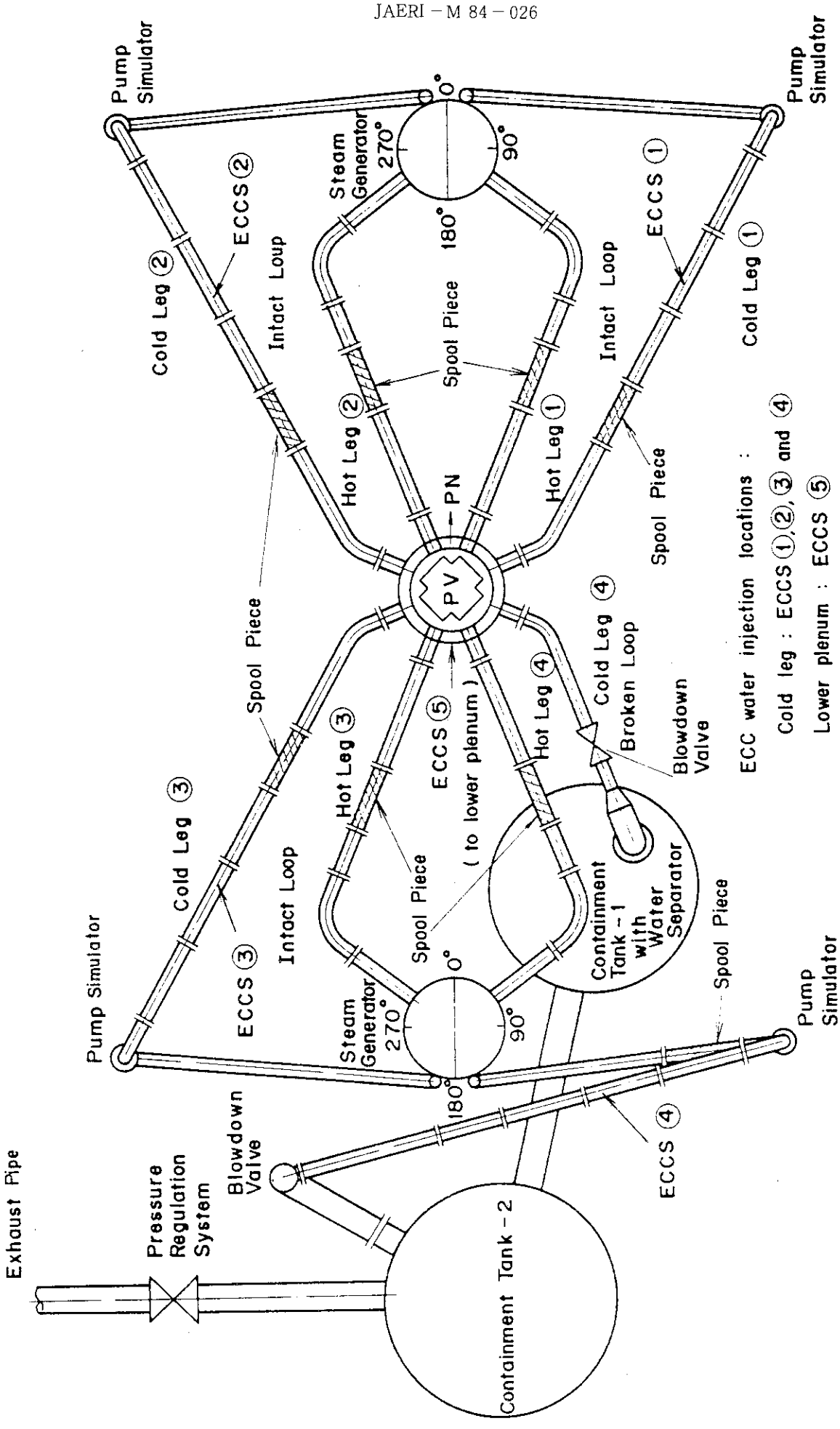

Fig. 2.7 Primary loop piping (top view)

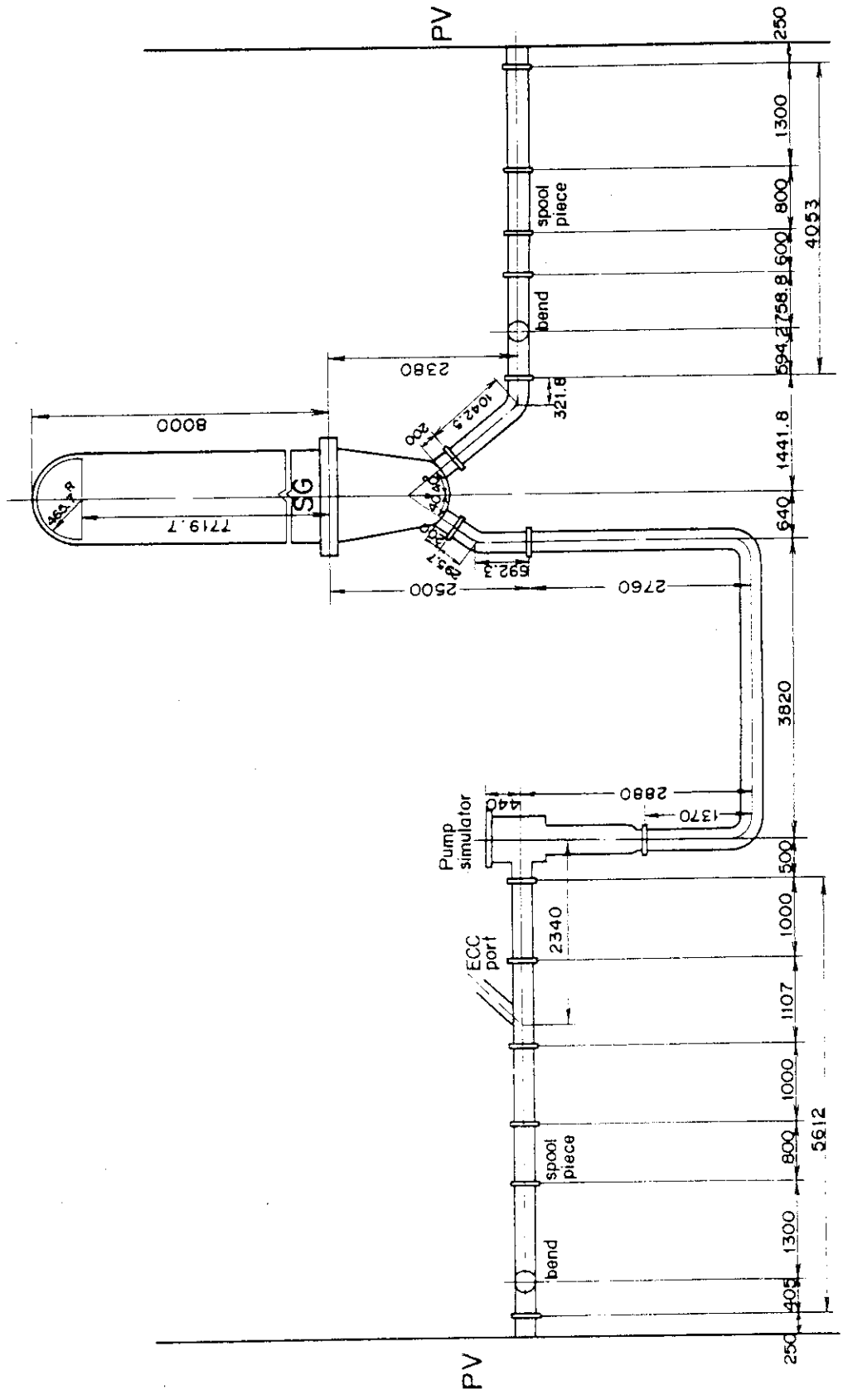

Fig. 2.8 Primary loop (side view)

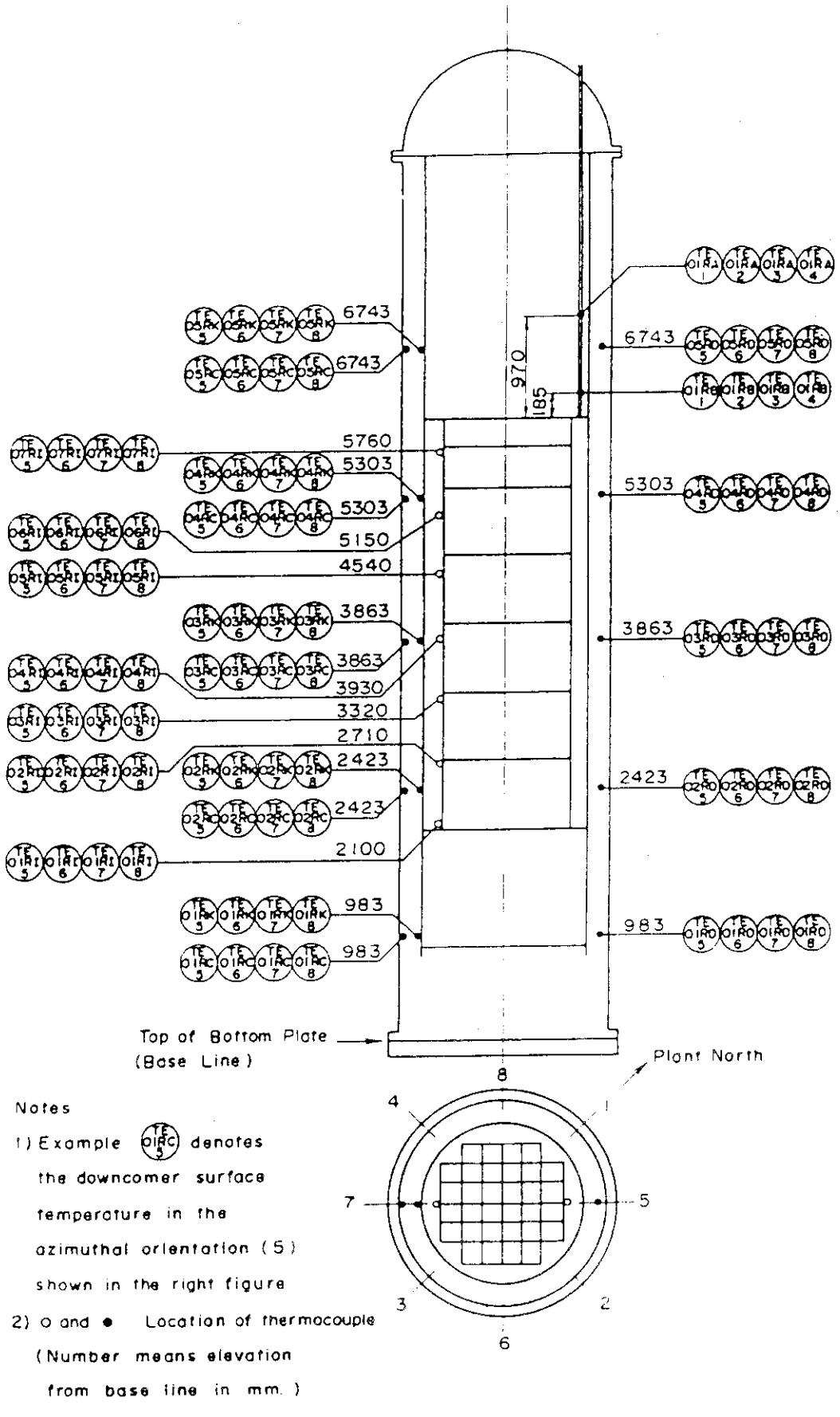

Fig. 2.9 Thermocouple locations in pressure vessel

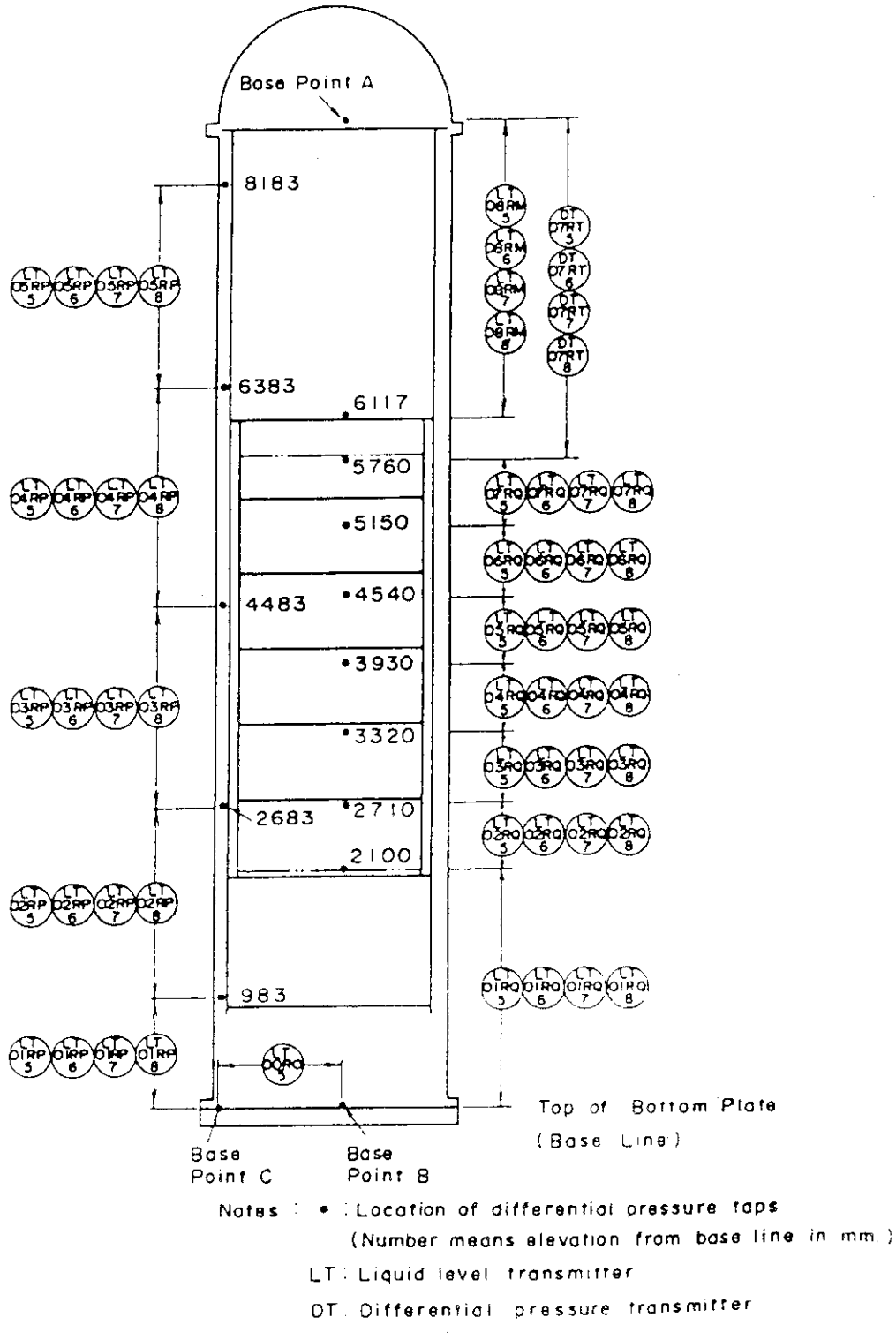

Fig. 2.10 Pressure, differential pressure and liquid level instrumentation locations in pressure vessel

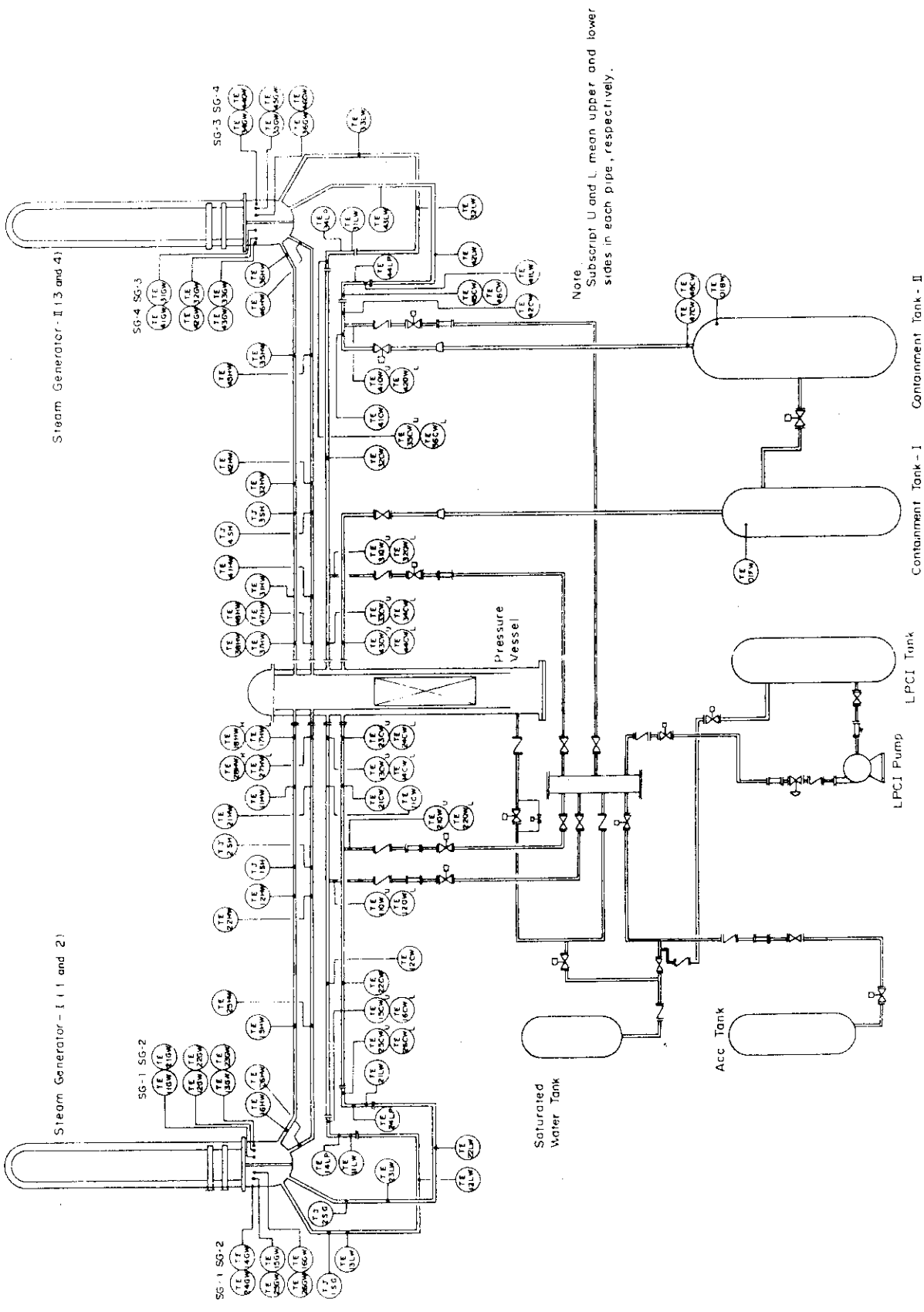

Fig. 2.11 Thermocouple locations except pressure vessel and steam generator simulators

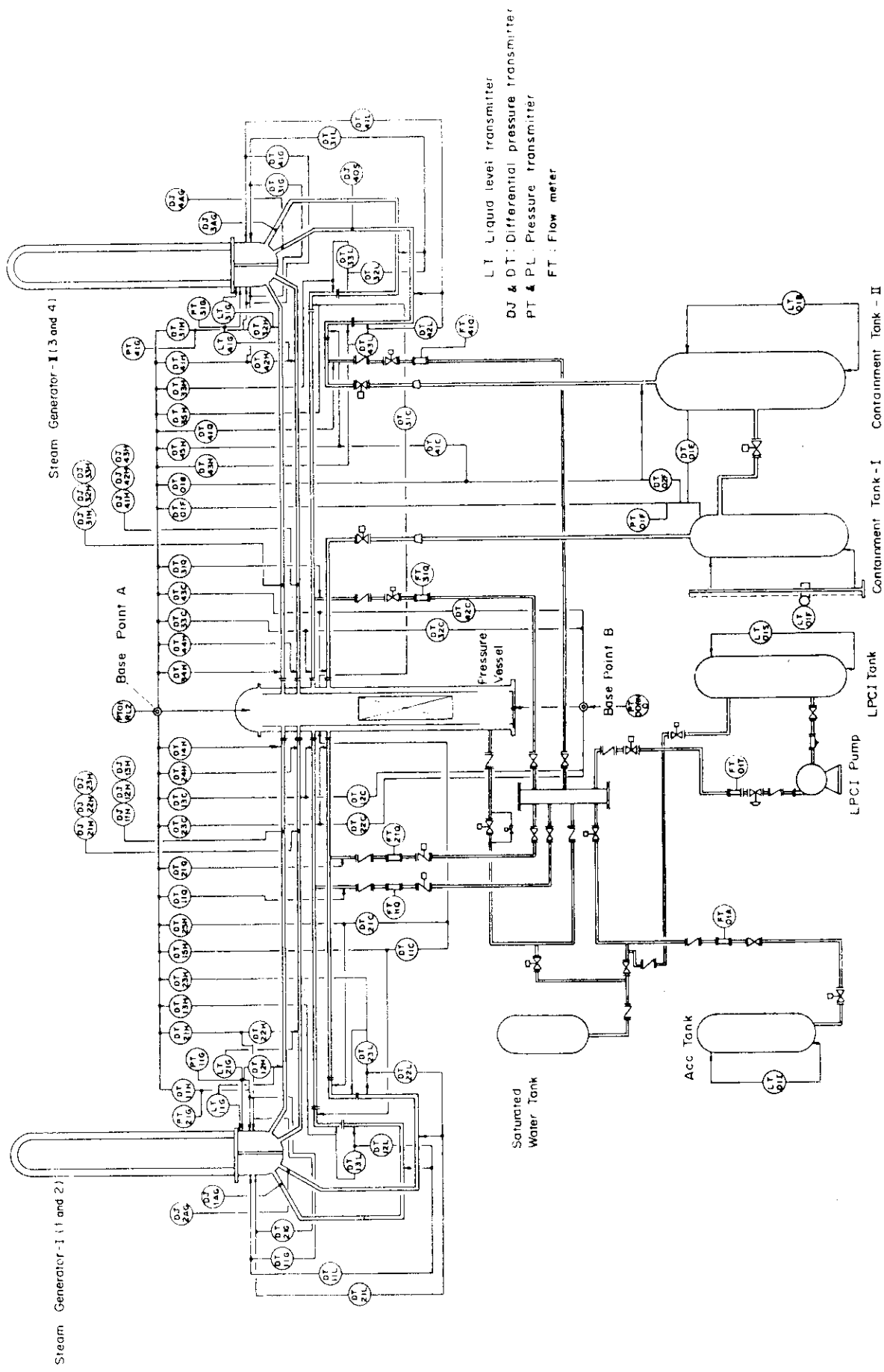

Fig. 2.12 Pressure, differential pressure and liquid level instrumentation locations except pressure vessel

3. Results and discussion

3.1 System behavior

With higher initial clad temperature, the following responses were observed for overall system behaviors:

(1) Water accumulation in vessel

Differential pressures, and hence water accumulations in the core, downcomer and upper plenum tend to be lower as shown in Fig. 3.1. But the water accumulations in the lower plenum, which was filled with water for the most of the transient, are almost identical between two tests.

The water accumulation in the core remains lower only until about 100 s of the transient. This shows the direct effect of the initial stored energy which prevents the water from accumulating in the core. It is noted that the water accumulations in the downcomer behave almost identically with each other. The observed much higher water accumulation in the upper plenum can be attributed to the higher core outlet liquid mass flow rate in an early reflood transient. This is because that the water accumulation in the upper plenum is reported to be strongly governed by the core outlet liquid mass flow rate[5].

It should also be noted that the differential pressure oscillation observed before 30 s is larger with higher initial clad temperature.

(2) Pressure drop and mass flow rate in primary loop

Broken and intact loop pressure drops are slightly higher in the early reflood transient as shown in Fig. 3.2. This implies that the loop mass flow rate is also higher, by removing the heat with steam from the larger initial stored energy in the core. This can be qualitatively verified by the steam mass flow rate in the broken hot leg measured with spool pieces as shown in Fig. 3.3.

The pressure drop across the broken cold leg nozzle is higher as shown in Fig. 3.4. The pressure drop is defined as the pressure difference between the top part of the downcomer and the nozzle outlet of the broken cold leg, and it accounts for the large difference between the broken and intact loop pressure drops shown in Fig. 3.2.

The water mass flow rate through the broken cold leg nozzle is higher as shown in Fig. 3.5 only in an early reflood transient. But it is rather smaller from about 60 to 100 s. However, the steam mass flow rate at the exit of the containment tank 2 is higher as shown in Fig.

3.6. It is considered that the larger pressure drop shown in Fig. 3.4 is mainly attributed to the higher steam mass flow rate, resulting in the higher two-phase mixture velocity through the broken cold leg nozzle.

3.2 Core inlet flow conditions

With higher initial clad temperature, the following responses were observed for the core inlet flow conditions:

(1) Pressure and fluid temperature

The pressure at the core inlet is little affected as shown in Fig. 3.7, however, it is slightly higher up to about 250 s of the reflood transient. This is primarily due to the higher pressure drop across the broken cold leg nozzle (shown in Fig. 3.4) which dominates over the slightly lower pressure drop in the downcomer (shown in Fig. 3.1).

The fluid temperature at the core inlet shown in Fig. 3.8 is also little affected, but it is slightly higher from about 20 to 40 s of the transient. It was found that the fluid temperatures in the downcomer and the lower plenum were almost the same between two tests, and that the fluid temperature at the core inlet showed the coincident oscillation with the differential pressure oscillation. It is therefore considered that the slightly higher core inlet fluid temperature from 20 to 40 s is the result of the better mixing of hot water in the lower part of the core with cold water in the lower plenum due to the larger oscillation.

(2) U-tube flow oscillation

The differential pressure oscillation in the lower plenum and the core bottom is larger, and the oscillation period is shorter as shown in Fig. 3.9. The oscillation which corresponds to the U-tube flow oscillation between the core and the downcomer lasted from the reflood initiation until about 20 s. The larger amplitude can be attributed to the larger heat generation in the core, causing the more rapid pressurization in the upper plenum. The shorter period, on the other hand, is probably due to the larger steam condensation rate at ECC ports with Acc water, when the steam mass flow rate is larger as suggested from Figs. 3.2 and 3.3. The oscillation ceases after about 20 s when the injected water was largely reduced from Acc to LPCI injection mode. Hence it appears to give little effect on the overall system behaviors on a long-term base.

(3) Liquid mass flow rate

The integrated core inlet liquid mass flow rate is lower as shown

in Fig. 3.10. The integrated mass is estimated from differential pressure measurement in the core and the upper plenum, and flow measurement at the pump simulating orifice in the primary loops.

The core inlet mass flow rate i.e., the derivative of the integrated mass is lower from about 15 to 30 s. This is probably due to the higher pressurization in the upper plenum which tends to retard the core inlet mass flow initially. This trend becomes a little reversed after 30 s and almost null after 250 s. It is noted that the average core inlet mass flow rate in LPCI period after 30 s is about 4.6 kg/s, which corresponds to core flooding velocity of about 1.9 cm/s.

3.3 Core thermo-hydraulic behavior

With higher initial clad temperature, the following responses were observed for the core thermo-hydraulic behaviors:

(1) Temperature history of heater rod

The maximum (turnaround) temperature is higher and the quench time is longer in the high (A), medium (B) and low (C) power regions as shown in Figs. 3.11 through 3.13 (Definition of power regions is shown in Fig. 2.5). The peak clad temperature is found at 2.44 m elevation from the bottom of the heated length in A region. It is noted that the temperature curves with different initial clad temperature become almost alike after about 200 s with each other, indicating the similar core hydraulics between the two cases.

(2) Turnaround and quench times

The turnaround time is earlier and the quench time tends to be later in the high (A) power region along the core as shown in Fig. 3.14. Indicated in the figure are the mean values with a standard deviation of totally 65 measurement points. The earlier turnaround time is the result of the larger heat removal from the heater rod, which is discussed in the following section. It is noted that the turnaround at 2.035 m occurred remarkably earlier than other neighbouring location. As indicated in Fig. 3.14, the elevation 2.035 m is only 9.5 cm apart from the upper edge of the third grid spacer. It will be therefore due to the heat transfer enhancement effect of grid spacers[6] in the downstream region.

The averaged quench times in medium (B) and low (C) power regions are also later as shown in Fig. 3.15. The difference of quench time

between the two tests is generally smaller in high power region than medium or low power region. This can be attributed to the radially more skewed power distribution, i.e. the higher local power in high power region in the case of lower initial clad temperature as shown in Table 2.3. The quench time above 3 m has not a smooth change with elevation as indicated by the large scattering of data in Fig. 3.14. It will be due to random occurrence of the top-down quenching in the top part of the core.

(3) Turnaround and quench temperatures, and temperature rise

The turnaround temperature is higher except in the top part of the core, and quench temperature tends to be higher in the bottom section of the core as shown in Fig. 3.16. The temperature rise, which is the difference between the turnaround and initial clad temperatures, is lower along the core heated length as shown in the figure. It is noted again that the turnaround temperature, and hence the temperature rise is noticeably small at 2.035 m elevation due to the heat transfer enhancement of grid spacers.

The turnaround temperatures in medium and low power regions are also higher as shown in Fig. 3.17. The difference of the turnaround temperatures between the two tests tends to be smaller with higher elevation. This situation is shown in Fig. 3.18 by considering the difference of the radial power distributions between two tests. It is found that the turnaround temperature depends almost linearly on the local power at 1.83 and 2.44 m elevations. The temperature rise is generally larger with higher local power, but it tends to be slightly lower with higher local power when the initial clad temperature is high. This may show that the multi-dimensional effect for homogenizing the flow in the core is larger with higher initial clad temperature.

(4) Heat transfer coefficient and heat flux

The heat transfer coefficients at 1.83 and 2.44 m elevations are slightly lower from about 20 to 50 s as shown in Figs. 3.19 through 3.21. This can be attributed to the initially suppressed core inlet mass flow rate by the higher initial stored energy as already shown in Fig. 3.10. However, the difference of the heat transfer coefficients between two tests is small for the rest of the transient.

The heat fluxes at 1.83 and 2.44 m elevations are larger for the most of the transient as shown in Figs. 3.22 through 3.24. This is

because that the temperature difference between the rod wall and the saturated fluid is too large to be cancelled by the difference of heat transfer coefficients. This then causes the larger heat removal from the heater rod with higher initial clad temperature, decreasing the temperature rise as already shown in Figs. 3.16 and 3.18.

(5) Water distribution in core

The water accumulation, and hence the sectional differential pressure in the core is lower as shown in Fig. 3.25. This trend is more clearly observed below 1.83 m elevation in the core before about 150 s of the transient. This will be due to the larger initial stored energy which works to reduce the initial core inlet mass flow rate and to retard the quench front propagation upward in the lower part of the core. It is noted that the differential pressure, and hence the void fraction in the upper part of the core is not much affected by the initial clad temperature. This then causes the similar heat transfer coefficients between the two cases as already shown in Figs. 3.19 through 3.21.

3.4 Comparison of test results with CCTF-I and FLECHT data

(1) Experimental conditions

The observed phenomena described previously are compared with the test results of CCTF Core-I and FLECHT data concerning the effect of initial clad temperature in the following. Table 3.1 summarizes the experimental conditions between CCTF Core-I, CCTF Core-II and FLECHT tests. The ECC water is injected into downcomer through cold legs in both CCTF tests (gravity feed), whereas it is constantly injected into the core in FLECHT test (forced feed) with no other system simulations. It is noted that both Acc and LPCI flow rates of CCTF Core-II are about 30% higher than those of CCTF Core-I.

(2) System responses in CCTF Core-I and Core-II

Table 3.2 compares the responses between CCTF Core-I and Core-II to higher initial clad temperature. The overall responses of the present CCTF Core-II test are similar to those in CCTF Core-I test in spite of modified core geometry and different ECC conditions. It means that the observed phenomena may have a characteristic feature of a PWR-LOCA conditions, concerning the effect of the initial clad temperature.

The water accumulation in the downcomer, however, is somewhat

different between CCTF Core-I and Core-II as shown in Table 3.2. This will be the direct effect of about 30% higher Acc and LPCI flow rates in CCTF Core-II than Core-I, because the downcomer water in CCTF Core-II began to overflow much earlier in Acc period when the loop steam flow rate was fairly small, causing little difference of the downcomer water head between two tests in CCTF Core-II.

(3) Core thermal behavior

Figure 3.26 compares the temperature rise and the quench time of the peak powered rod at the midplane between CCTF Core-I, Core-II and FLECHT tests. Also shown in the figure is the result of Evaluation Model (EM) test[7] in CCTF Core-I with nominal initial clad temperature of 1143 K and same ECC flow rate as CCTF Core-II test. The temperature rise is smaller and the quench time is longer with higher initial clad temperature in all tests as shown in Fig. 3.26.

The temperature rise in both CCTF tests is generally smaller than FLECHT data. This can be attributed to the larger core flooding rate in CCTF tests during Acc period. The temperature rises in three CCTF Core-I parametric tests are slightly higher than those in CCTF Core-II or CCTF Core-I EM test. Since the peak linear power is nearly same among those tests as shown in Table 3.1, this will be due to about 30% lower Acc flow rate in CCTF Core-I parametric tests.

The quench time in CCTF Core-II with higher initial clad temperature (Test C2-4) was somewhat earlier than expected. The radial power distribution in test C2-4 is less skewed than test C2-AC1, in which the highest local power is about 10% higher than test C2-4. This shows that the quench time much depends on the local power as well as the initial stored energy. The quench times of CCTF tests are in the same range of FLECHT data with the flooding rate of 2.0 cm/s. This implies that the quench time is much affected by the long-term flooding rate in LPCI period, but not by the initial high flooding rate in Acc period.

(4) Analysis with REFLA code

The effect of the flooding rate on the turnaround temperature and the quench time has been analyzed with REFLA code[8], the result of which is shown in Fig. 3.27. Shown in the figure are the calculated temperature histories at the midplane under five core inlet flow conditions for the simulated CCTF core geometry. The input pressure and the fluid temperature at the core inlet were 0.2 MPa and 373 K, respectively.

As shown in Fig. 3.27, the turnaround temperature, and hence the temperature rise is strongly affected by the flooding rate before 10 s which simulates Acc period. The quench time, on the other hand, is much affected by the flooding rate after 10 s which simulates LPCI period. It means that the initial flooding rate is cruciel for decreasing the temperature rise and that the long-term flooding rate determines the complete cooling of the core. Although the temperature rise tends to be lower with higher initial clad temperature, the higher initial flooding rate rather than the long-term flooding rate is important for further decreasing the temperature rise.

Table 3.1 Comparison of experimental conditions between CCTF Core-I, Core-II and FLECHET tests on effect of initial clad temperature

Conditions	CCTF-I	CCTF-II	FLECHT[1]
ECC injection method	Gravity feed	Gravity feed	Forced feed
Number of rods	2,048	2,048	100
Axial peaking factor	1.49	1.40	1.66
System pressure (MPa)	0.20	0.20	0.28
Peak linear power (kW/m)	2.6	2.7∿2.9	2.8
Average flooding rate (cm/s)	10∿2[1)]	12∿2[1)]	2.0, 3.8
Inlet subcooling (K)	29∿7[2)]	30∿4[2)]	78

Note 1) Varies with time. CCTF-II is higher in Acc period before 20 s.

2) Decreases with time in LPCI period after 80 s.

Table 3.2 Comparison of CCTF Core-I and Core-II responses to higher initial clad temperature

Item	Response to higher initial clad temperature	
	CCTF-I	CCTF-II
(1)System behavior [1]		
Water accumulation in core	Lower	Lower
Water accumulation in upper plenum	Lower	Lower
Water accumulation in downcomer	Higher	Not clear[2]
Loop mass flow rate	Higher	Higher
Broken cold leg nozzle pressure drop	Higher	Higher
(2)Core inlet flow condition [1]		
Pressure	Nearly same	Nearly same
Fluid temperature	Higher	Slightly higher
Mass flow rate	Slightly lower[3]	Lower[4]
U-tube flow oscillation	Larger	Larger
(3)Core thermo-hydraulic behavior		
Turnaround temperature	Higher	Higher
Quench time	Longer	Longer
Temperature rise	Lower	Lower
Heat flux	Higher	Higher
Void fraction	Higher	Higher

Note 1) Responses are different only in an early transient.

2) Nearly same before the initiation of downcomer overflow and slightly lower afterwards.

3) Almost same after about 20 s.

4) Higher after about 20 s until 250 s.

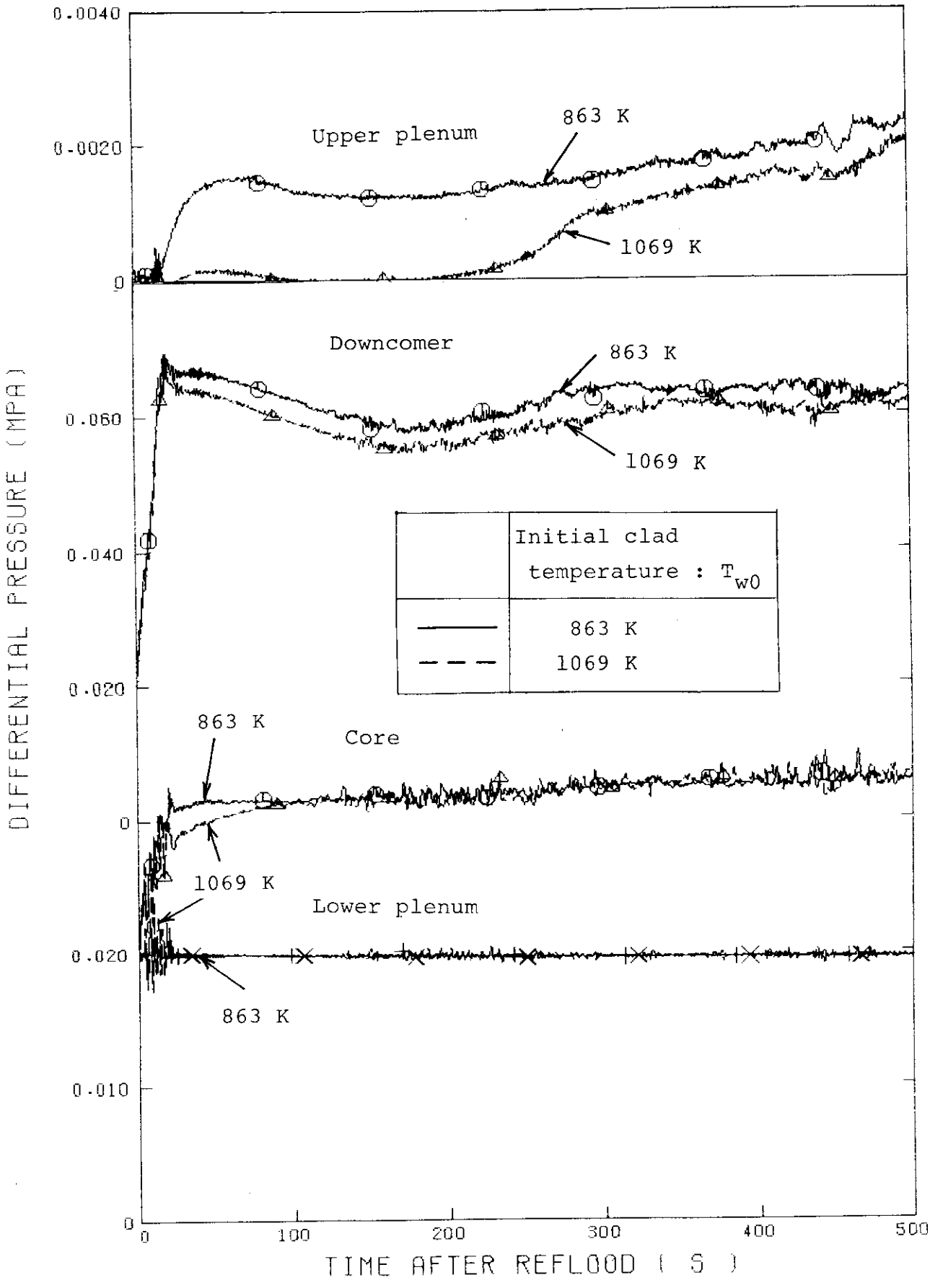

Fig. 3.1 Effect of initial clad temperature on differential pressures in lower plenum, core, downcomer and upper plenum

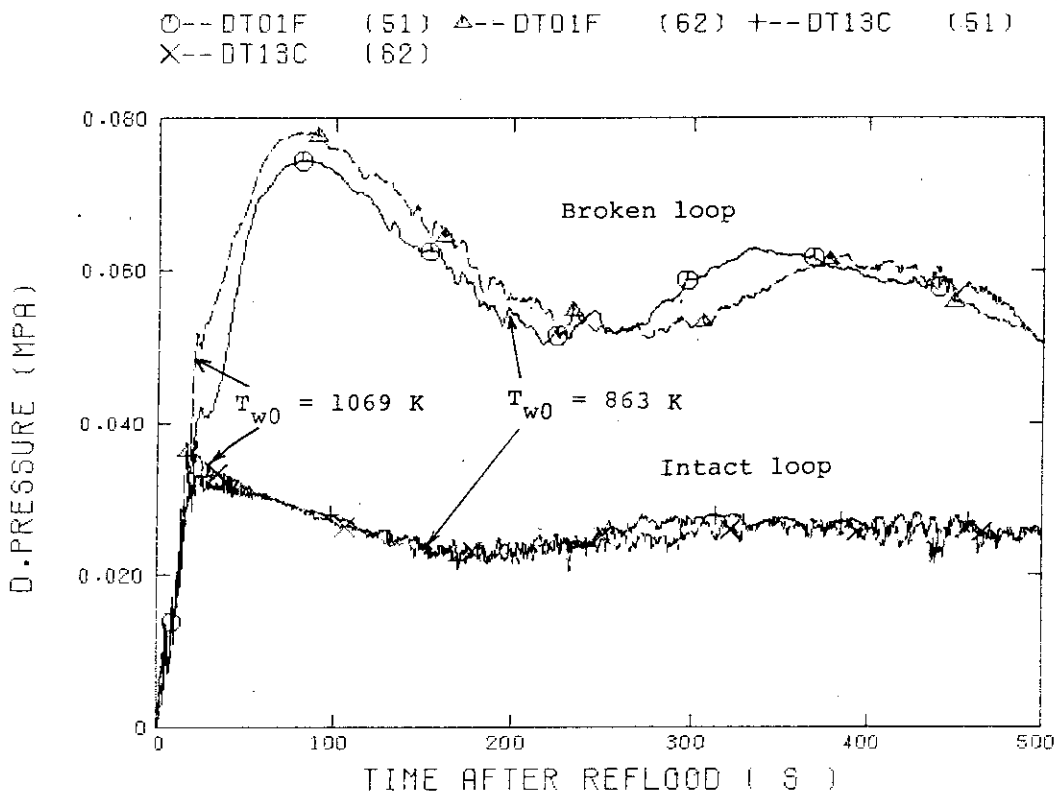

Fig. 3.2 Effect of initial clad temperature on loop pressure drop

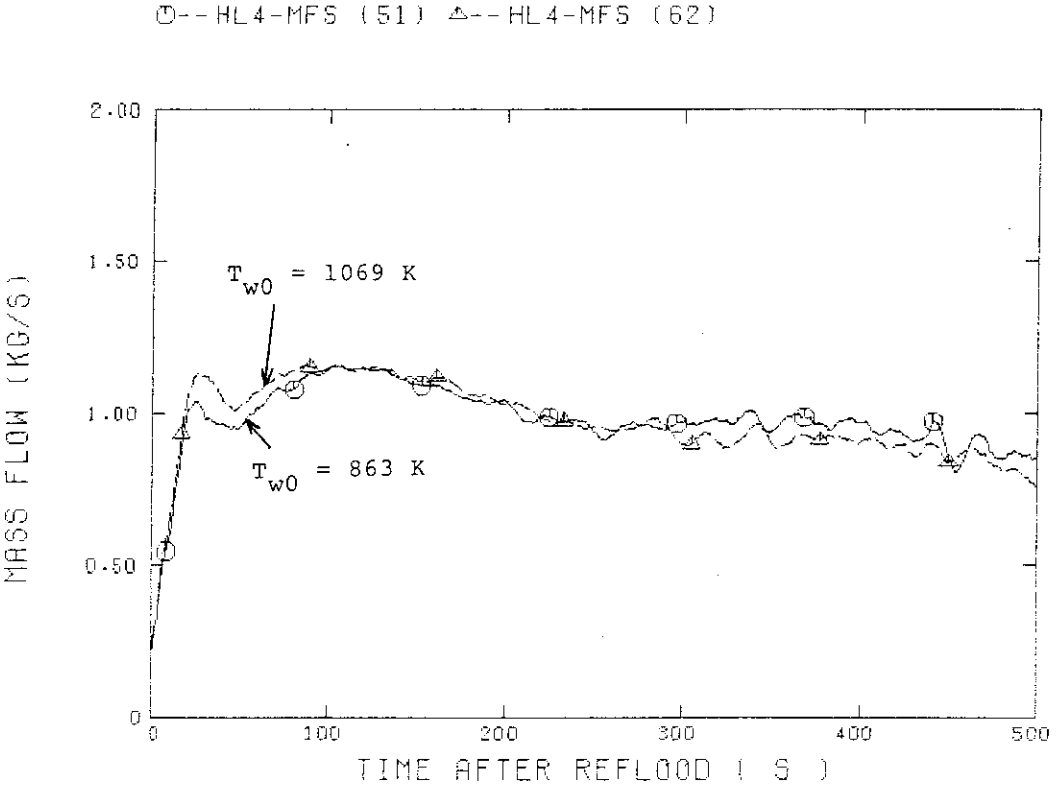

Fig. 3.3 Effect of initial clad temperature on steam mass flow rate through hot legs

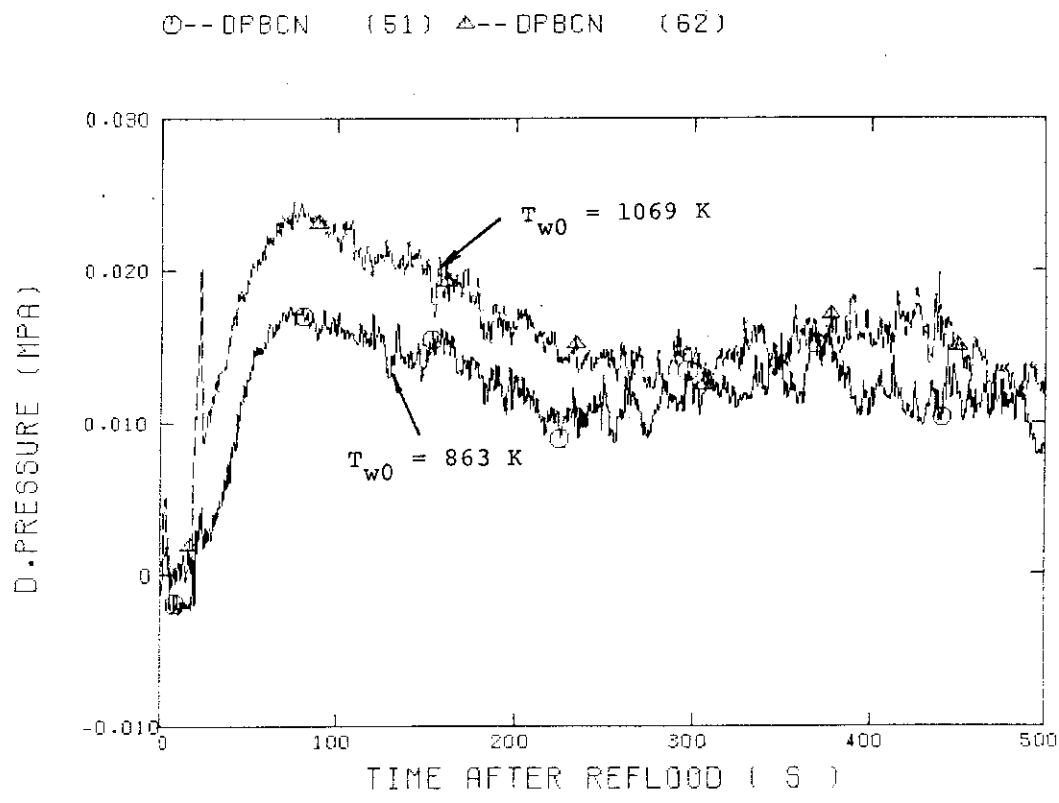

Fig. 3.4 Effect of initial clad temperature on pressure drop at broken cold leg nozzle

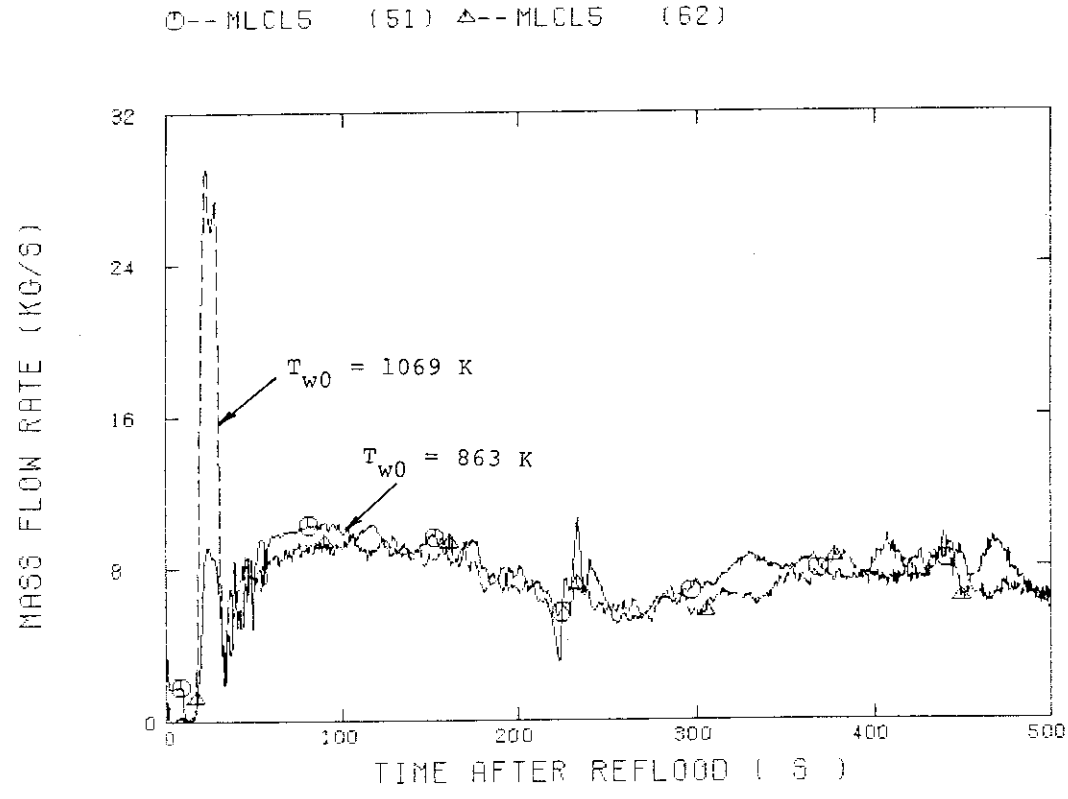

Fig. 3.5 Effect of initial clad temperature on water mass flow rate through broken cold leg nozzle

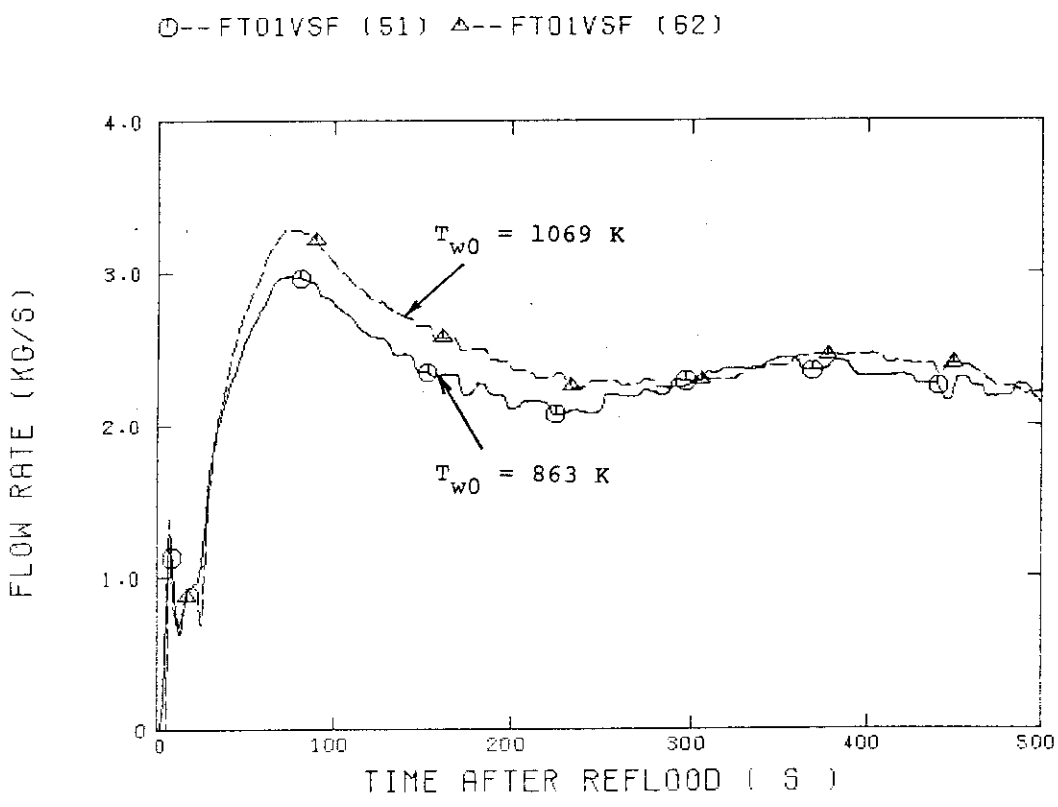

Fig. 3.6 Effect of initial clad temperature on exit steam mass flow rate from containment tank 2

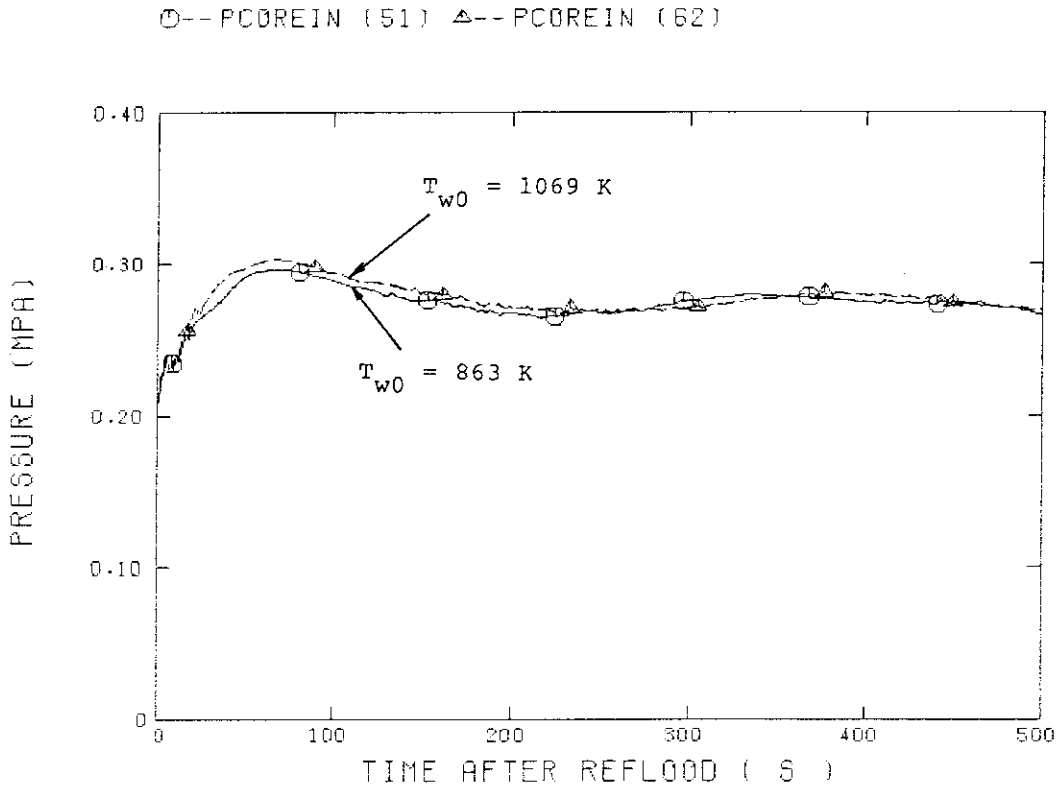

Fig. 3.7 Effect of initial clad temperature on pressure at core inlet

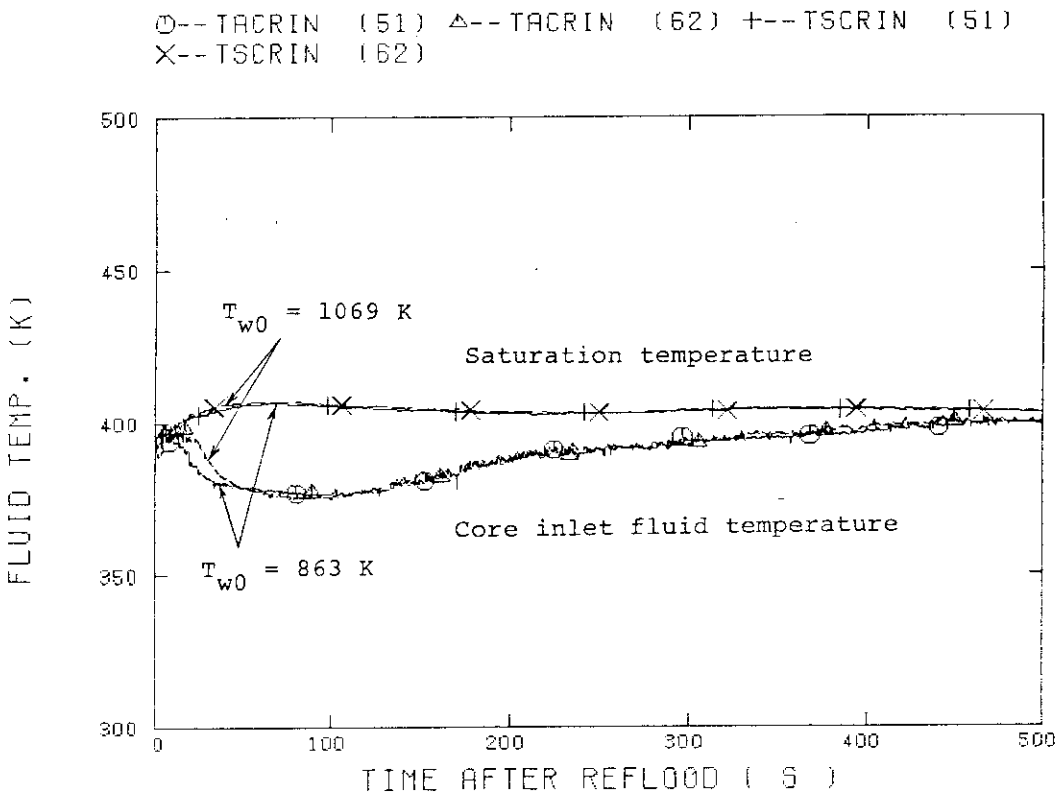

Fig. 3.8 Effect of initial clad temperature on fluid temperature at core inlet

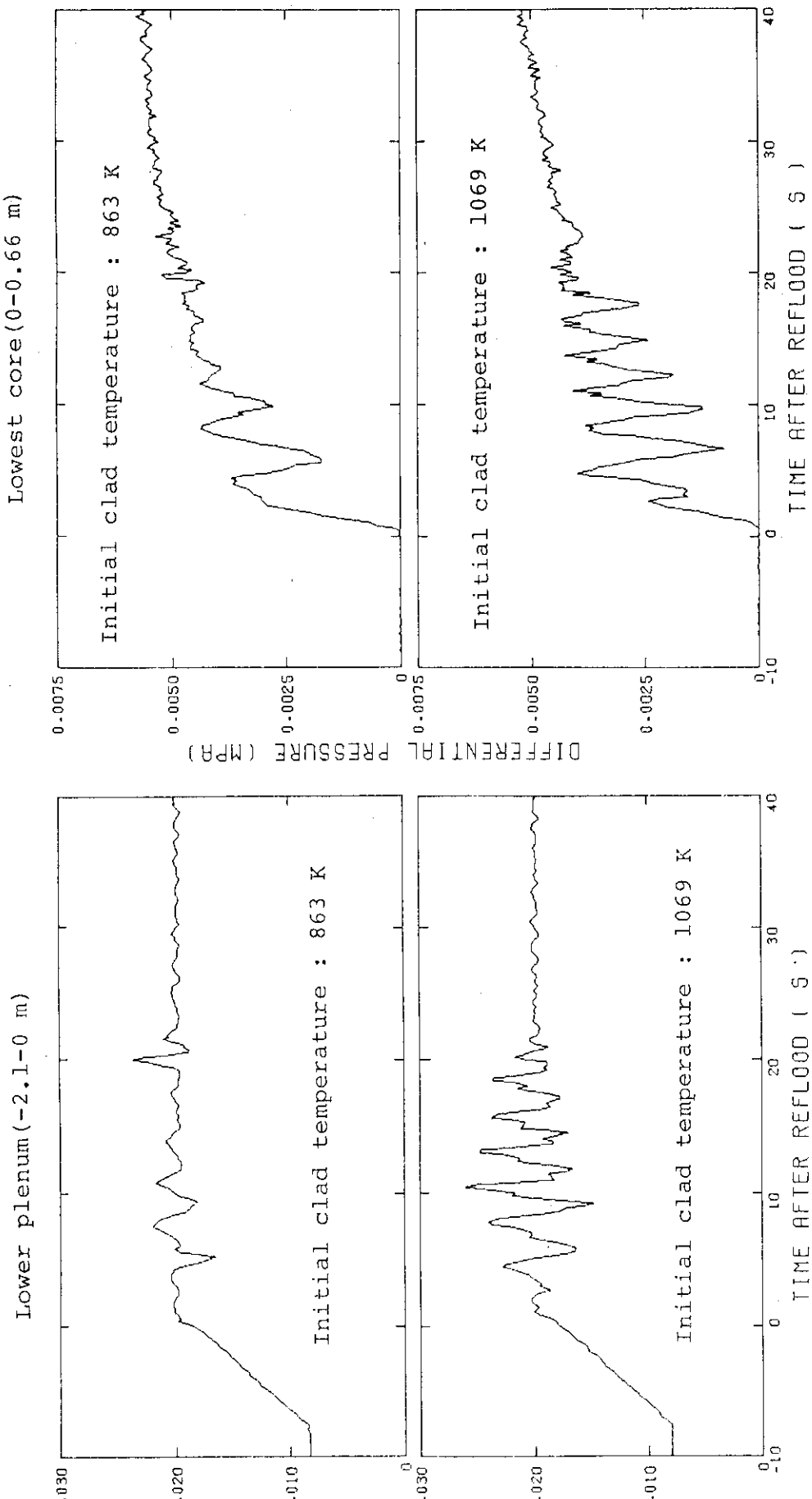

Fig. 3.9 Effect of initial clad temperature on dynamic behavior of differential pressure in lower plenum and lowest part of core

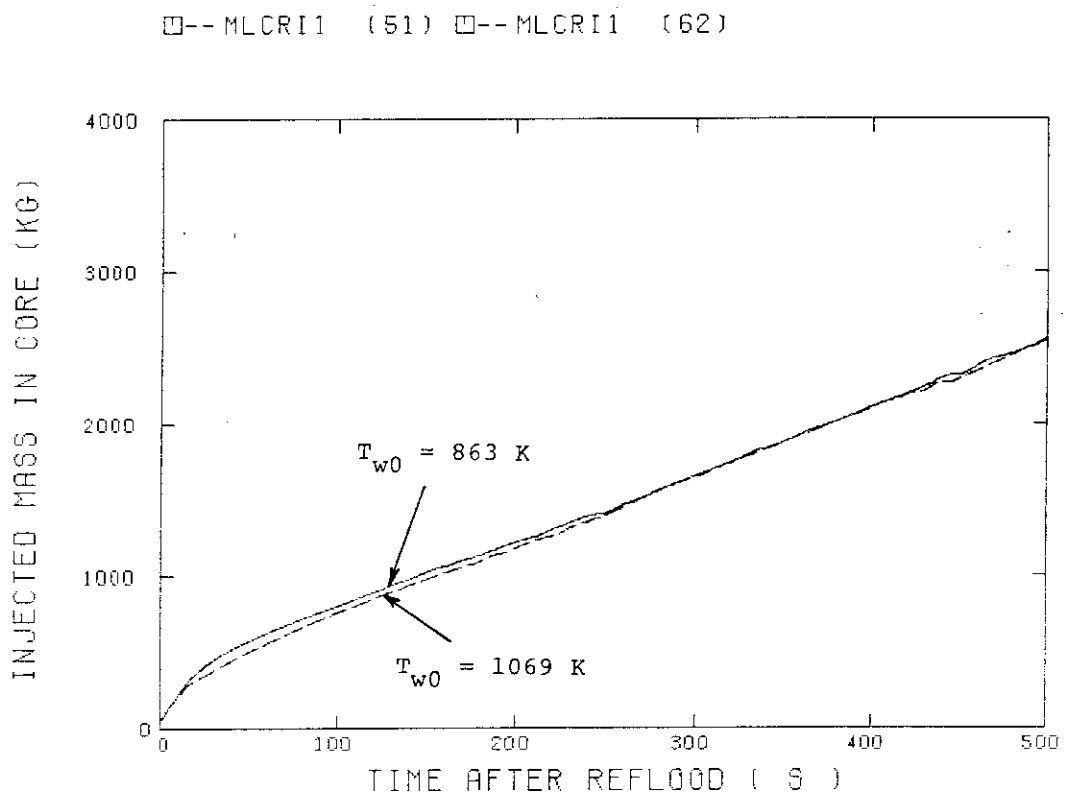

Fig. 3.10 Effect of initial clad temperature on integrated core inlet mass flow rate

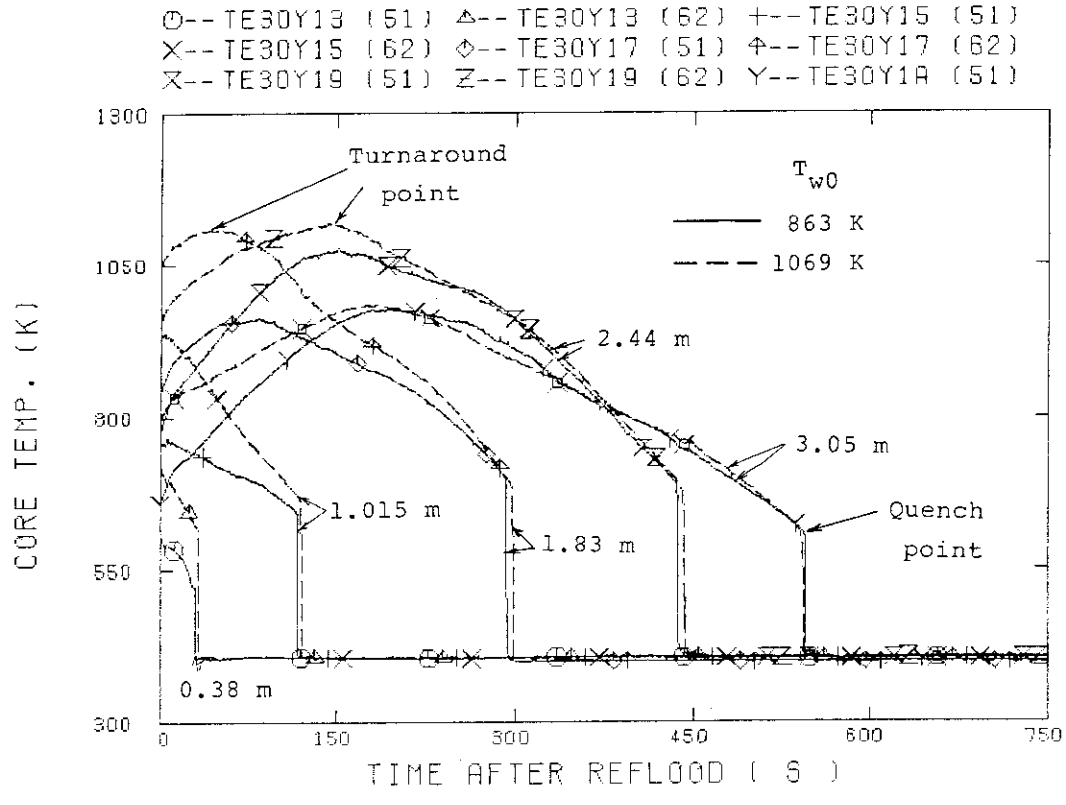

Fig. 3.11 Effect of initial clad temperature on temperature histories of heated rod in high power region

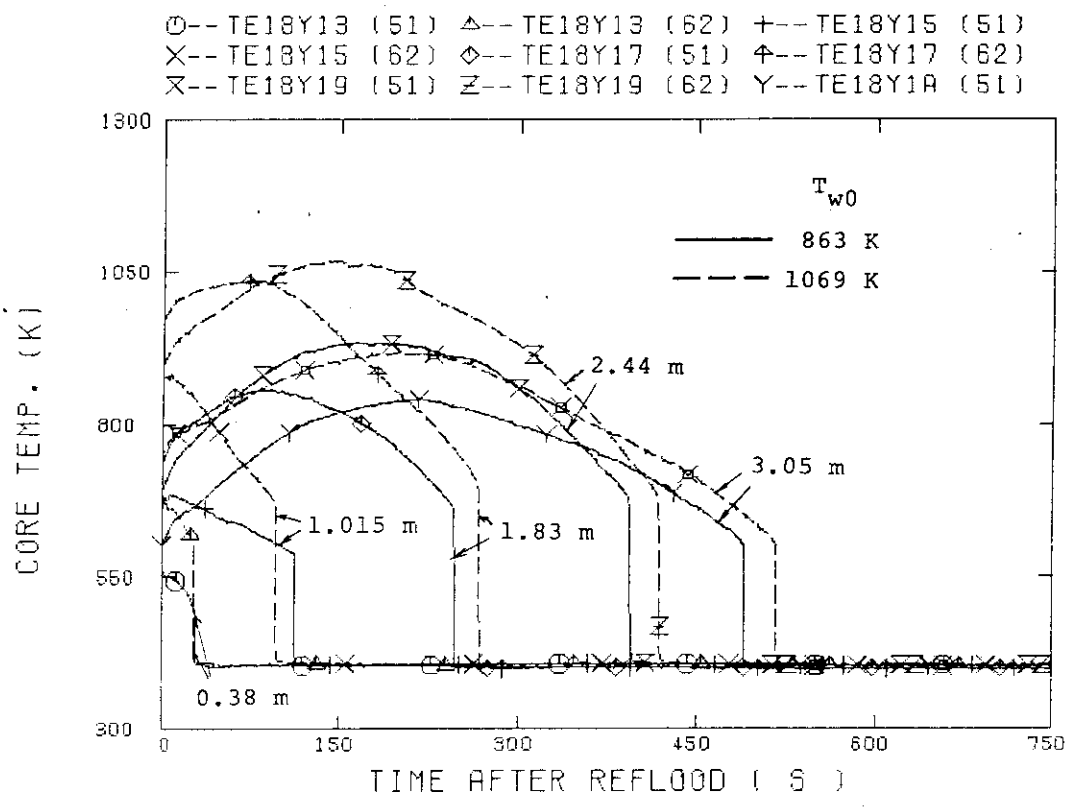

Fig. 3.12 Effect of initial clad temperature on temperature histories of heated rod in medium power region

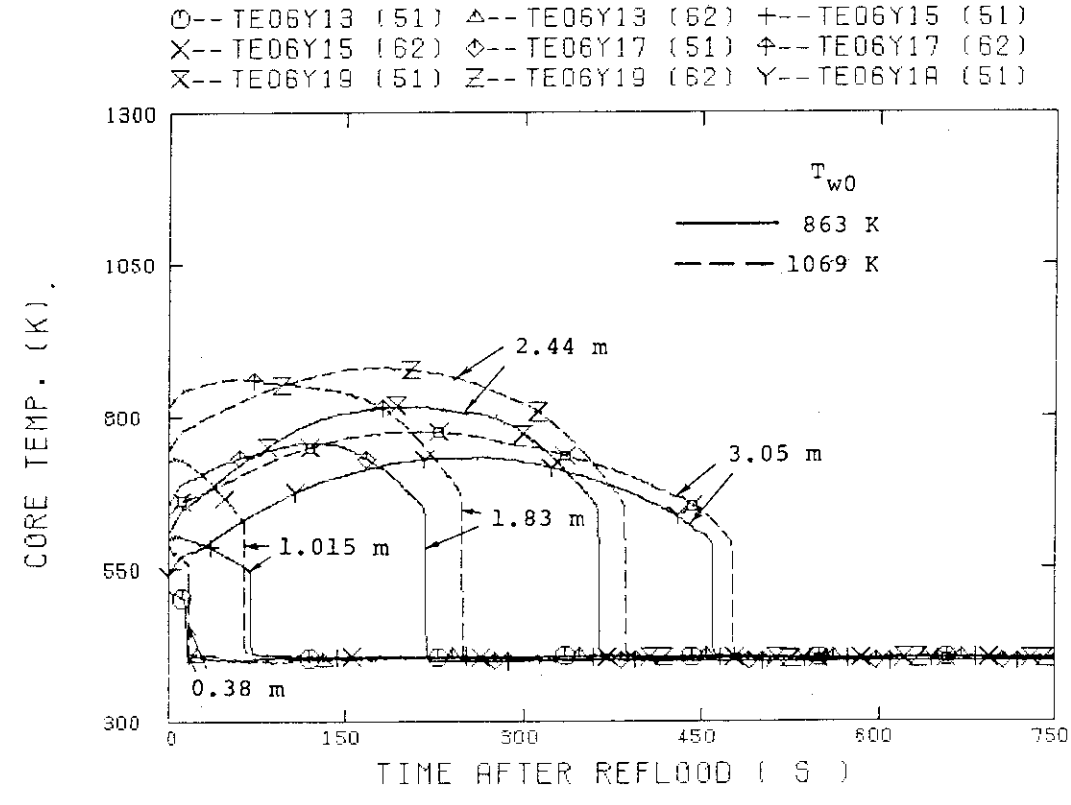

Fig. 3.13 Effect of initial clad temperature on temperature histories of heated rod in low power region

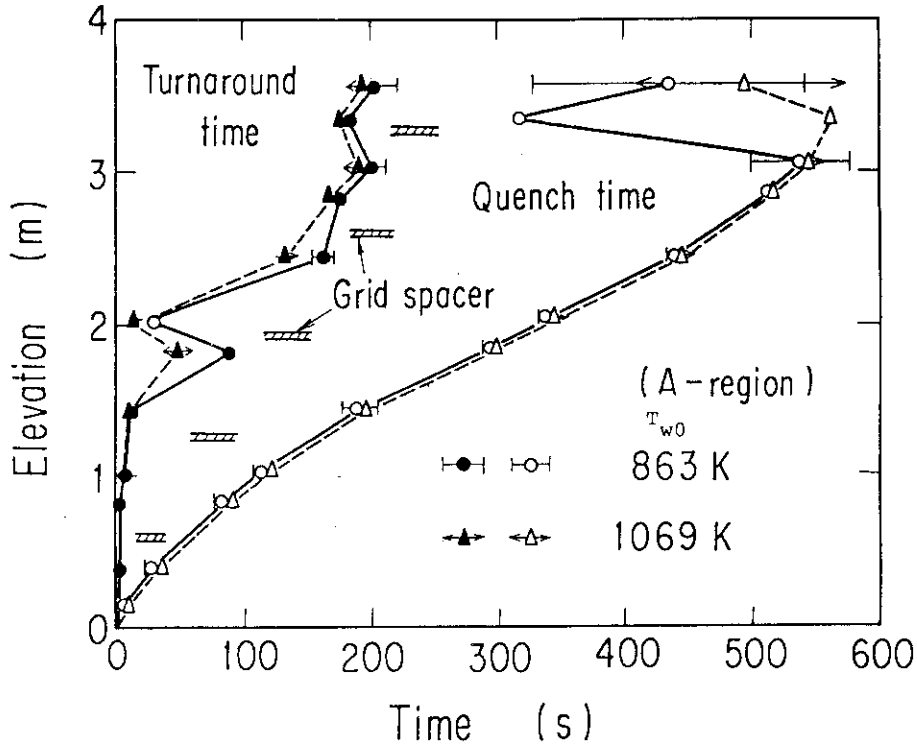

Fig. 3.14 Effect of initial clad temperature on turnaround and quench times in high power region

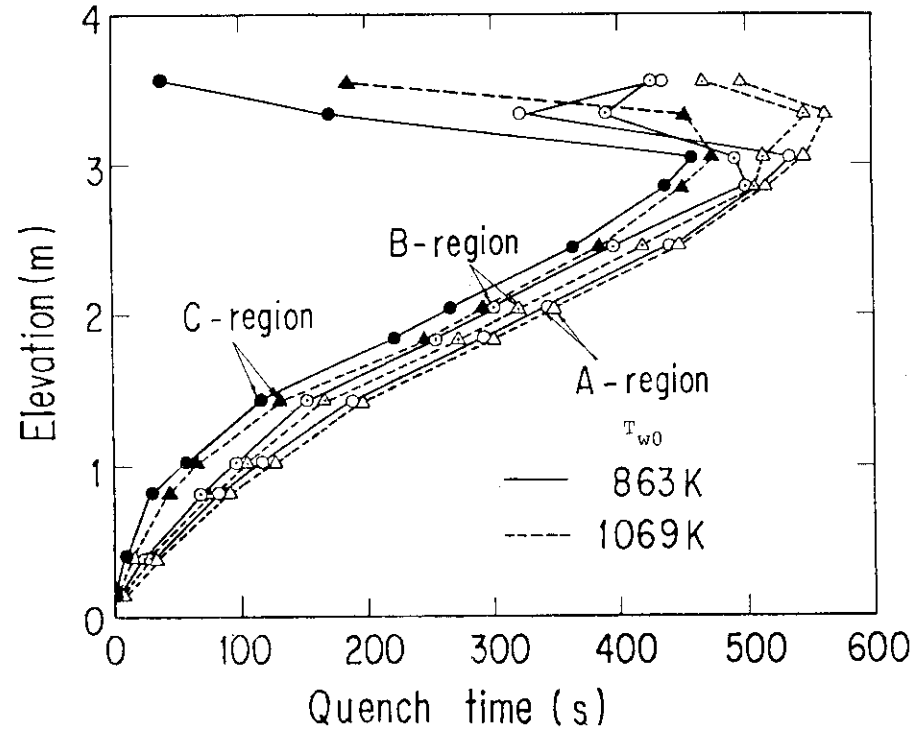

Fig. 3.15 Effect of initial clad temperature on quench times in three power regions

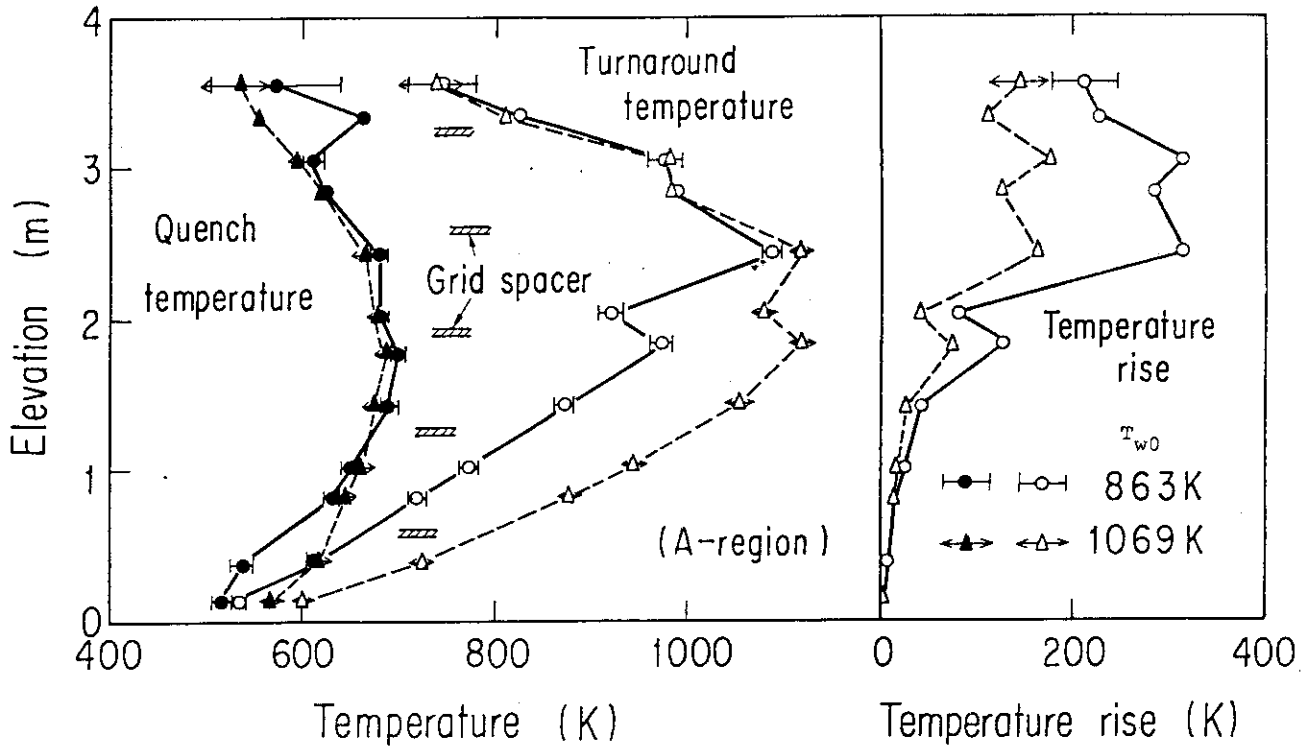

Fig. 3.16 Effect of initial clad temperature on turnaround and quench temperatures, and temperature rise in high power region

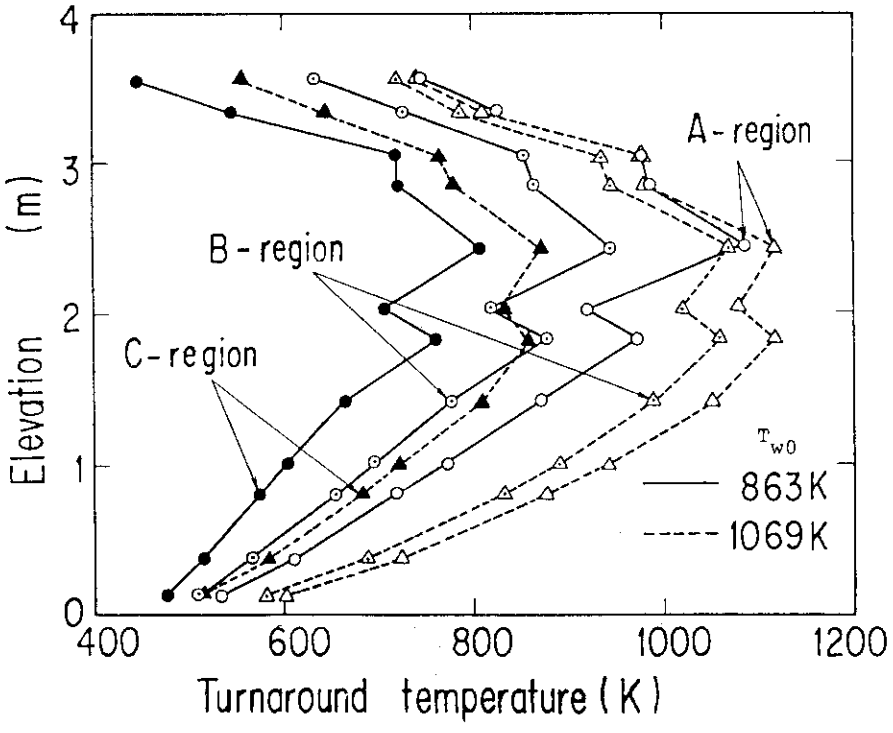

Fig. 3.17 Effect of initial clad temperature on turnaround temperatures in three power regions

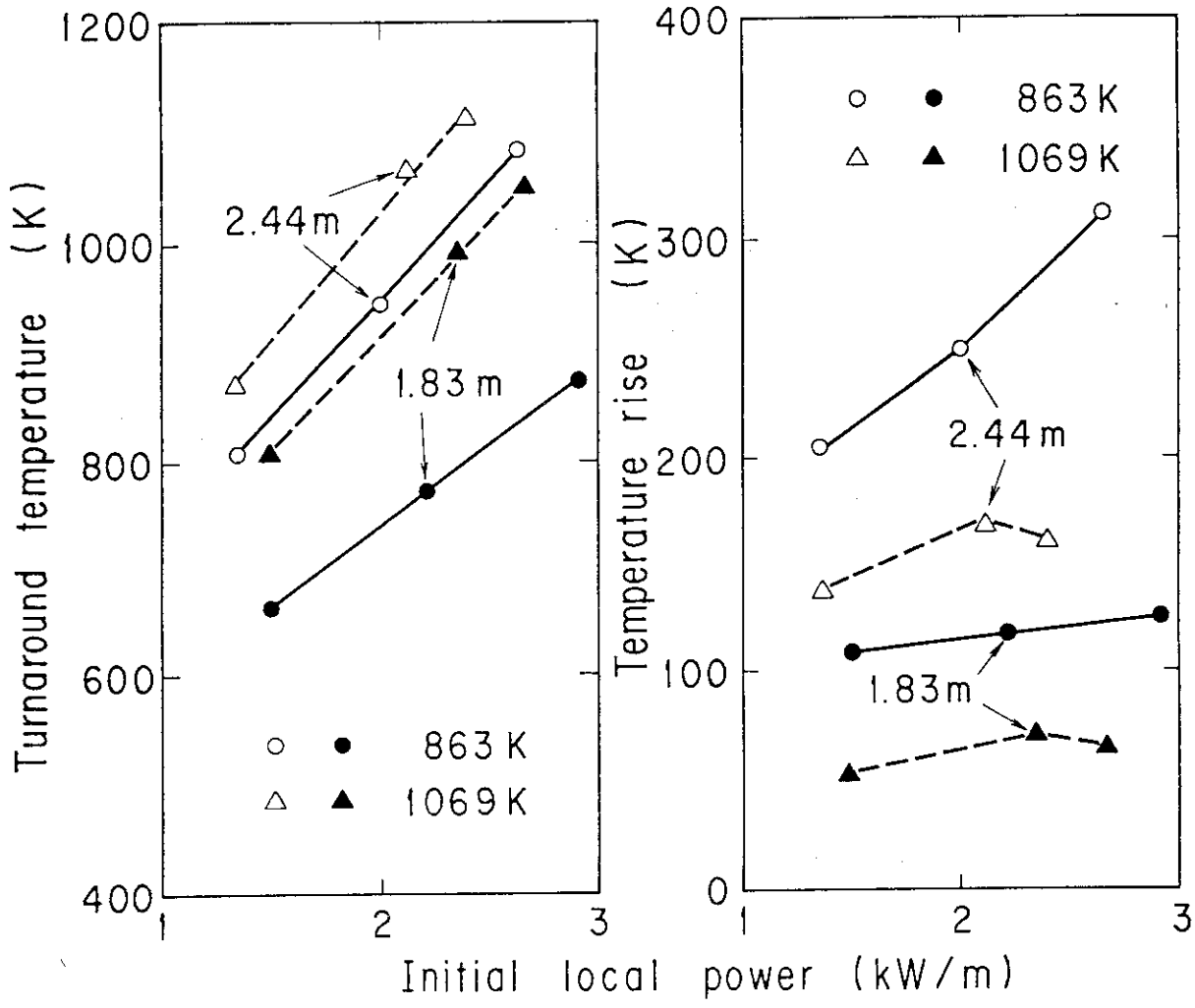

Fig. 3.18 Effect of initial clad temperature on turnaround temperature and temperature rise with regard to initial local power

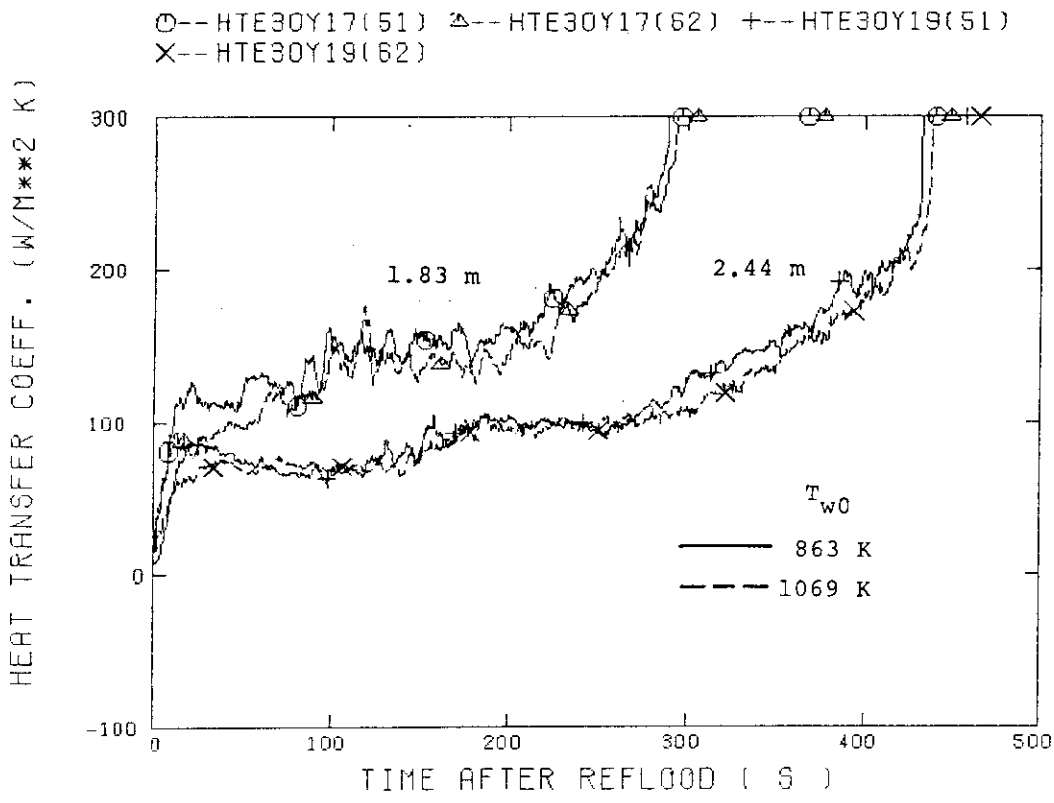

Fig. 3.19 Effect of initial clad temperature on heat transfer coefficient in high power region

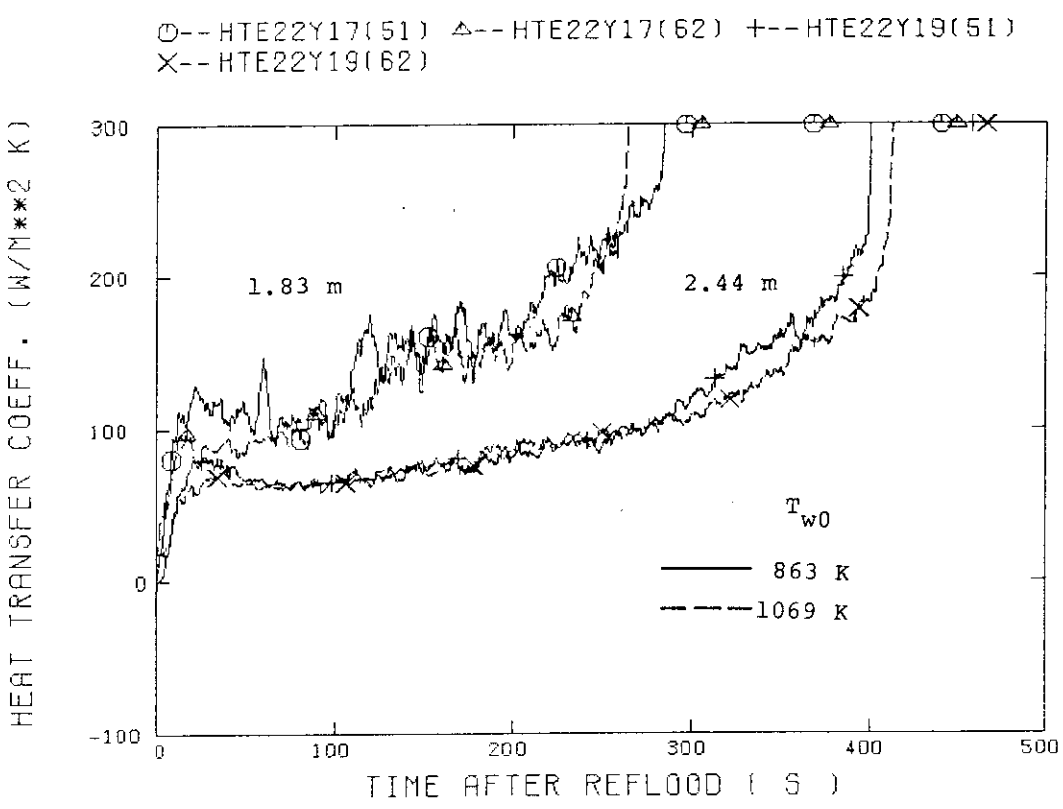

Fig. 3.20 Effect of initial clad temperature on heat transfer coefficient in medium power region

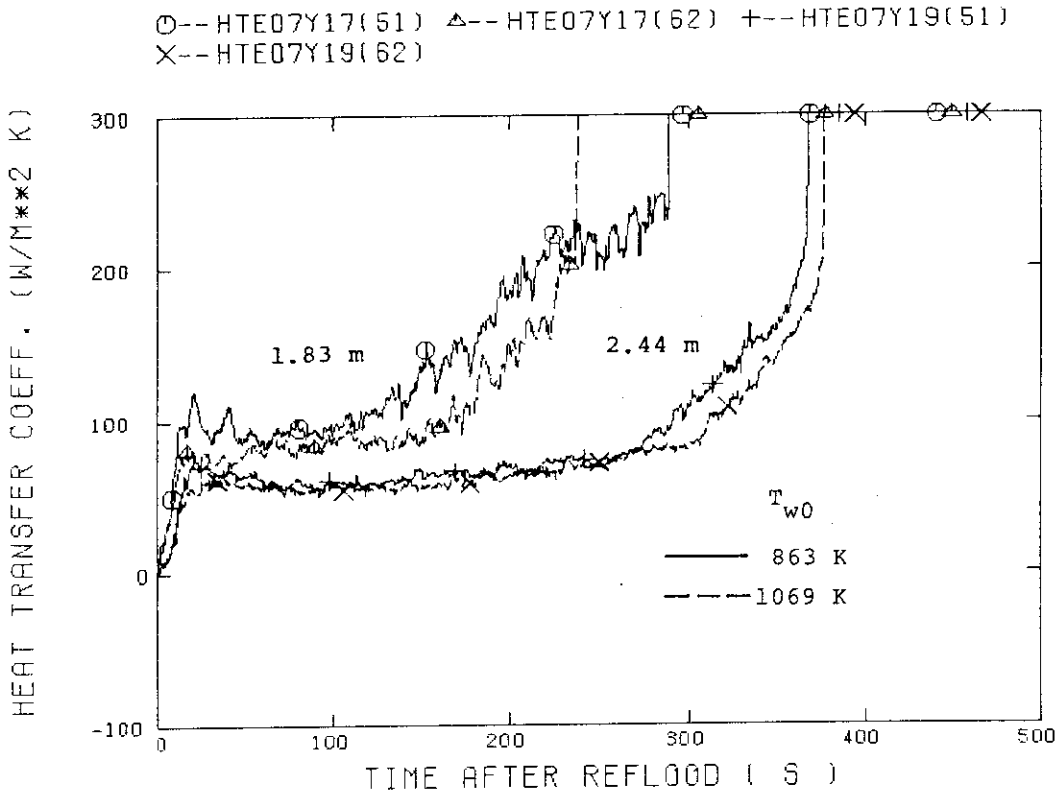

Fig. 3.21 Effect of initial clad temperature on heat transfer coefficient in low power region

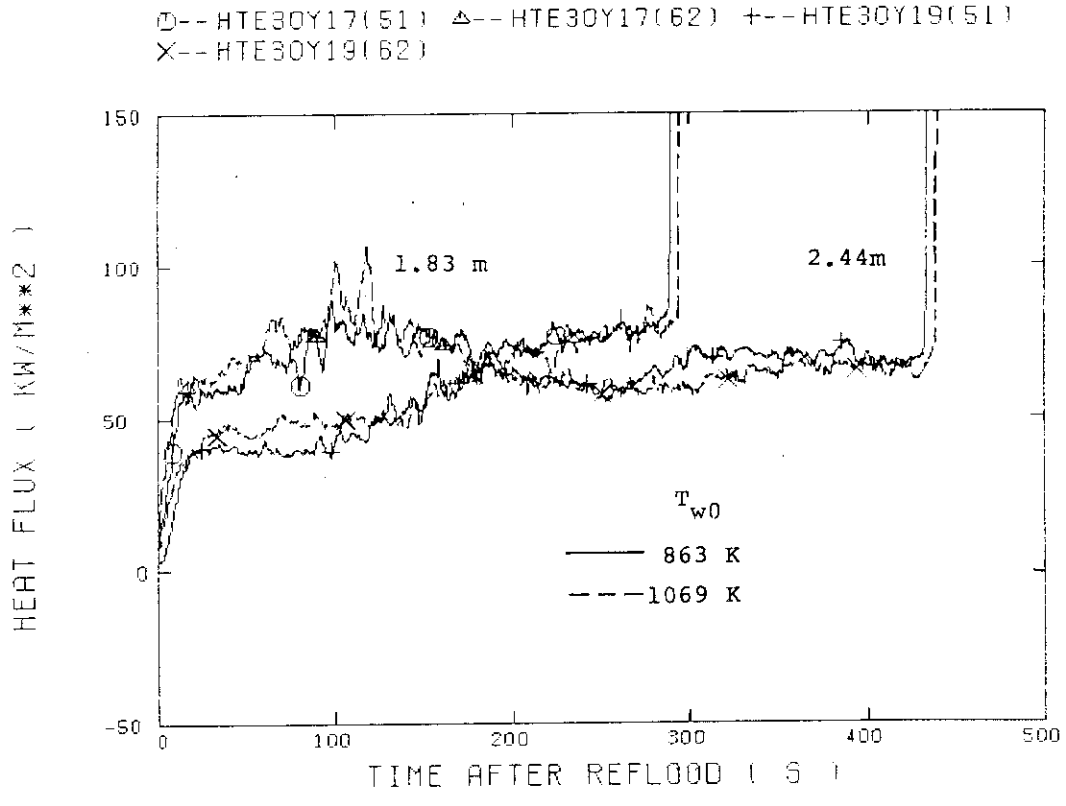

Fig. 3.22 Effect of initial clad temperature on heat flux in high power region

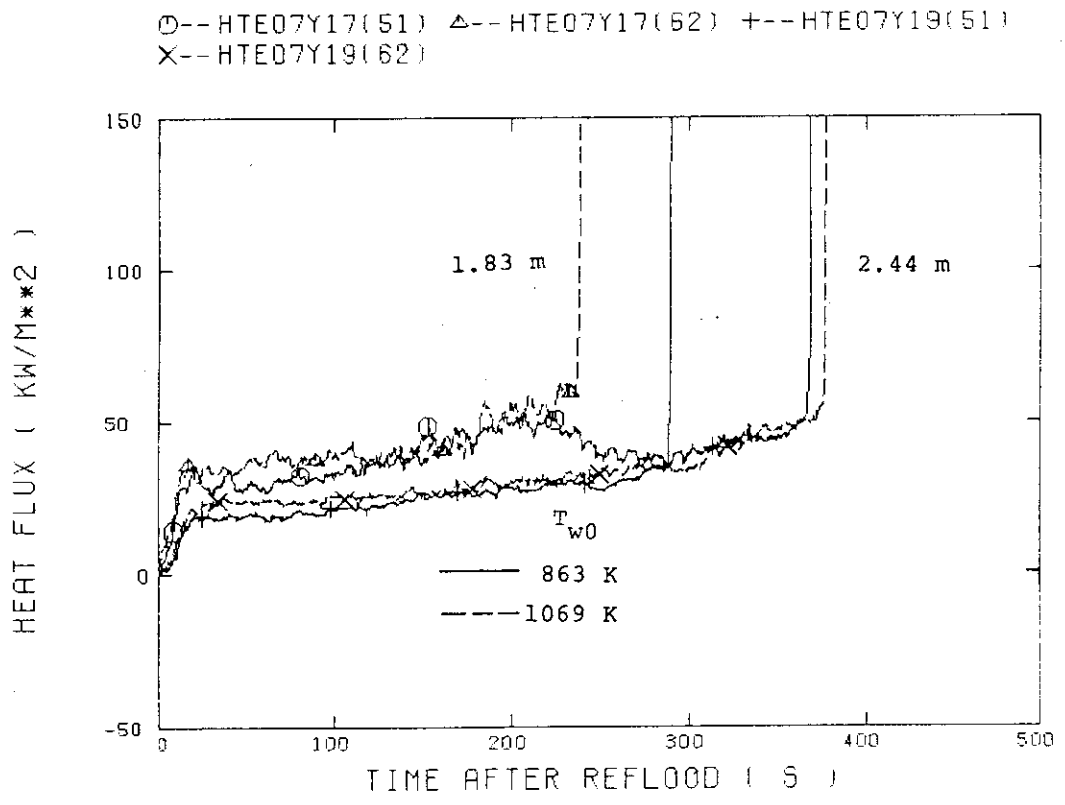

Fig. 3.23 Effect of initial clad temperature on heat flux in medium power region

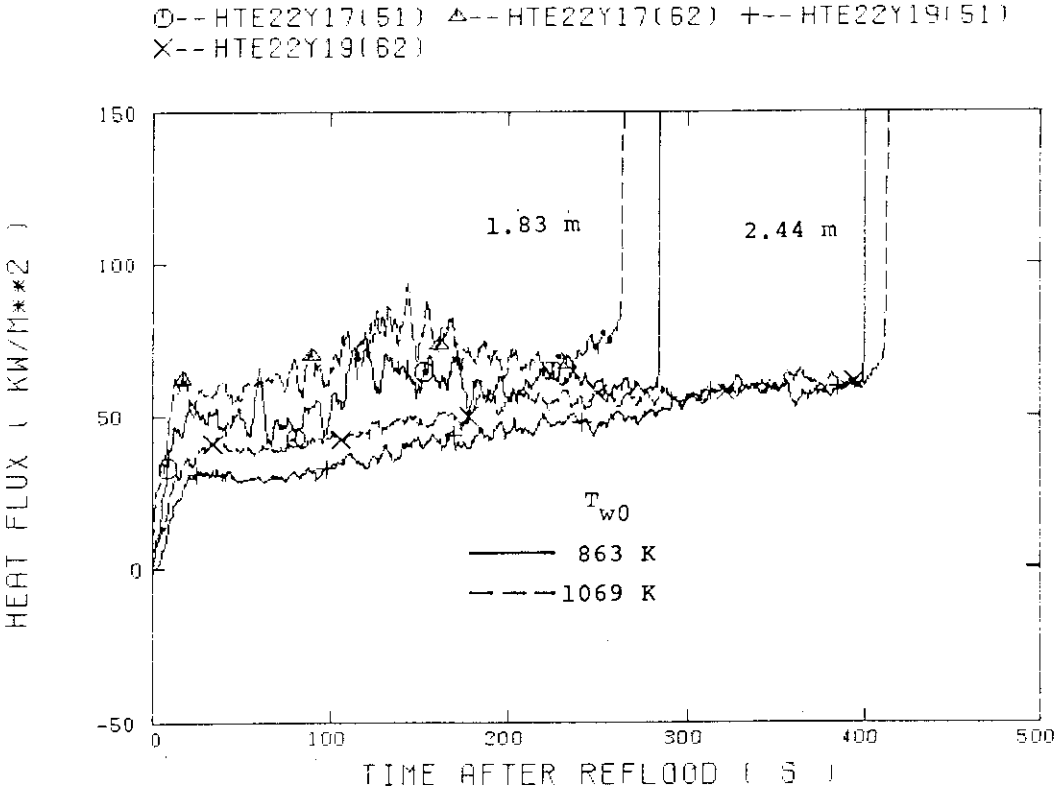

Fig. 3.24 Effect of initial clad temperature on heat flux in low power region

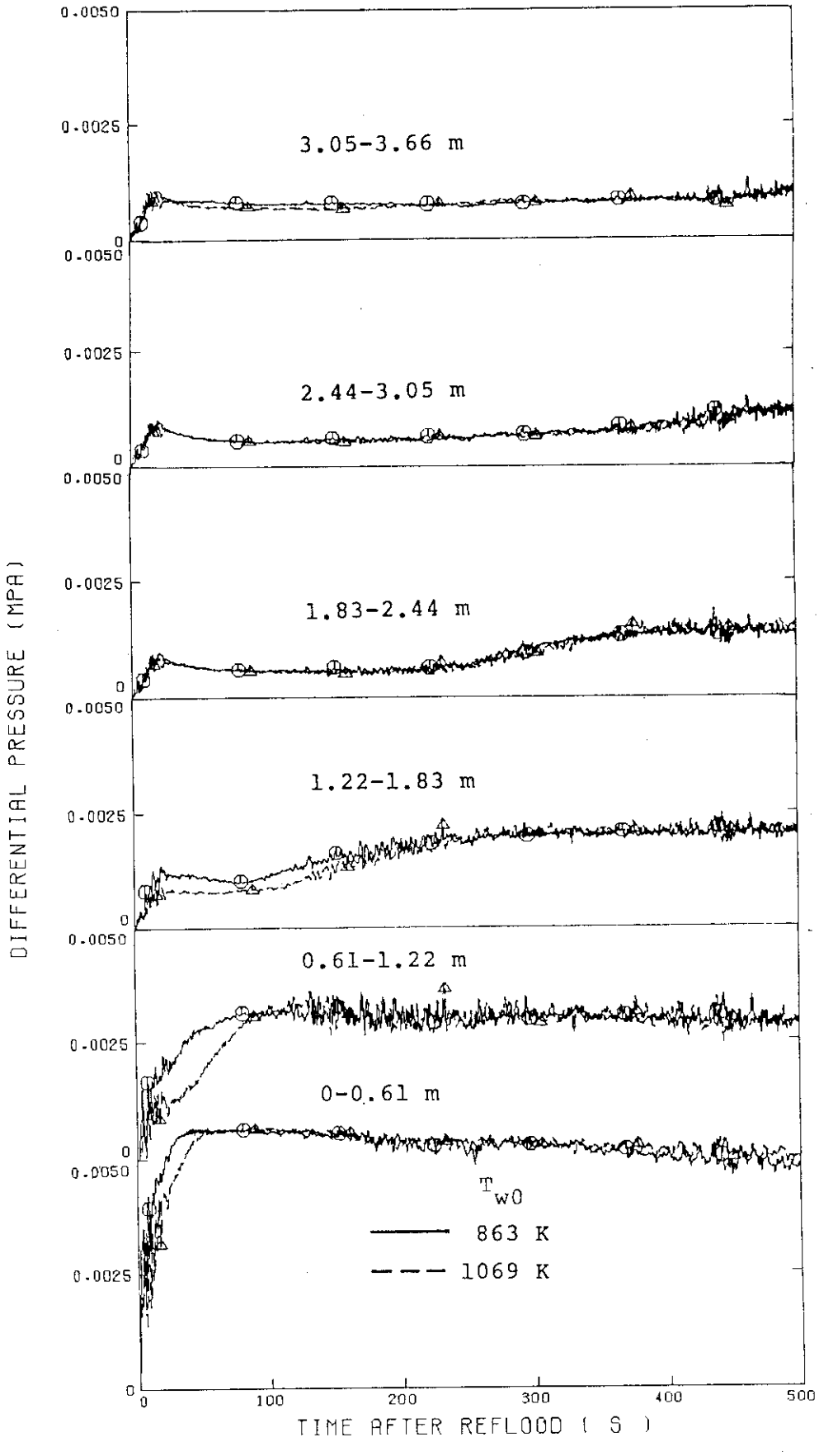

Fig. 3.25 Effect of initial clad temperature on sectional differential pressure in core

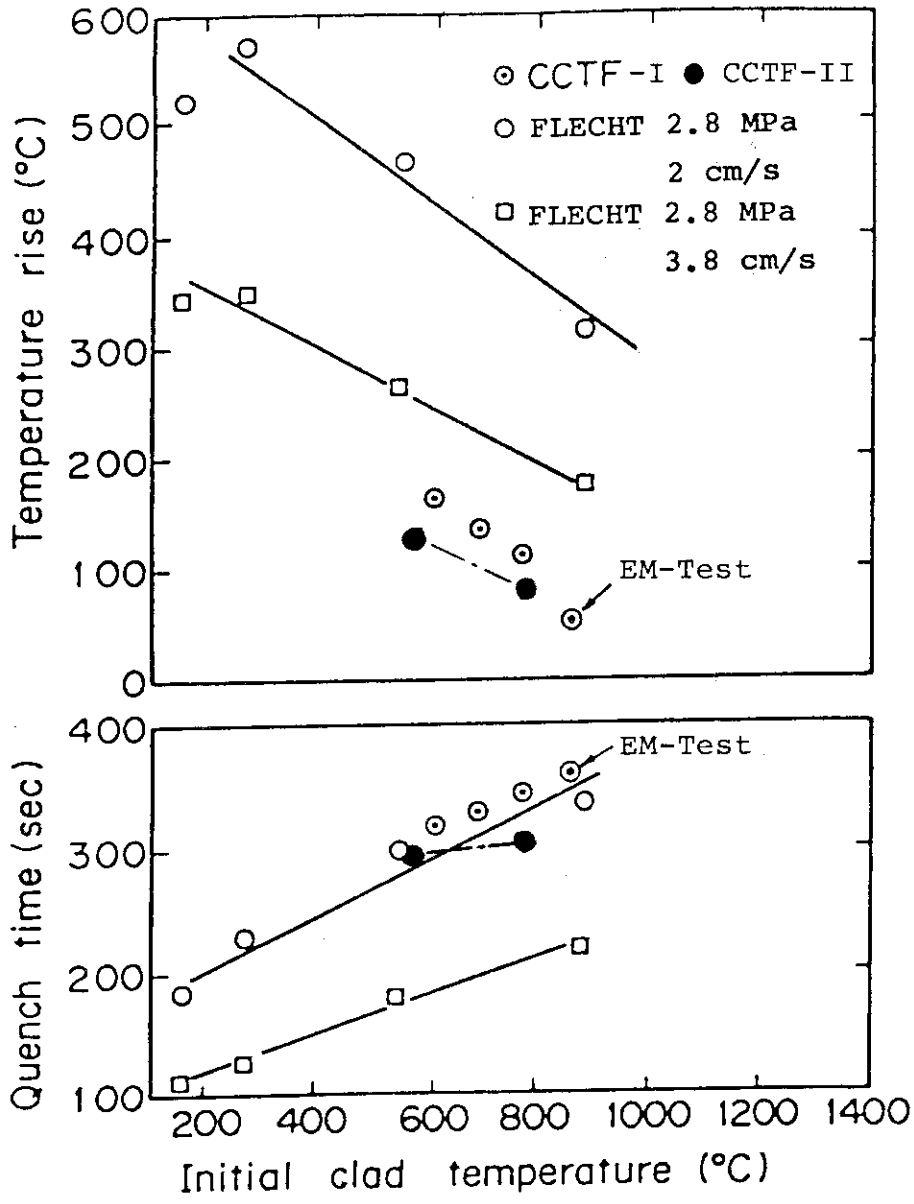

Fig. 3.26 Comparison of temperature rise and quench time at midplane

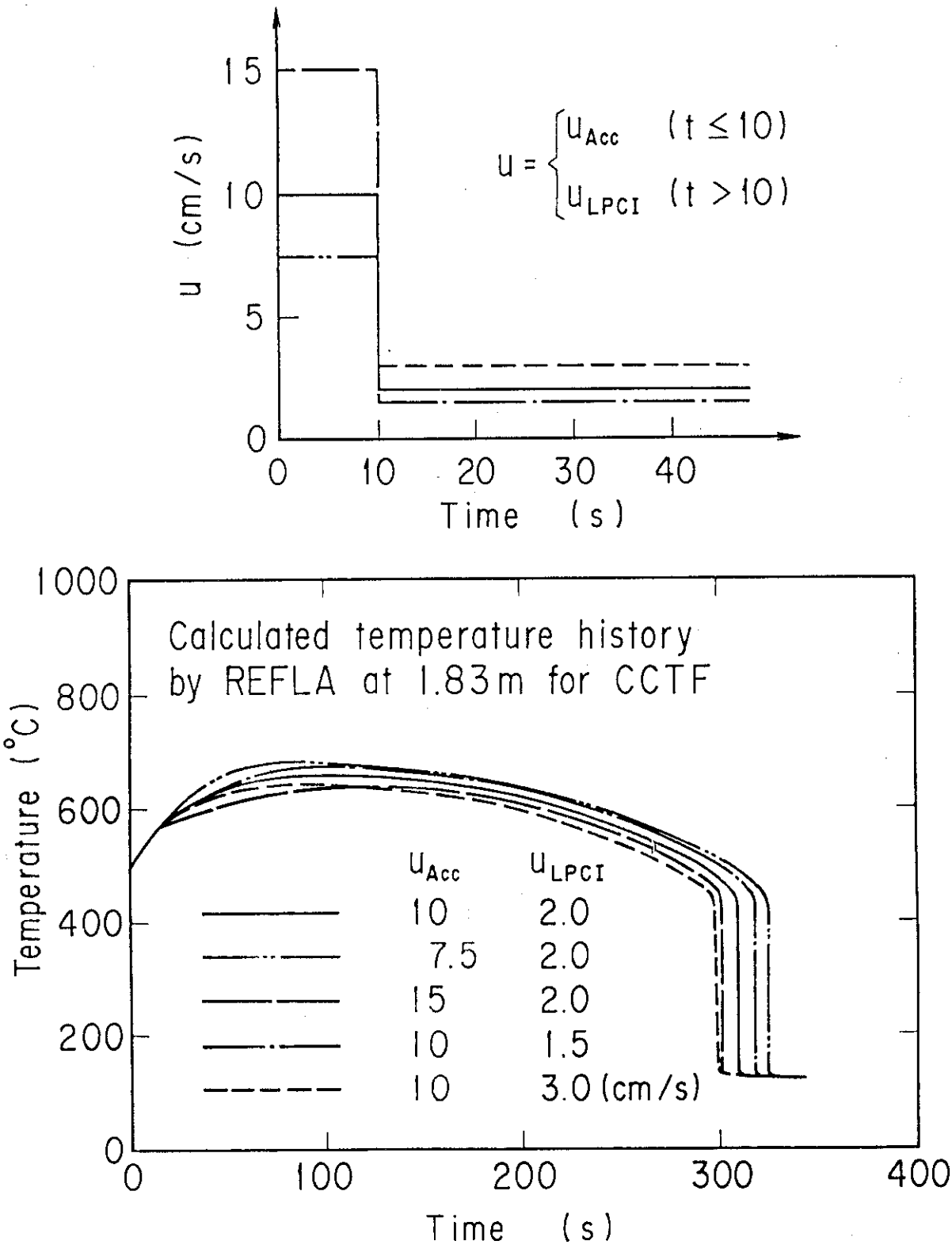

Fig. 3.27 Effect of initial and long-term flooding rates on calculated temperature responses

4. Conclusions

The effect of the initial clad temperature on the reflood phenomena was investigated in CCTF Core-II. The initial peak clad temperature in the two tests were 863 and 1069 K, respectively. The following conclusions were obtained:

(1) The higher initial clad temperature has revealed lower water accumulation in the core and the uppler plenum, higher loop mass flow rate, and larger differential pressure across the broken cold leg nozzle in an early reflood transient. These effects can be attributed to larger release of stored energy in the core.

(2) Pressure and fluid temperature at the core inlet were little affected by the initial clad temperature. The core inlet mass flow rate was suppressed by the higher initial clad temperature only just after the reflood initiation, due to the more rapid vapor generation in the core. However, the core inlet mass flow rate was little affected for the rest of the transient.

(3) The U-tube flow oscillation between the core and the downcomer was observed just after the reflood initiation. Amplitude of the oscillation was larger with higher initial clad temperature. This can also be attributed to the more rapid vapor generation in the core. The oscillation lasted for less than 20 s, and hence it appears to give little effect on the overall system behaviors.

(4) In the core, with higher initial clad temperature, higher turnaround temperature and later quench time were observed. The heat transfer coefficient was slightly lower only in an early reflood transient, but the heat flux was larger, which resulted in lower temperature rise. The water accumulation in the lower part of the core was smaller in the higher initial clad temperature test in which the core flooding and quench front propagation were more suppressed than in the lower temperature test.

(5) The effect of the initial clad temperature on system responses in CCTF Core-II were similar to those observed in CCTF Core-I. The core thermal behaviors in CCTF Core-I, Core-II and FLECHT tests were also similar with each other. The general trend of the lower temperature rise with higher initial clad temperature was thus confirmed. Analysis by the REFLA code has revealed that higher initial flooding rate rather than the long-term flooding rate is important for further decreasing the temperature rise.

Acknowledgments

The authors are very grateful to Dr. M. Nozawa, Deputy Director General of Tokai Research Establishment of JAERI, Dr. S. Katsuragi, Director of Nuclear Safety Research center, Dr. M. Hirata, Director of Department of Nuclear Safety Research, and Dr. K. Hirano, Deputy Director of Department of Nuclear Safety Research, respectively, for their guidance and encouragement.

They are deeply indebted to Mr. T. Sudoh, Mr. K. Okabe, Dr. H. Akimoto, and Mr. T. Okubo for their valuable suggestions and discussion.

They would like to express their appreciation to the SCTF analysis group, Mr. H. Adachi, Dr. Y. Sudo, Mr. M. Sobajima, Mr. T. Iwamura, Mr. M. Osakabe, Mr. A. Ohnuki, and Mr. Y. Abe for their useful discussion.

References

(1) Lilly, G.P., et al.: "FLECHT cosine low flooding rate test series evaluation report", WCAP-8838, March (1977).

(2) Sugimoto, J., et al.: "Evaluation report on CCTF Core-I reflood tests C1-5 (Run 14), C1-7 (Run 16) and C1-14 (Run 23) - Effects of initial clad temperature -", JAERI-M 83-026, February (1983).

(3) Sugimoto, J., et al.: "Experimental study of effect of initial clad temperature on reflood phenomena during PWR-LOCA", J. Nucl. Sci. Technol., 20 [8], 656∿667 (1983).

(4) Sudoh, T., et al.: "Evaluation report on CCTF Core-II reflood Test C2-SH1 (Run 53)", JAERI-M, to be published.

(5) Iguchi, T., et al.: "Water accumulation phenomena in upper plenum during reflood phase of PWR-LOCA by using CCTF data", J. Nucl. Sci. Technol., 20 [6], 453∿466 (1983).

(6) Sugimoto, J., et al.: "Effect of grid spacers on reflood heat transfer in PWR-LOCA", J. Nucl. Sci. Technol., 21 [2], 103∿114 (1984).

(7) Murao, Y., et al.: "Evaluation report on CCTF Core-I reflood test C1-19 (Run 38) - Experimental assessment of the evaluation model for the safety analysis on the reflood phase of a PWR-LOCA - ", JAERI-M 83-029 (1983).

(8) Murao, Y.: "Analytical study of thermo-hydrodynamic behavior of reflood phase during LOCA", J. Nucl. Sci. Technol. 16 [11], 802∿817 (1979).

Acknowledgments

The authors are very grateful to Dr. M. Nozawa, Deputy Director General of Tokai Research Establishment of JAERI, Dr. S. Katsuragi, Director of Nuclear Safety Research center, Dr. M. Hirata, Director of Department of Nuclear Safety Research, and Dr. K. Hirano, Deputy Director of Department of Nuclear Safety Research, respectively, for their guidance and encouragement.

They are deeply indebted to Mr. T. Sudoh, Mr. K. Okabe, Dr. H. Akimoto, and Mr. T. Okubo for their valuable suggestions and discussion.

They would like to express their appreciation to the SCTF analysis group, Mr. H. Adachi, Dr. Y. Sudo, Mr. M. Sobajima, Mr. T. Iwamura, Mr. M. Osakabe, Mr. A. Ohnuki, and Mr. Y. Abe for their useful discussion.

References

(1) Lilly, G.P., et al.: "FLECHT cosine low flooding rate test series evaluation report", WCAP-8838, March (1977).

(2) Sugimoto, J., et al.: "Evaluation report on CCTF Core-I reflood tests C1-5 (Run 14), C1-7 (Run 16) and C1-14 (Run 23) - Effects of initial clad temperature -", JAERI-M 83-026, February (1983).

(3) Sugimoto, J., et al.: "Experimental study of effect of initial clad temperature on reflood phenomena during PWR-LOCA", J. Nucl. Sci. Technol., 20 [8], 656∿667 (1983).

(4) Sudoh, T., et al.: "Evaluation report on CCTF Core-II reflood Test C2-SH1 (Run 53)", JAERI-M, to be published.

(5) Iguchi, T., et al.: "Water accumulation phenomena in upper plenum during reflood phase of PWR-LOCA by using CCTF data", J. Nucl. Sci. Technol., 20 [6], 453∿466 (1983).

(6) Sugimoto, J., et al.: "Effect of grid spacers on reflood heat transfer in PWR-LOCA", J. Nucl. Sci. Technol., 21 [2], 103∿114 (1984).

(7) Murao, Y., et al.: "Evaluation report on CCTF Core-I reflood test C1-19 (Run 38) - Experimental assessment of the evaluation model for the safety analysis on the reflood phase of a PWR-LOCA - ", JAERI-M 83-029 (1983).

(8) Murao, Y.: "Analytical study of thermo-hydrodynamic behavior of reflood phase during LOCA", J. Nucl. Sci. Technol. 16 [11], 802∿817 (1979).

Appendix A

Definitions of Tag IDs

Figure List

1. Definition of Tag. ID for clad surface temperatures and heat fransfer coefficients

Notation : TEnnYlm (temperature)

HTEmmYlm (heat transfer coefficient)

nn : Bundle number (see Fig. A.1)

m : Elevation number

	Elevation (m)	Axial power factor
3	0.38	0.651
5	1.015	1.147
7	1.83	1.40
9	2.44	1.256
A	3.05	0.854

2. Definition of power zone and boundle number

See Fig. A.1

3. Definition of Tag. ID for void fraction

See Fig. A.2

4. Definition of Tag. ID for average linear power of heater rod in each power unit zone

See Fig. A.3

5. Definition of Tag. ID for differential pressure through downcomer, upper plenum, core and lower plenum

See Fig. A.4

6. Definition of Tag. ID for differential pressure through intact and broken loop and broken cold leg nozzle

See Fig. A.5

7. Definition of Tag. ID for fluid temperature in inlet and outlet plenum and secondary side of steam generator

See Fig. A.6

8. Definition of Tag. ID for ECC water injection rate, ECC water temperature and vented steam flow rate

See Fig. A.7

9. Definition of initial temperature, turnaround temperature quench temperature, temperature rise, turnaround time and quench time. (See Fig. A.8)

T_i : Initial temperature (Clad surface temperature at reflood initiation)

T_t : Turnaround temperature (Maximum clad surface temperature in each temperature history)

ΔT_r : Temperature rise ($= T_t - T_i$)

T_q : Quench temperature (Clad surface temperature at quenching)

10. Definition of quenching

See Fig. A.8

Quench time t_t is determined as

$$t_t = i \times \Delta t - \text{(reflood initiation time)}$$

In above equation, i is determined by the following criteria.

(1) Clad surface temperature is high, compared with the saturation temperature.

$$T_i > T_{sat} + \Delta T_1$$

(2) Decreasing rate of clad surface temperature is large.

$$\frac{T_{i+1} - T_i}{\Delta t} < - C_{st}$$

(3) Clad surface temperature falls around the saturation temperature.

$$T_{i + k_1} \leq T_{sat} + \Delta T_1$$

(4) If the determined i is inadequate, the value i is manually re-determined.

Δt : Data sampling period (s)

T_i : Clad surface temperature (K)

T_{sat} : Saturation temperature at the pressure in upper plenum (K)

ΔT_1 : Temperature discrepancy (K)
Default value = 50.0

C_{st} : Decreasing rate of clad surface temperature (K/S)
Default value = 25.0

k_1 : Number of referred data (-)
Default value = 6

11. Definition of Tag. ID for core inlet mass flow rate, time-integral core inlet mass flow rate and carry-over rate fraction

(1) Core inlet mass flow rate : $\dot{m}_F$
Notation : MLCRI□ (□ = N, 1 or 11)

(2) Time-intefral core inlet mass flow rate : $\int \dot{m}_F dt$
Notation : IMLCRI□ (□ = N, 1 or 11)

(3) Carry-over rate fraction : $(\dot{m}_F - \dot{m}_{CR})/\dot{m}_F$
Natation : CRF□ (□ = N, 1 or 11)

where $\dot{m}_F$: Core inlet mass flow rate (See item 12)

$\dot{m}_{CR}$: Water accumulation rate in core

Suffix	$\dot{m}_F$ base on
N	Eq.(A.2)
1	Eq.(A.1) with K=15
11	Eq.(A.1) with K=20

12. Evaluation of core inlet mass flow rate

The reflood phenomena is a relatively slow transient and a steady state condition can be applied. In a steady state condition, based on the mass balance relations of the system, the core flooding mass flow rates $\dot{m}_F$s can be written as follows:

By using the data measured at the downstream of the core inlet, $\dot{m}_F$ is derived as,

$$\dot{m}_F = \dot{m}_C + \dot{m}_U + \dot{m}_B + \Sigma \dot{m}_I \quad , \qquad (A.1)$$

where $\dot{m}_C$ and $\dot{m}_U$ are the mass accumulation rates in the core and the upper plenum respectively. The $\dot{m}_B$ and $\dot{m}_I$ are the mass flow rates in the broken loop and the intact loop, respectively.

By using the data measured at the upstream of the core inlet, $\dot{m}_F$ is derived as,

$$\dot{m}_F = \Sigma \dot{m}_{DL} - \dot{m}_D - \dot{m}_O + \dot{m}_{ECC/LP} \quad , \tag{A.2}$$

where $\dot{m}_{DL}$ and $\dot{m}_O$ are the mass flow rates of the water flowing into and overflowing from the downcomer, $\dot{m}_{ECC/LP}$ and $\dot{m}_D$ are the mass flow rate of the ECC water injected into the lower plenum and the water accumulation rate in the dowmcomer respectively.

The $\dot{m}_I$s and $\dot{m}_B$ can be obtained from the pressure drops at the pump simulators with orifices by assuming the K-factor of the orifice is constant. The values of $\dot{m}_C$, $\dot{m}_D$ and $\dot{m}_U$ can be evaluated with the differential pressure ΔP_C, ΔP_D and ΔP_U, respectively, as follows:

$$\dot{m}_n = d(\Delta P_n S_n/g)/dt \quad (n : C, D, U) \quad , \tag{A.3}$$

where g is the gravitational acceleration and S_n is the cross sectional area. The value of $\dot{m}_O$ can be obtained from the liquid level X in the Containment tank 1 as,

$$\dot{m}_O = d(X\rho_\ell S_o)/dt \quad , \tag{A.4}$$

where ρ_ℓ is the liquid density and S_o is the cross sectional area of the containment tank 1.

The value of $\dot{m}_{DL}$, $\dot{m}_{DV}$ and h, which are liquid flow rate, steam flow rate and enthalpy of two phase mixture downstream each ECC port respectively, are obtained from the following mass and energy balance relations at each ECC port under the assumption of thermal equilibrium:

$$\dot{m}_{DV} + \dot{m}_{DL} = \dot{m}_{ECC} + \dot{m}_I \quad , \tag{A.5}$$

$$(\dot{m}_{DV} + \dot{m}_{DL})i = \dot{m}_{ECC}h_{ECC} + \dot{m}_I h_I \quad , \tag{A.6}$$

$$\text{if} \quad h_g \geq h \geq h_\ell \ , \ (\dot{m}_{DV} + \dot{m}_{DL})h = \dot{m}_{DV}h_g + \dot{m}_{DL}h_\ell$$

$$\text{if} \quad h \geq h_g \quad , \ \dot{m}_{DL} = 0 \quad , \tag{A.7}$$

$$\text{if} \quad h \geq h_\ell \quad , \ \dot{m}_{DV} = 0$$

where h is enthalpy of fluid and h_ℓ and h_g are enthalpies of liquid and steam at the saturation temperature, respectively.

The fluid temperatures can be measured with thermocouples immersed in the fluid and the enthalpies h_I and h_{ECC} can be estimated.

Mass balance calculations were performed with Eqs. (A.1) and (A.2). The K-factor of the orifice in the pump simulator was evaluated in the following two ways.

The K-factor of 20 was obtained with the steam and water single phase calibration tests using the flow meter and spool piece data. The K-factor of 15 was obtained with the Pitot tube measurement in a typical reflood condition assuming the flat velocity profile in the pipings. In the differentiation, higher frequency components of the data tends to be amplified more. Therefore, in the differentiation of the differential pressure data, the smoothing procedure was used to suppress the high frequency components of the data.

In the Acc injection period, the calculated $\dot{m}_F$s with Eqs. (A.1) and (A.2) are significantly different from each other. This discrepancy may be caused by inaccuracy of the mass flow rate injected into the system and by the unaccounting of the storage of water in the cold leg pipe. The former might be introduced from the slow time response of the flow meter (time constant 1 second) and the change of the gas volume in the injection line. In this period, especially before the steam generation from the core becomes noticeable, the mass flow rate, $\dot{m}_F$, calculated with Eq. (A.1) is probably reasonable, since the calculation uses the increasing rates of the masses in the core and the upper plenum and their accuracy is good enough for our estimation.

In the LPCI injection period, the calculated $\dot{m}_F$s are slightly different from each other. Judging from the time-integral values of both $\dot{m}_F$s, their average values are nearly proportional. The discrepancy was inferred to be caused by the disregard of the bypass of steam and liquid from the upper plenum without going through the hot legs in the calculation with Eq. (A.1). And additionally the discrepancy was caused by the disregard of the steam generation in the downcomer due to the hot wall of the pressure vessel in the calculation with Eq. (A.2). It was estimated that the disregard of the downcomer steam generation causes the error of 0.25 kg/s on predicted $\dot{m}_F$. The estimation was made by comparing the results of the tests with hot and cold downcomer conditions.

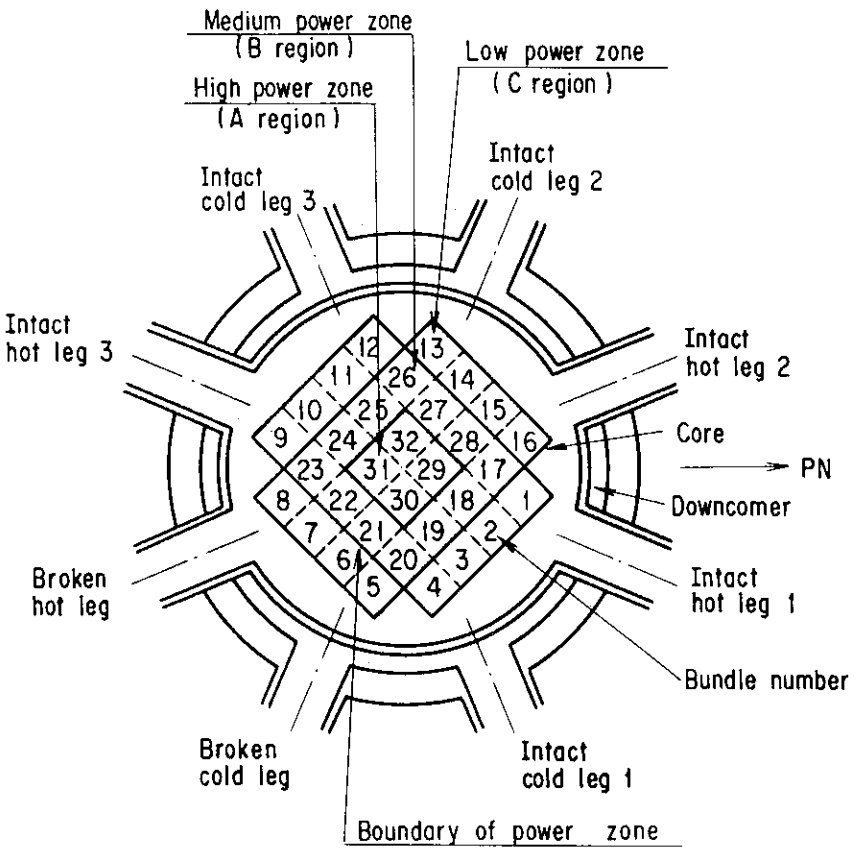

Fig. A.1 Definition of power zones and bundle numbers

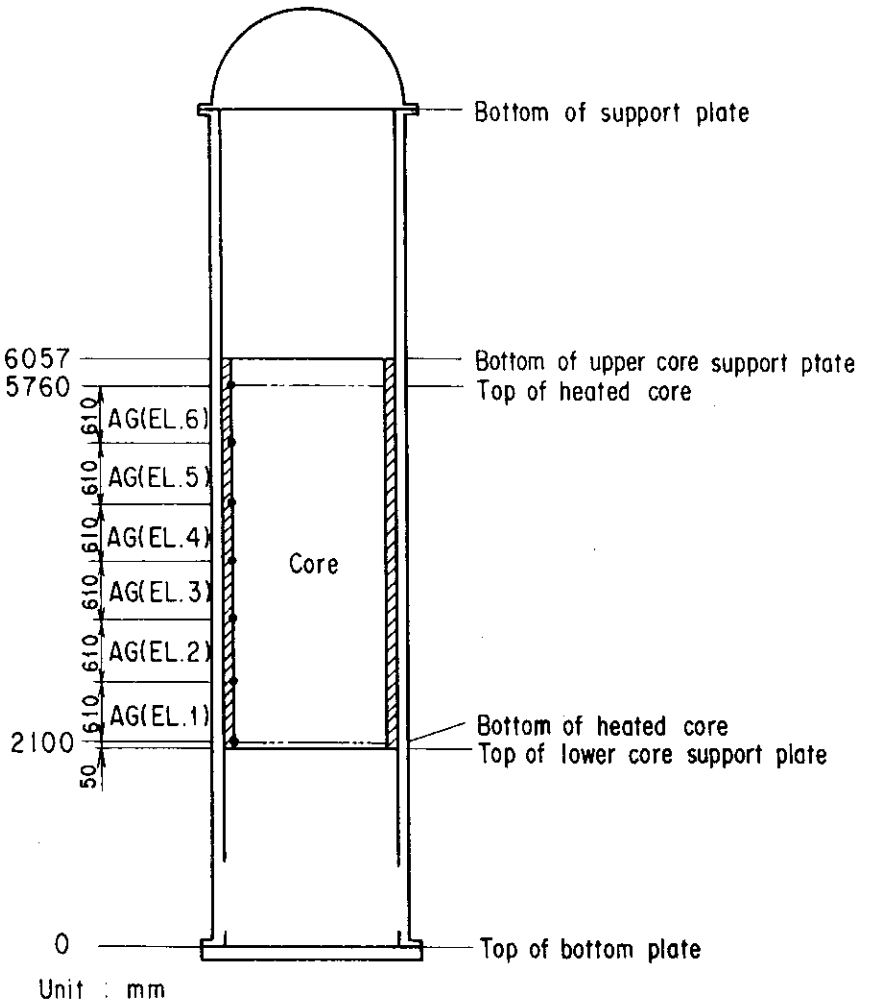

Fig. A.2 Definition of Tag. ID for void fraction (AG(EL.1) ∿ AG(EL.6))

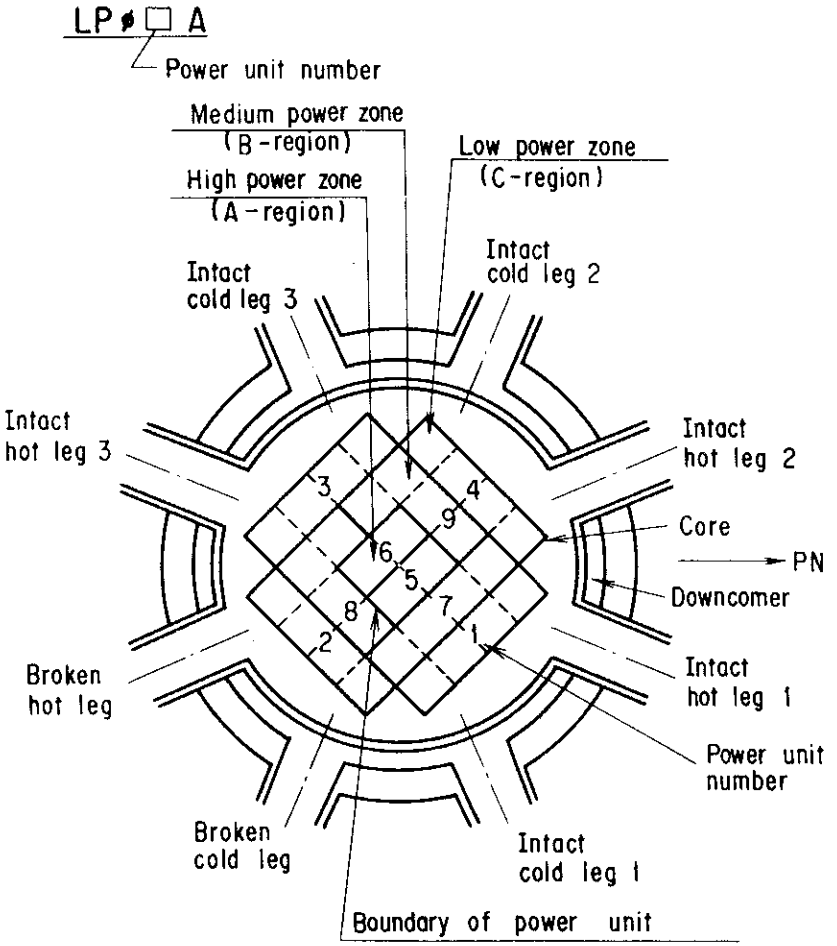

Fig. A.3 Definition of Tag. ID for average linear power of heater and in each power unit zone (LP01A ∿ LP09A)

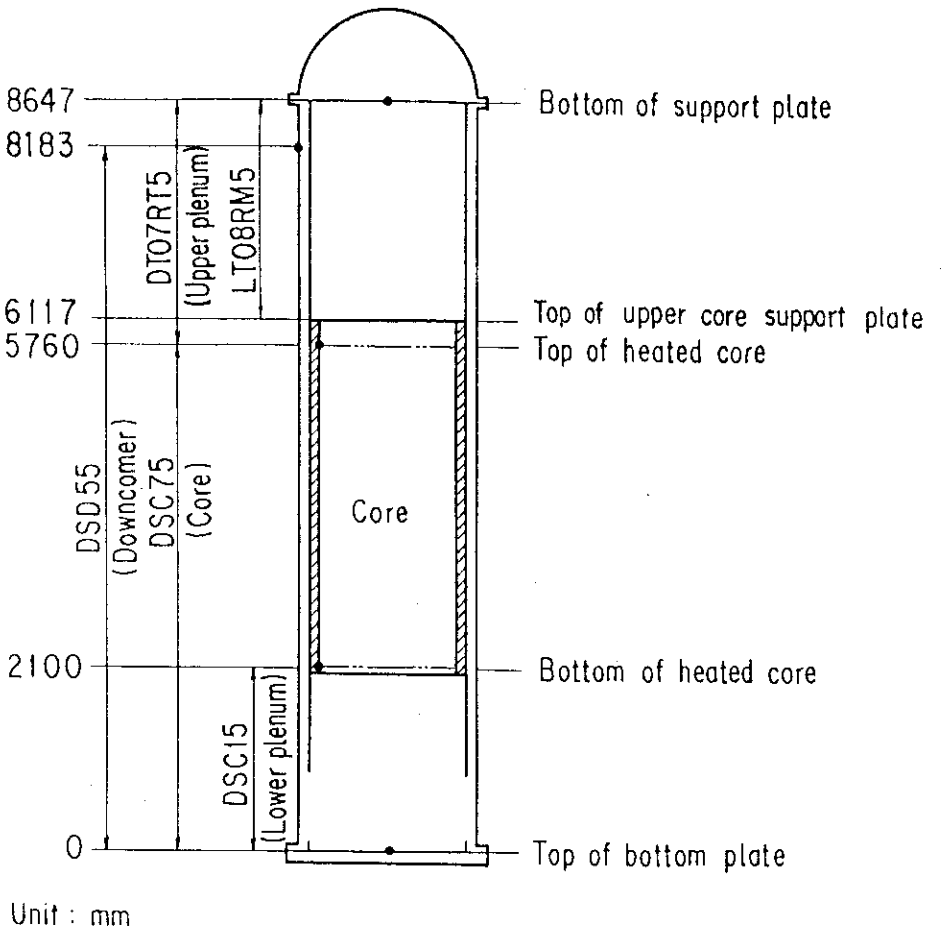

Fig. A.4 Definition of Tag. ID for differential pressure through downcomer, upper plenum, core, and lower plenum (DSD55, DT07RT5, LT08RM5, DSC75, DSC15)

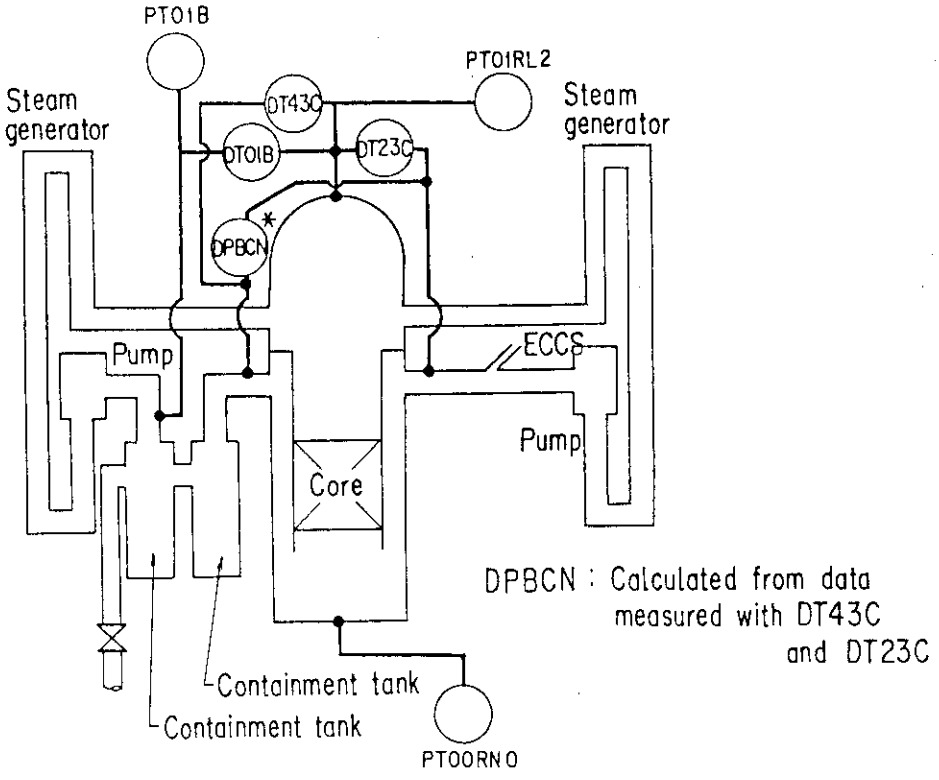

Fig. A.5 Definition of Tag. ID for differential pressure through intact and broken loop and broken cold leg nozzle (DT23C, DT01B, DPBCN)

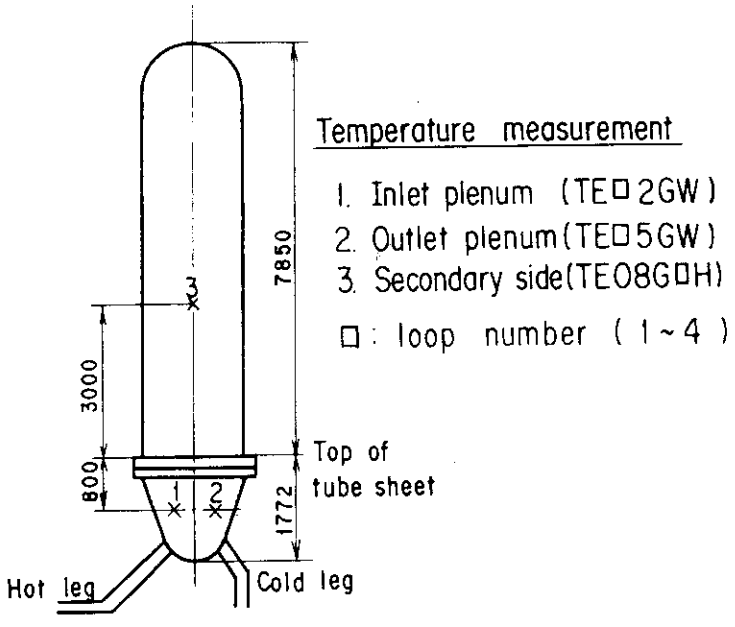

Fig. A.6 Definition of Tag. ID for fluid temperature iniinlet and outlet plenum and secondary of steam genrator (TE□2GW, TE□5GW, TE08G□H)

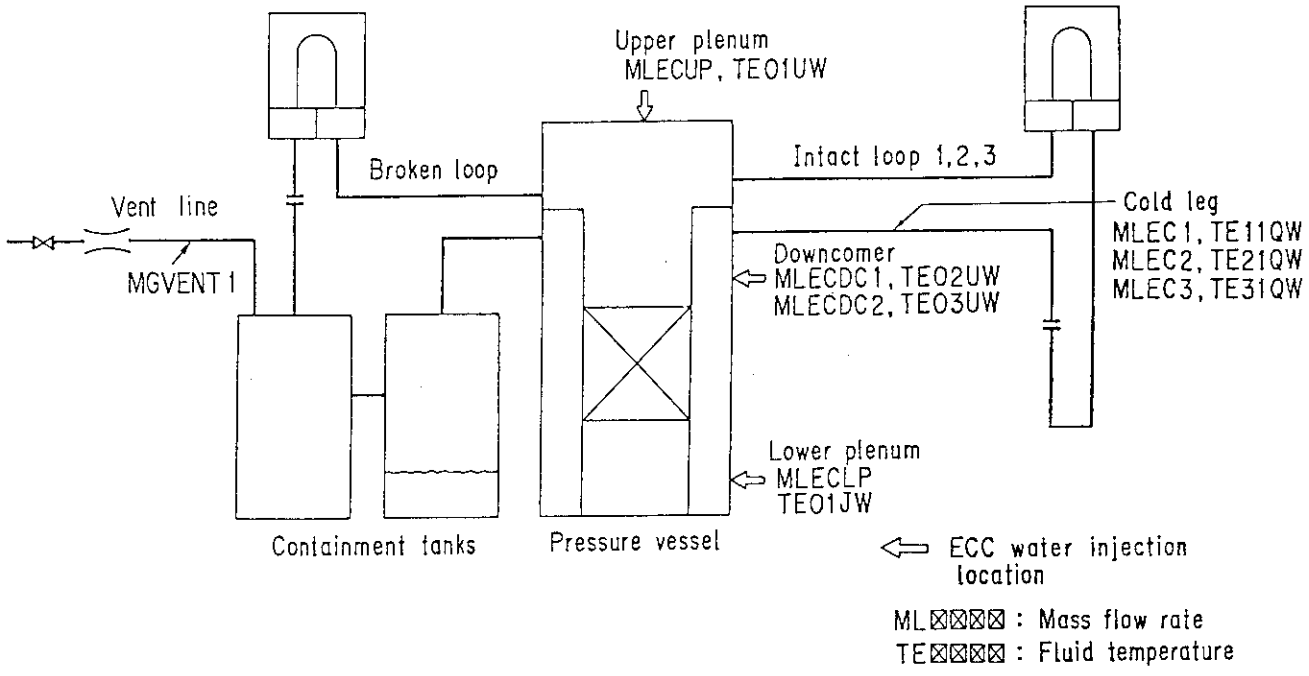

Fig. A.7 Definition of Tag. ID for ECC water injection rate, ECC water temperature and vented steam flow rate
(MLEC1, MLEC2, MLEC3, MLECLP, MLECUP, MLECDC1, MLECDC2, TE11QW, TE21QW, TE01JW, TE01UW, TE02UW, TE03UW, MGVENT1)

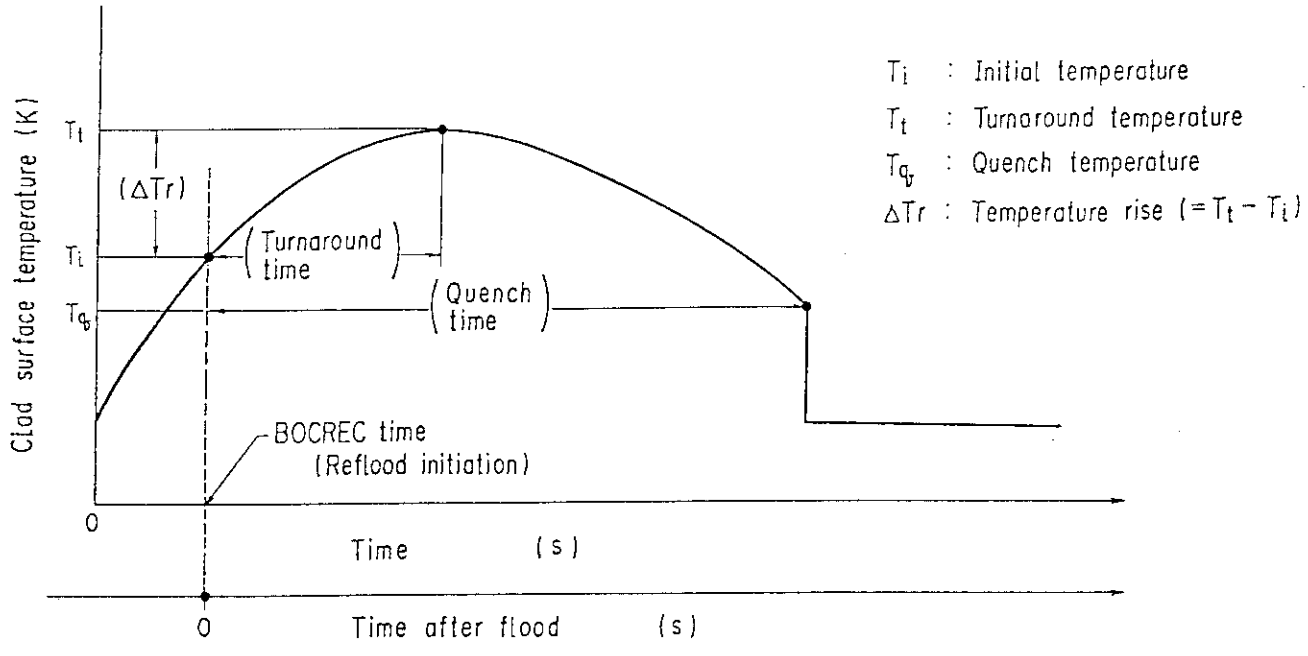

Fig. A.8 Definition of initial temperature, turnaround temperature, quench temperature, temperature rise, turnaround time and quench time

Appendix B

Selected data of CCTF Test C2-AC1 (Run 51)

Figure List

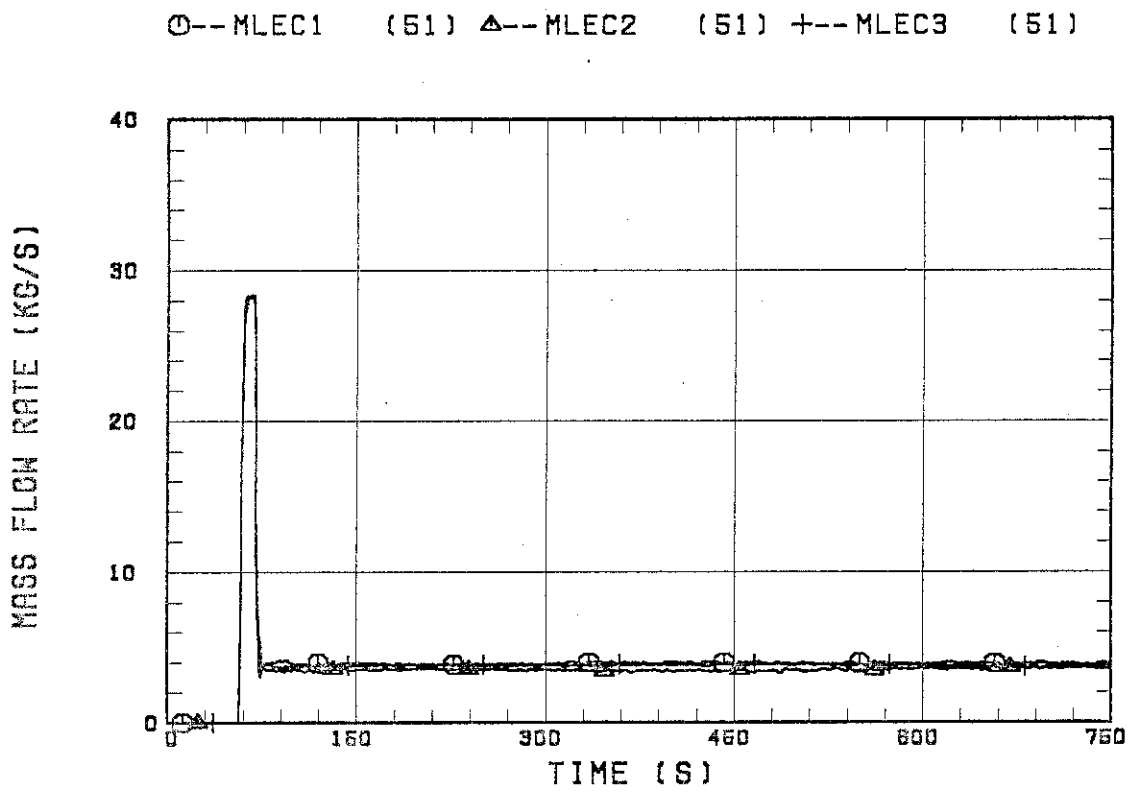

Fig. B.1　ECC water injection rates into the primary system.

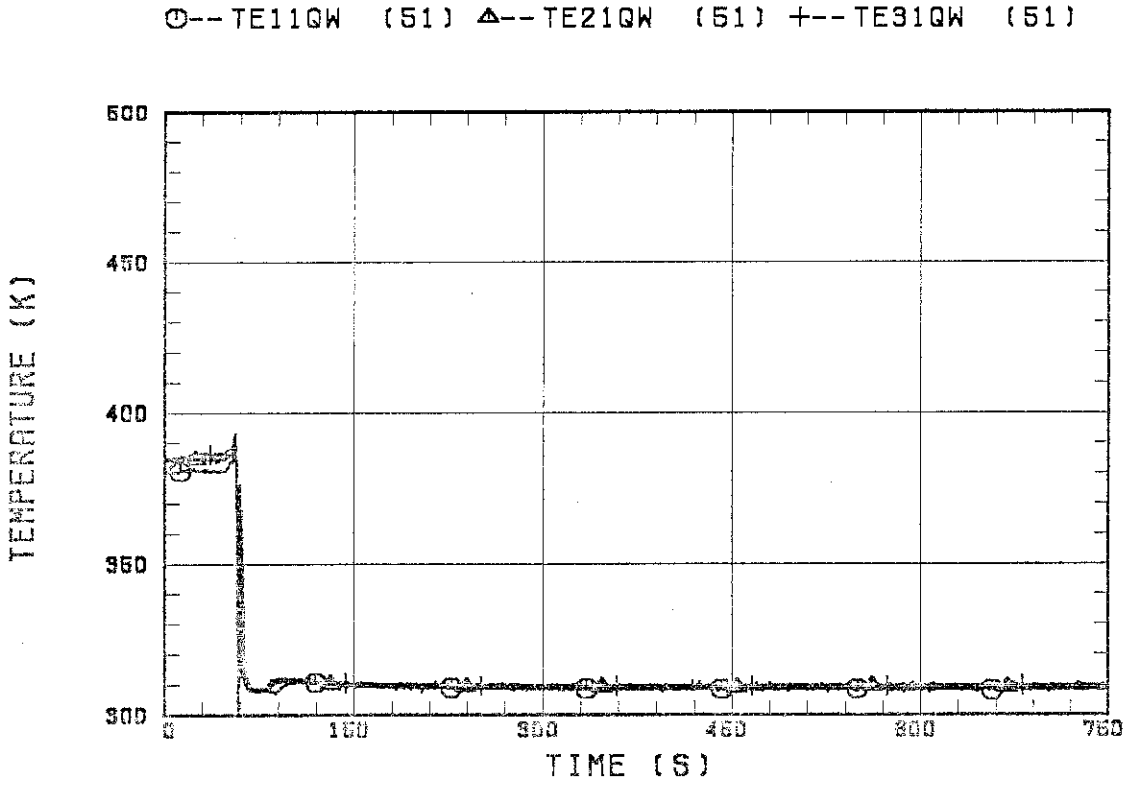

Fig. B.2　ECC water temperature.

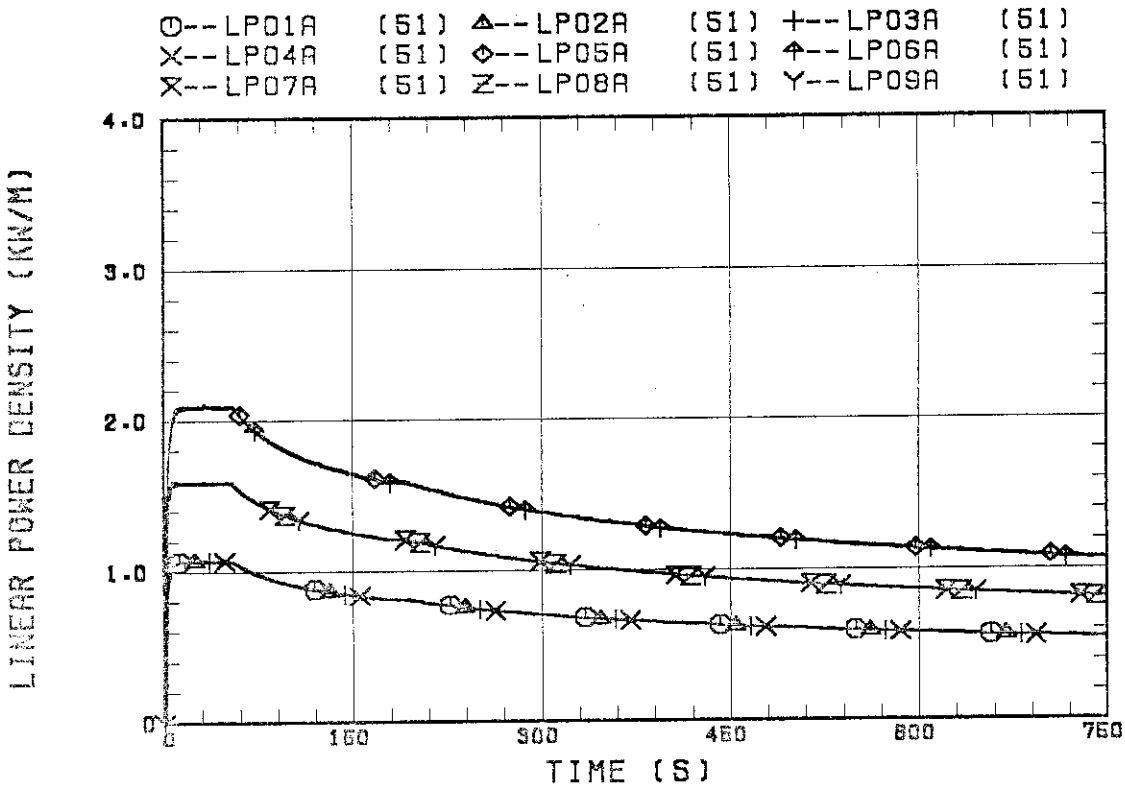

Fig. B.3 Average linear power of heater rod in each power unit zone.

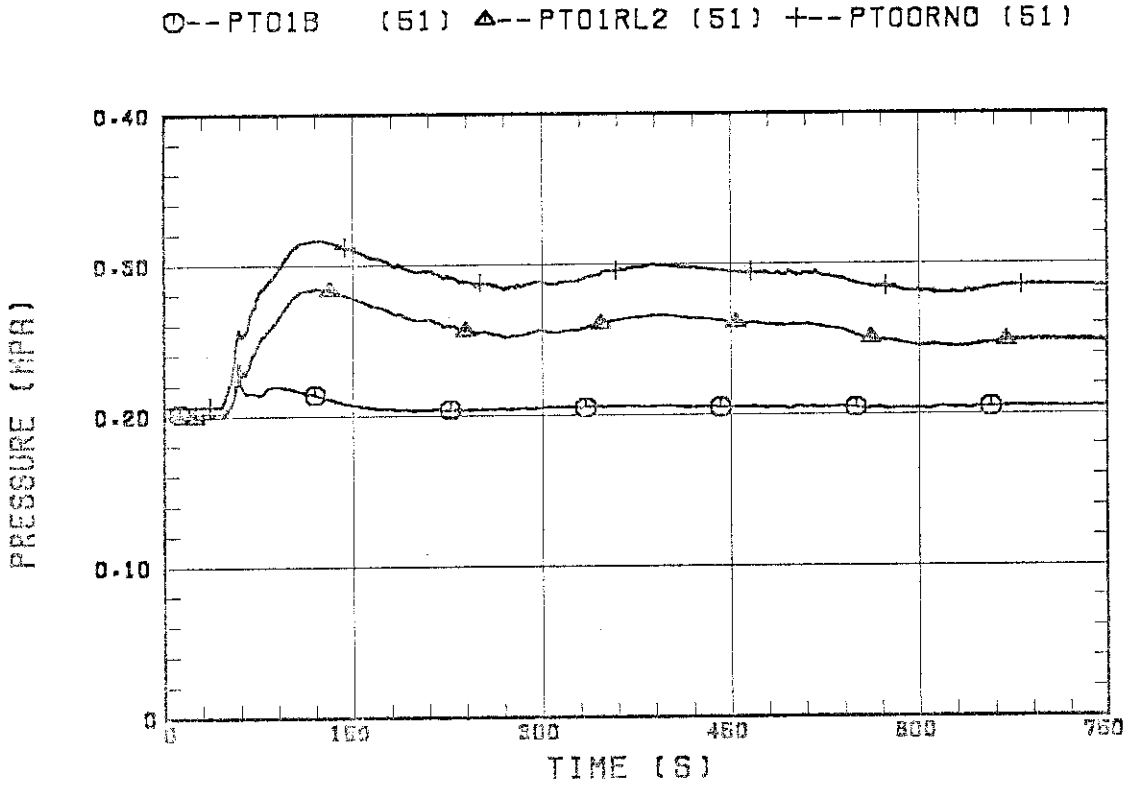

Fig. B.4 Pressure history in containment tank 2, upper plenum and lower plenum.

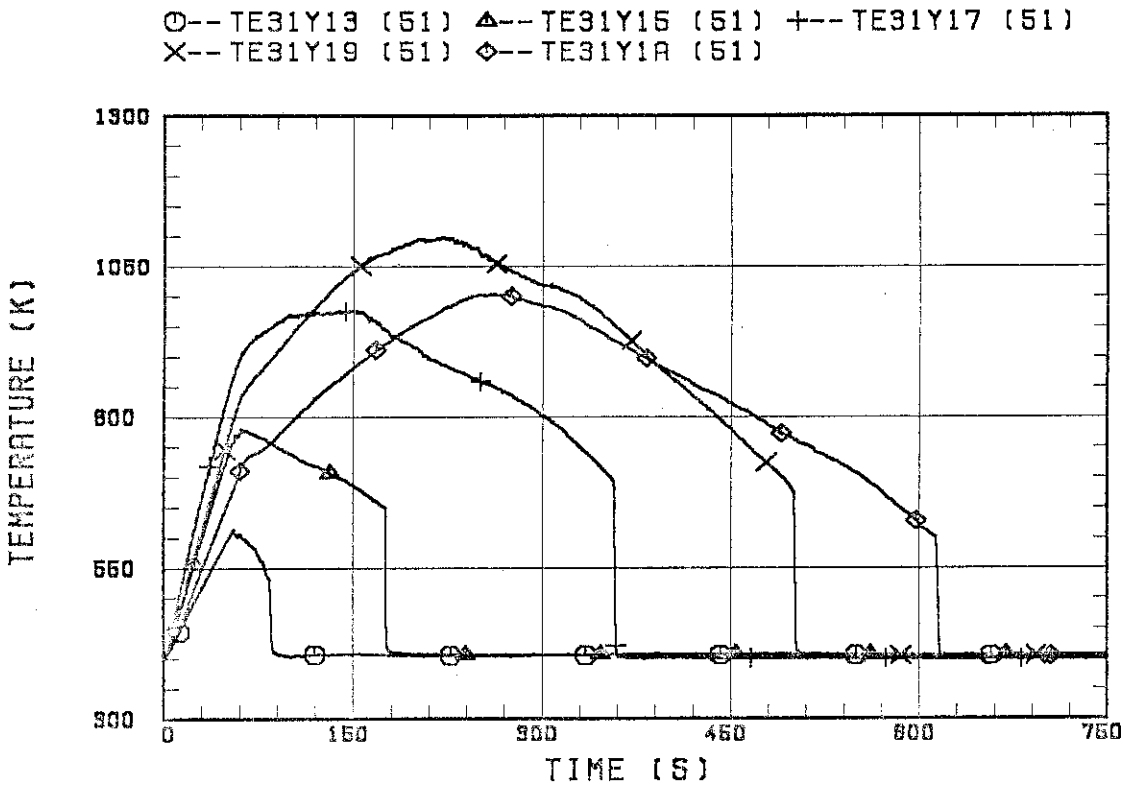

Fig. B.5 Clad surface temperature at various elevations along a heater rod in high power region (A region).

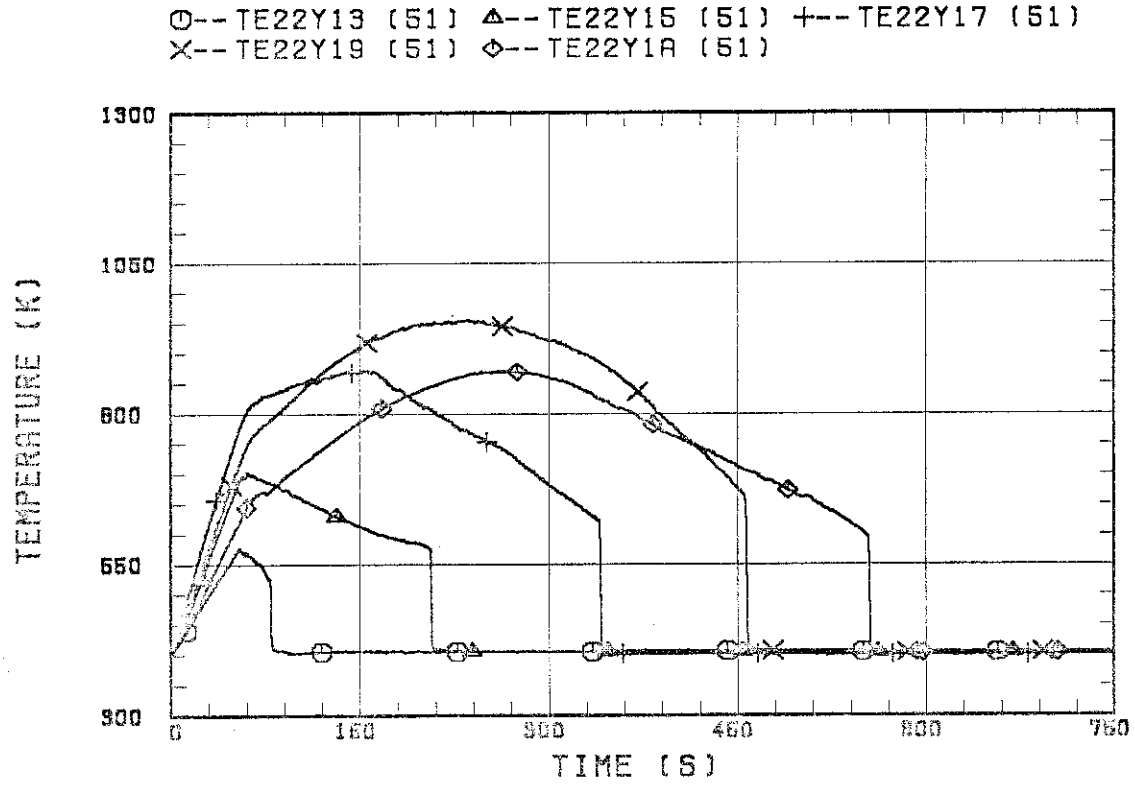

Fig. B.6 Clad surface temperature at various elevations along a heater rod in medium power region (B region).

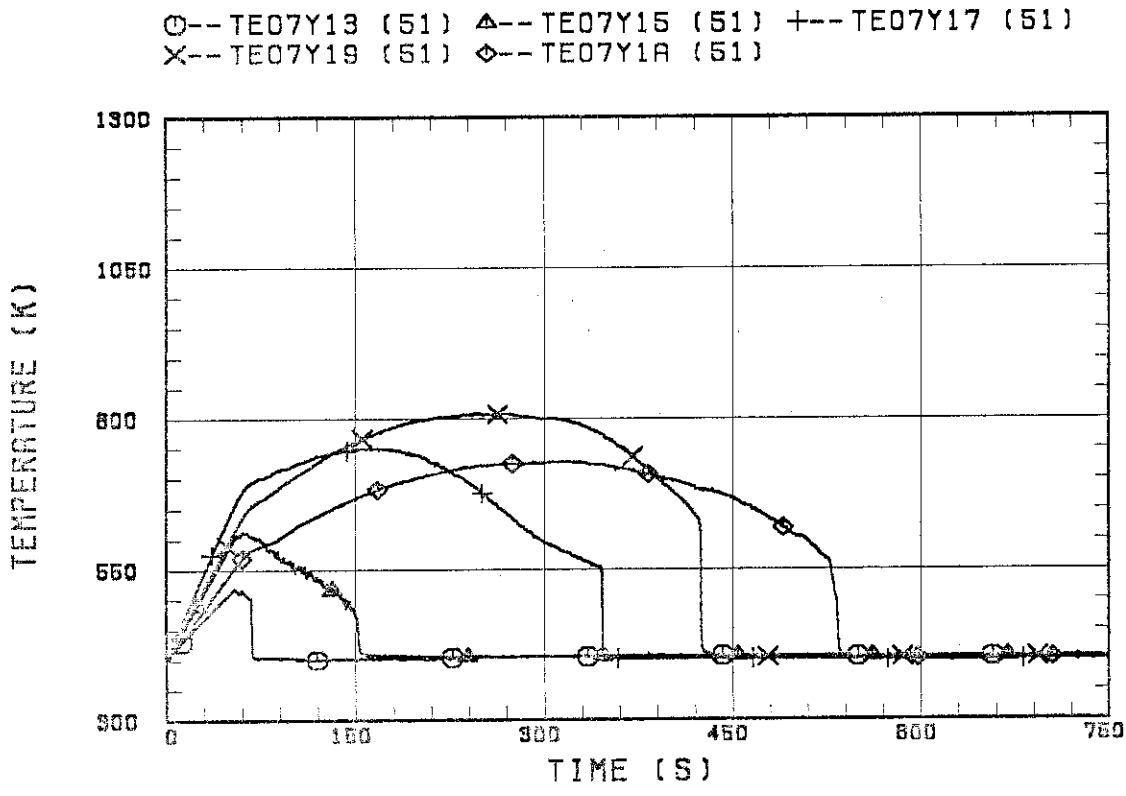

Fig. B.7 Clad surface temperature at various elevations along a heater rod in low power region (C region).

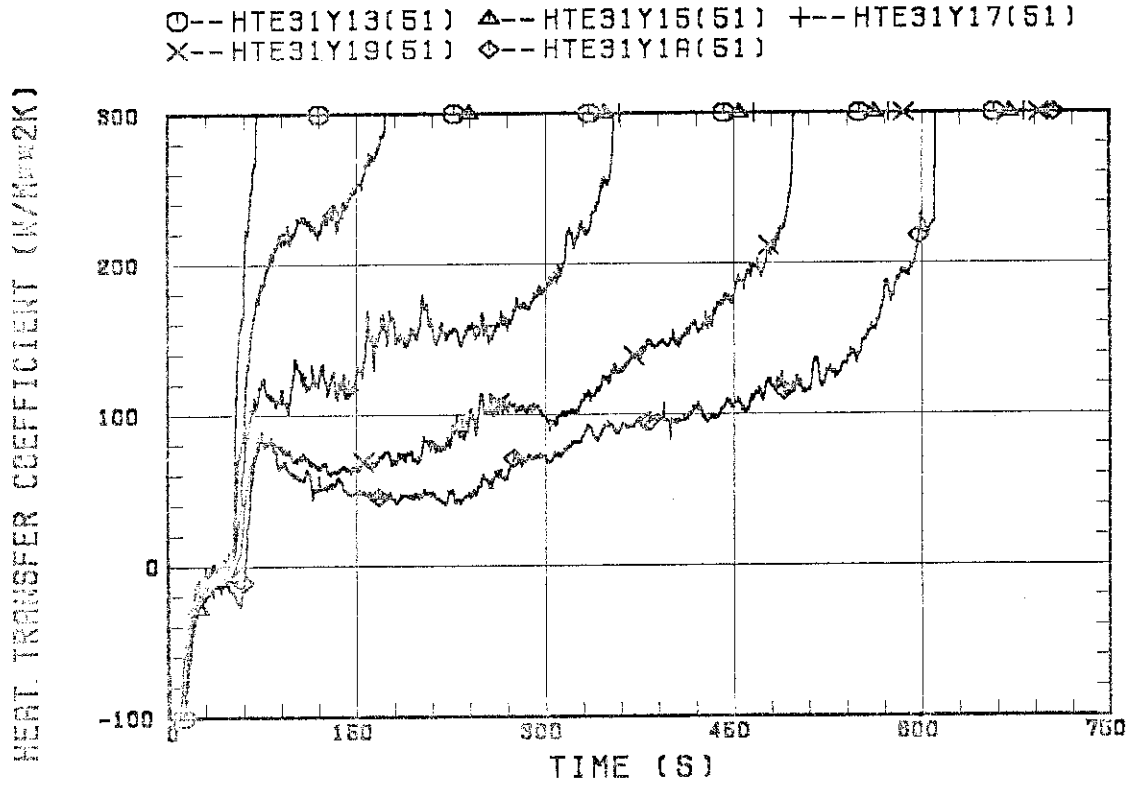

Fig. B.8 Heat transfer coefficient at various elevations along a heater rod in high power region (A region).

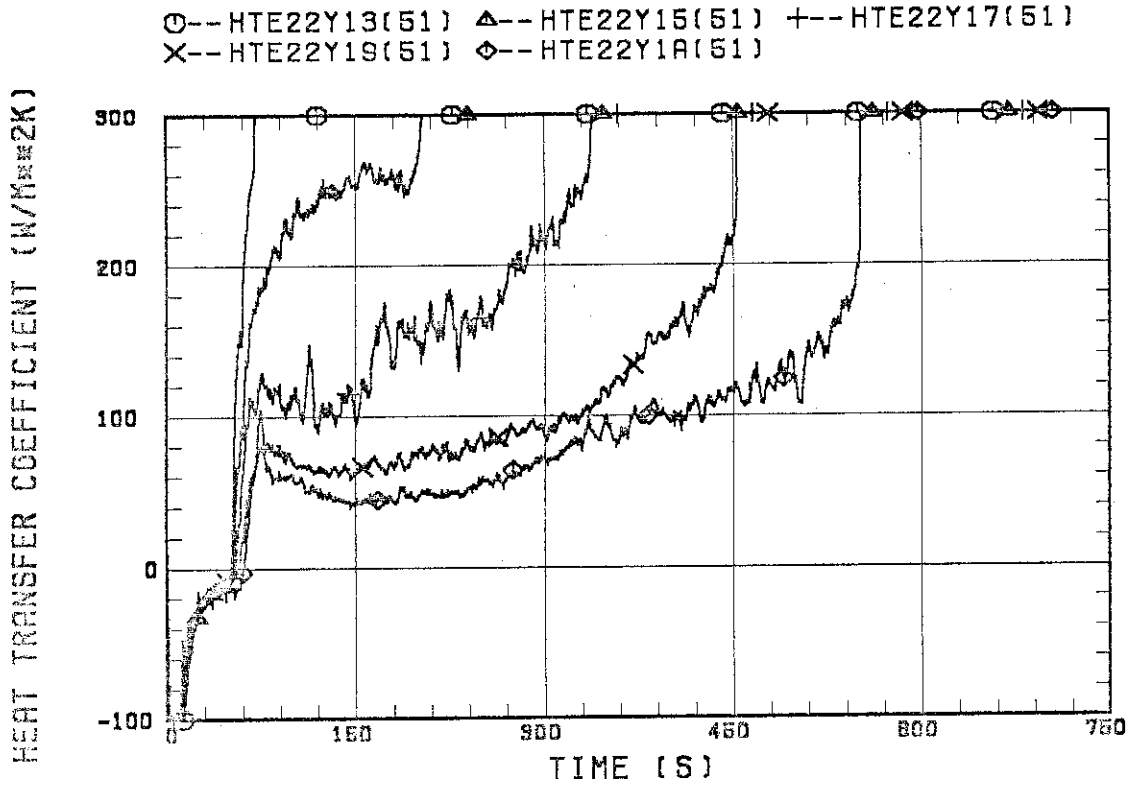

Fig. B.9 Heat transfer coefficient at various elevations along a heater rod in medium power region (B region).

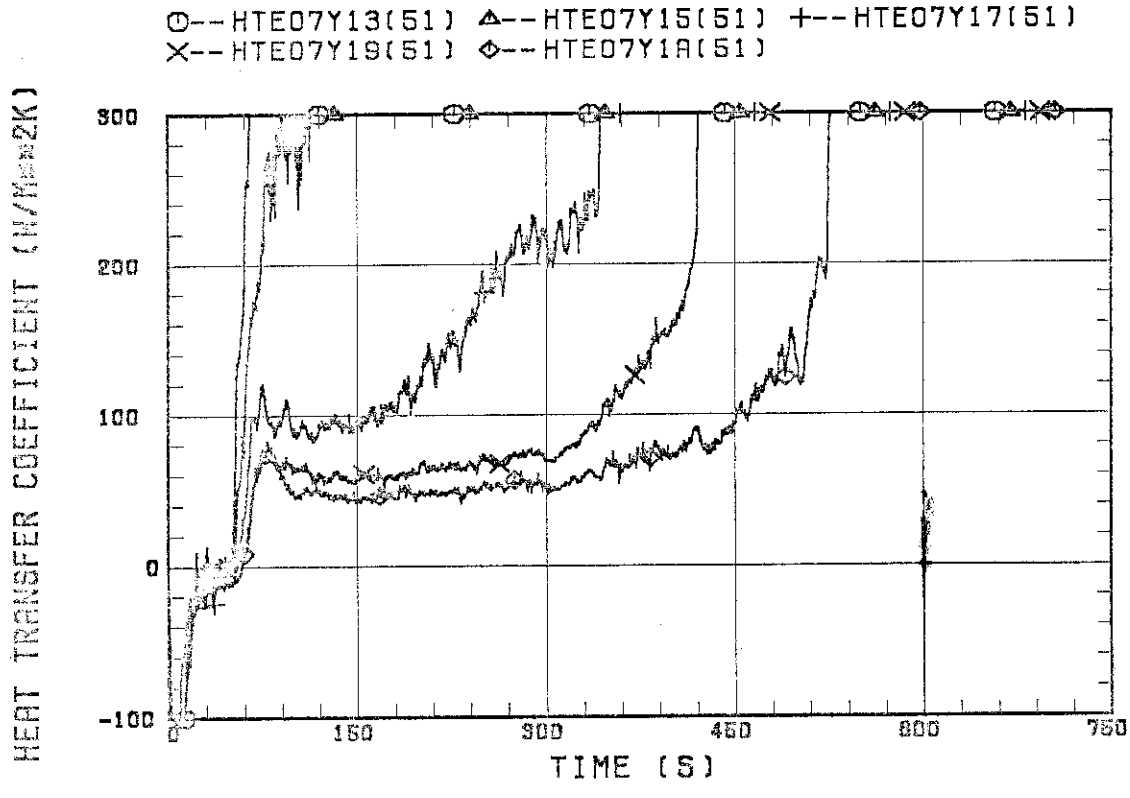

Fig. B.10 Heat transfer coefficient at various elevations along a heater rod in low power region (C region).

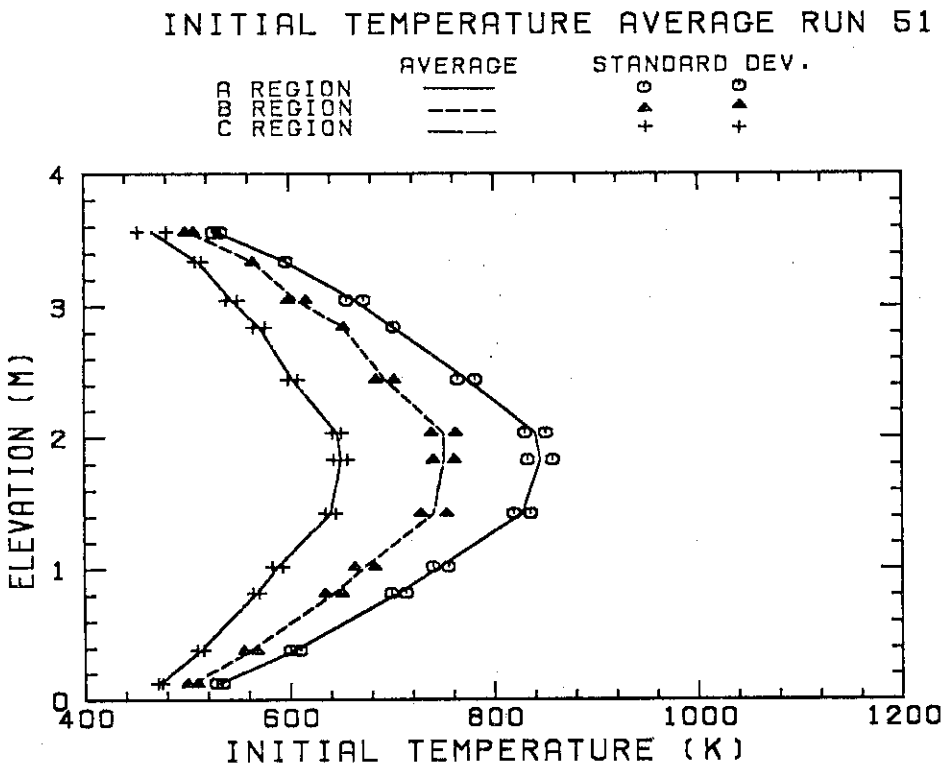

Fig. B.11 Initial clad surface temperature.

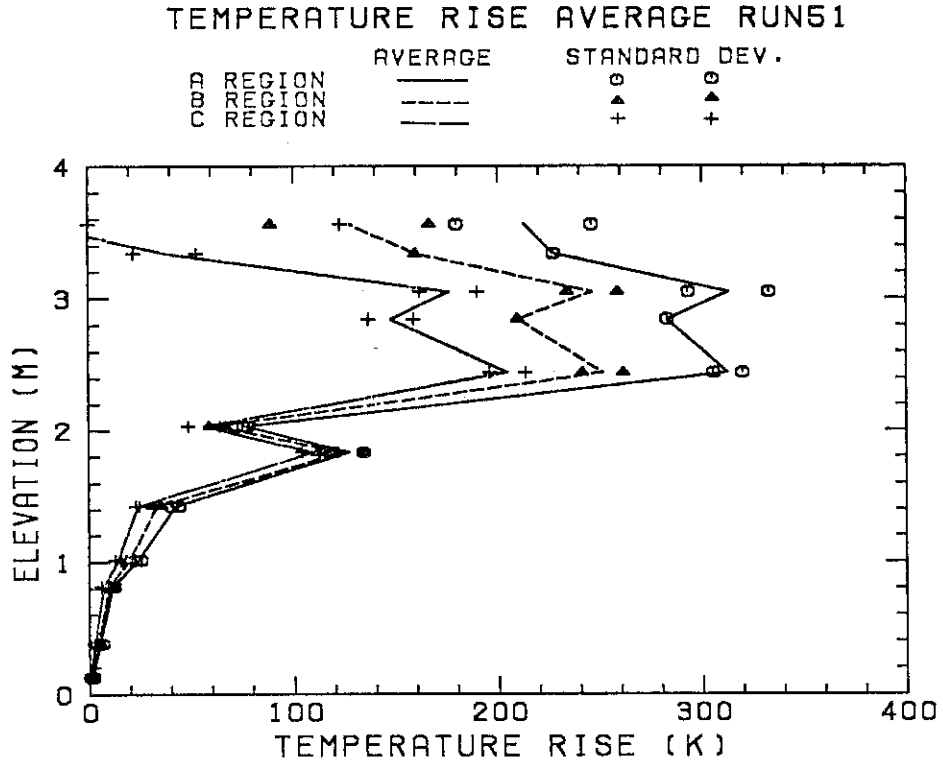

Fig. B.12 Temperature rise.

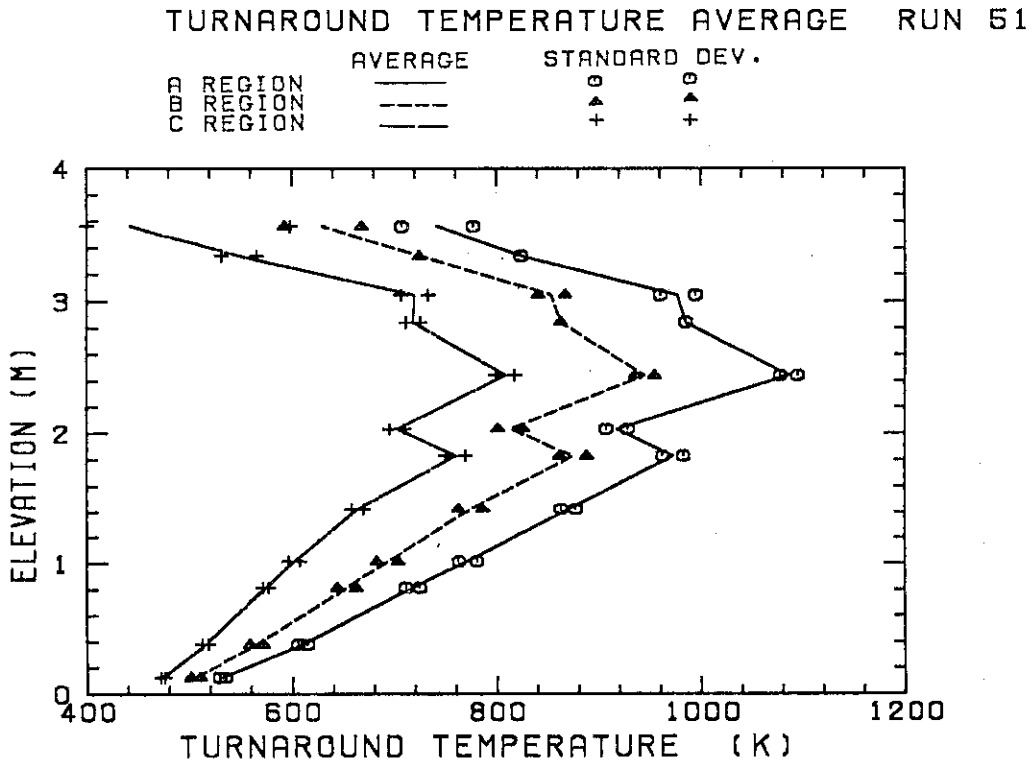

Fig. B.13 Turnaround temperature.

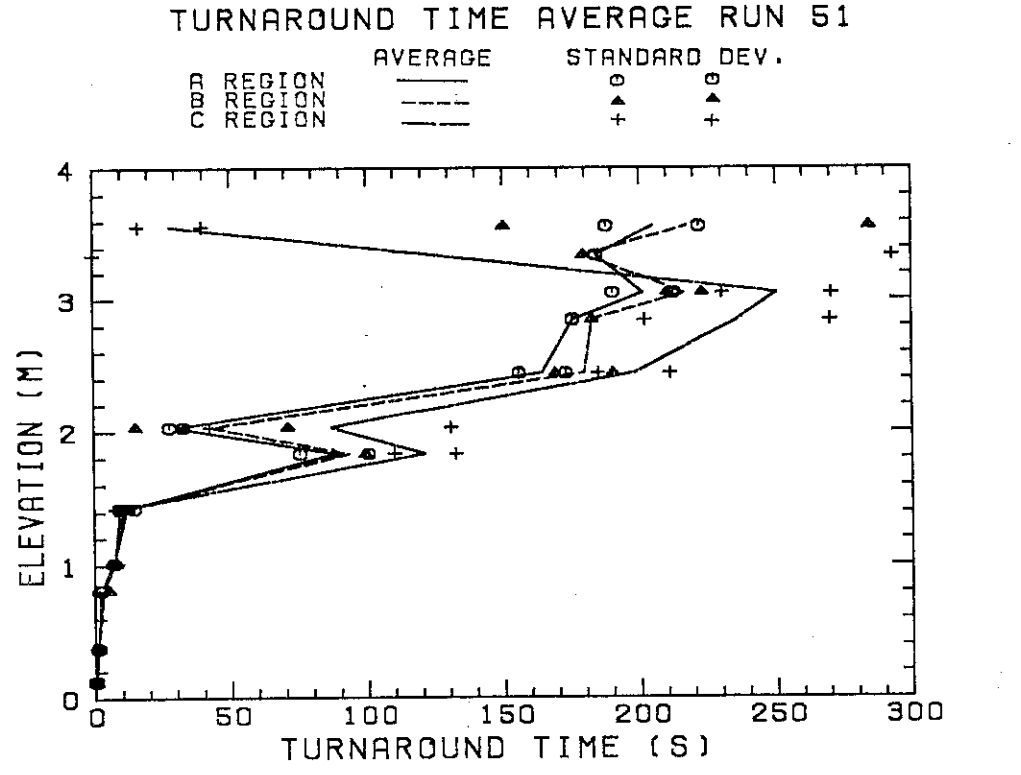

Fig. B.14 Turnaround time.

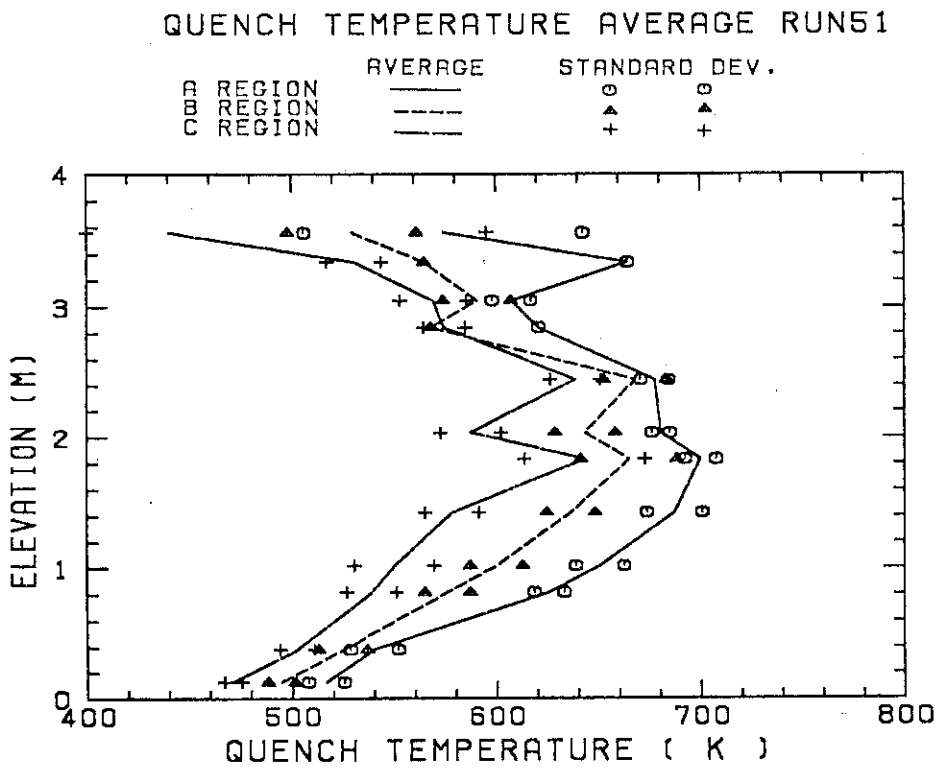

Fig. B.15 Quench temperature.

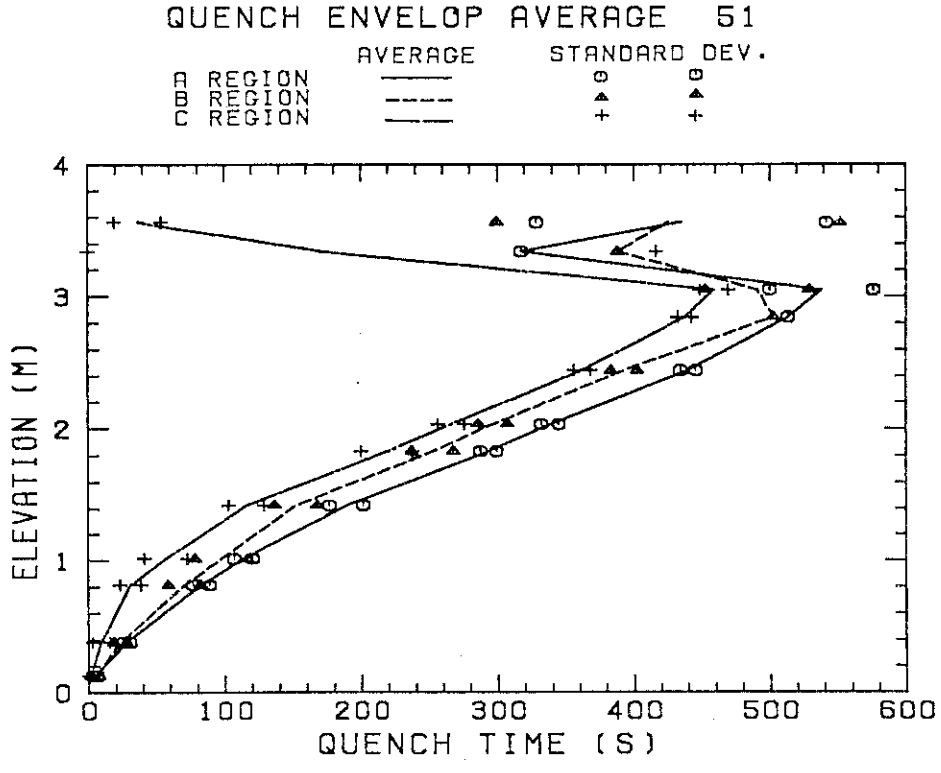

Fig. B.16 Quench time.

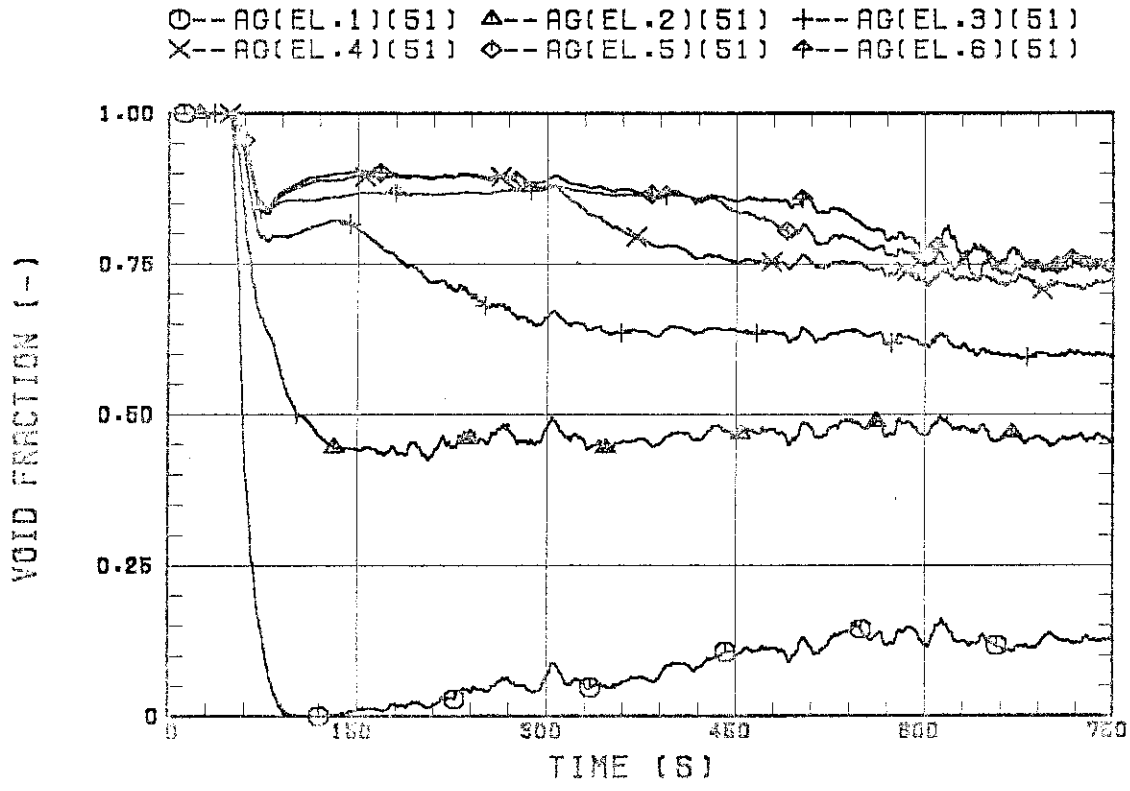

Fig. B.17 Void fraction in core.

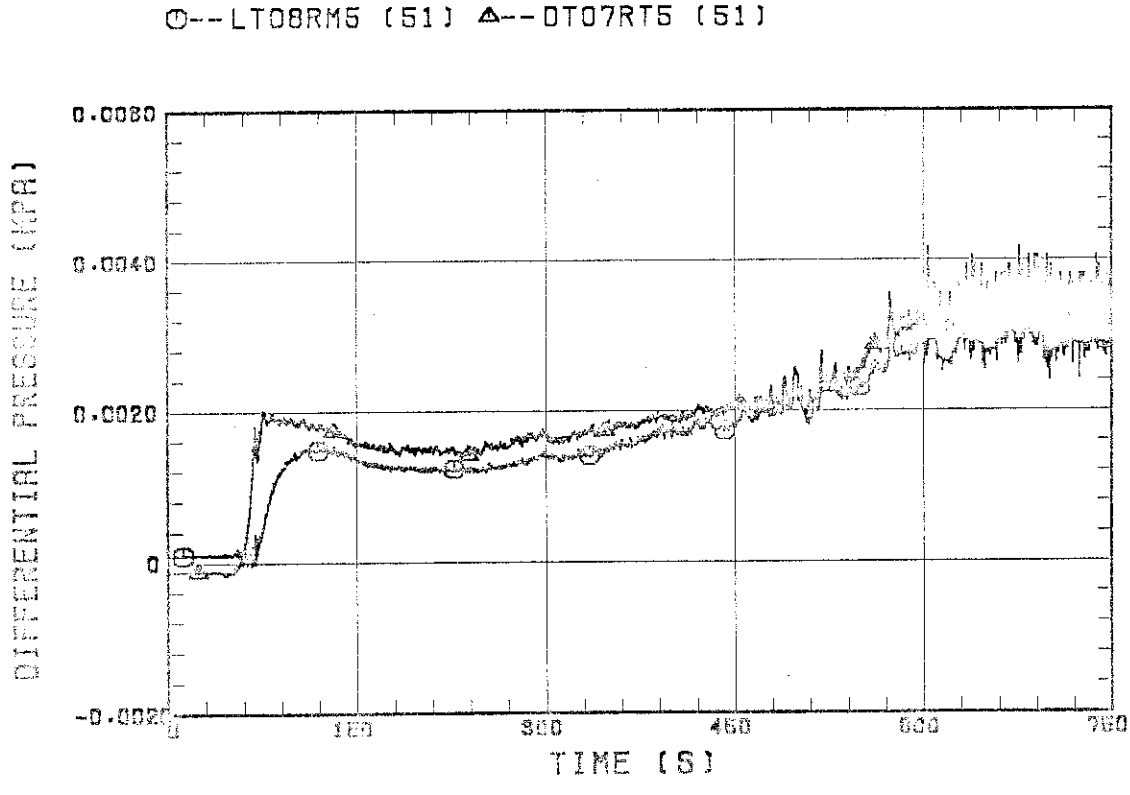

Fig. B.18 Differential pressure through upper plenum.

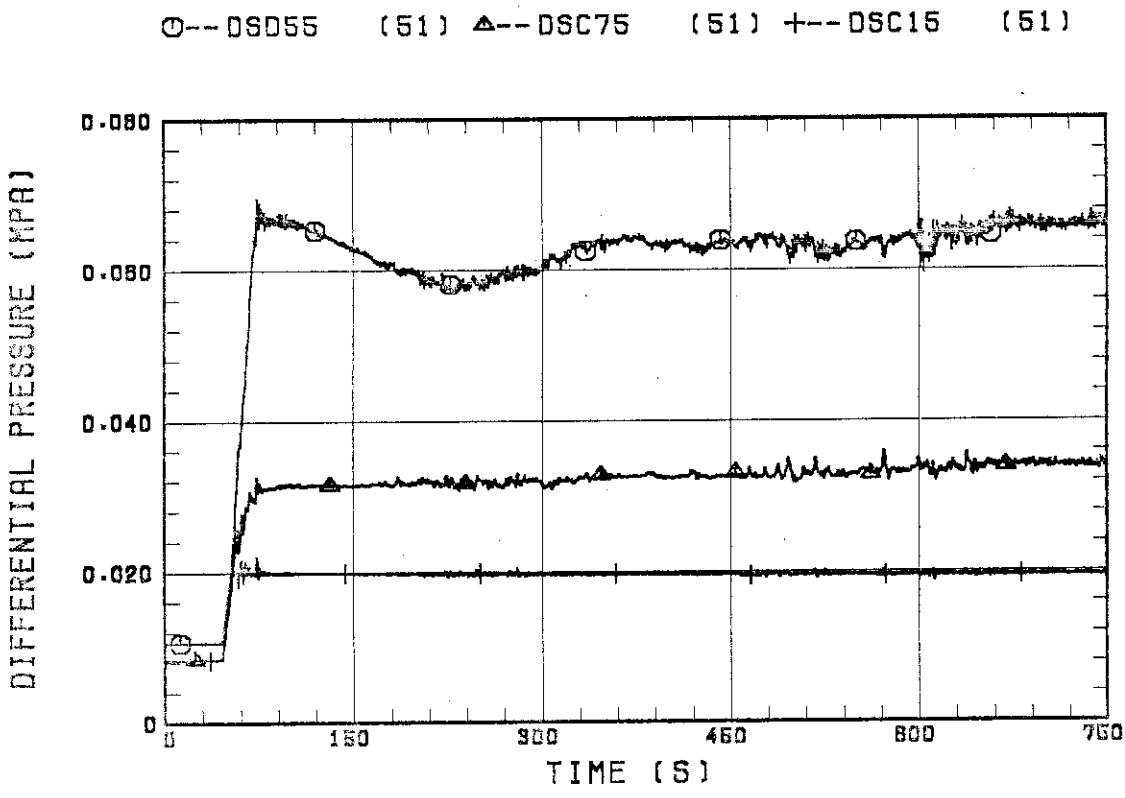

Fig. B.19 Differential pressure through downcomer, core, and lower plenum.

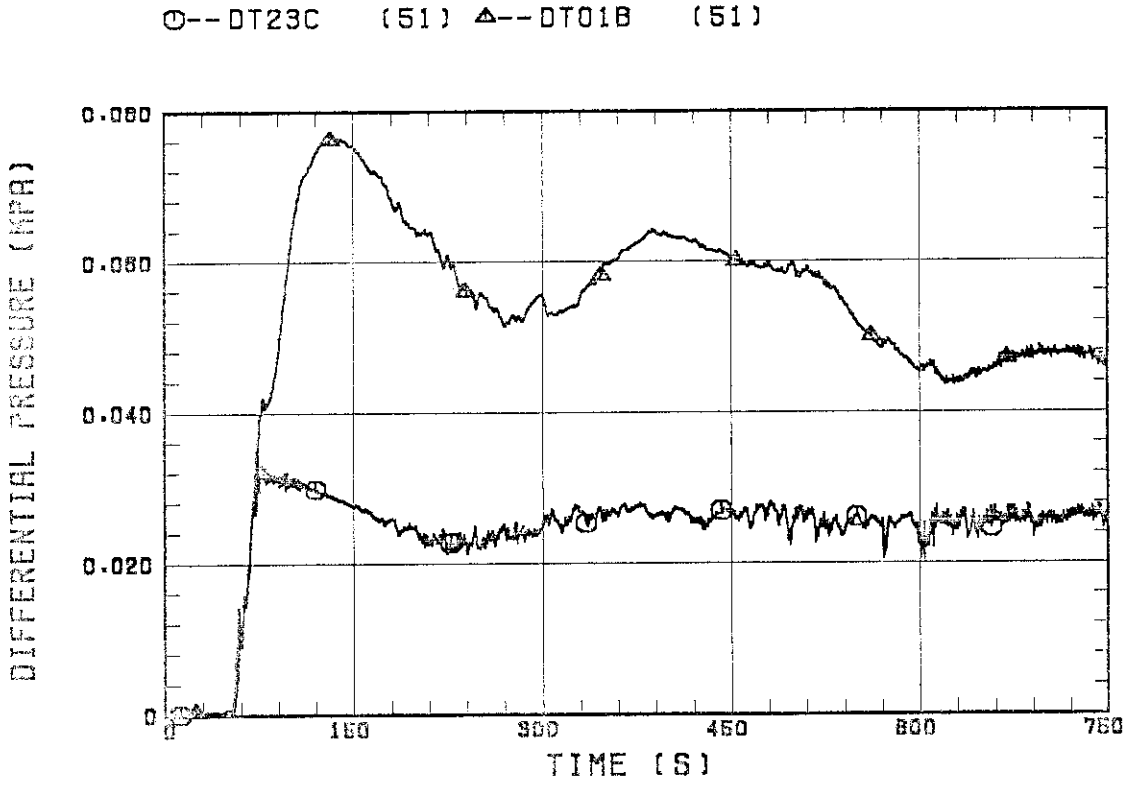

Fig. B.20 Differential pressure through intact and broken loops.

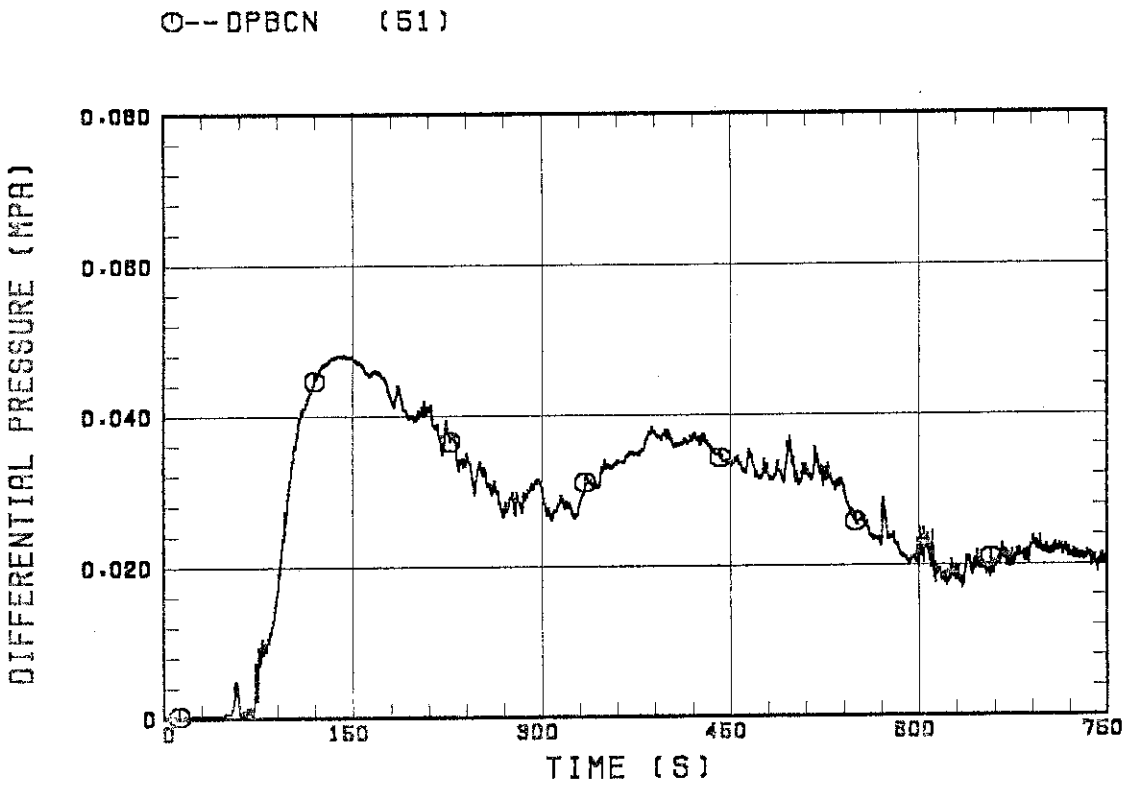

Fig. B.21 Differential pressure through broken cold leg nozzle.

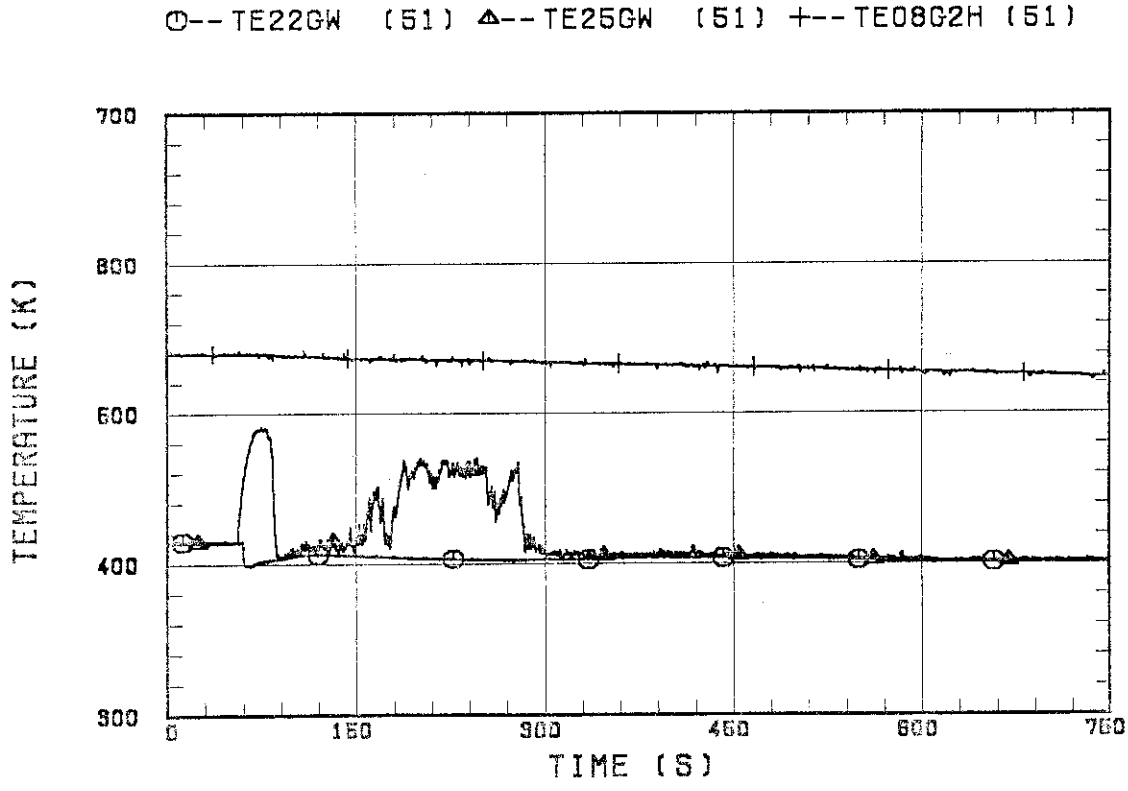

Fig. B.22 Fluid temperature in inlet plenum, outlet plenum, and secondary of steam generator 1.

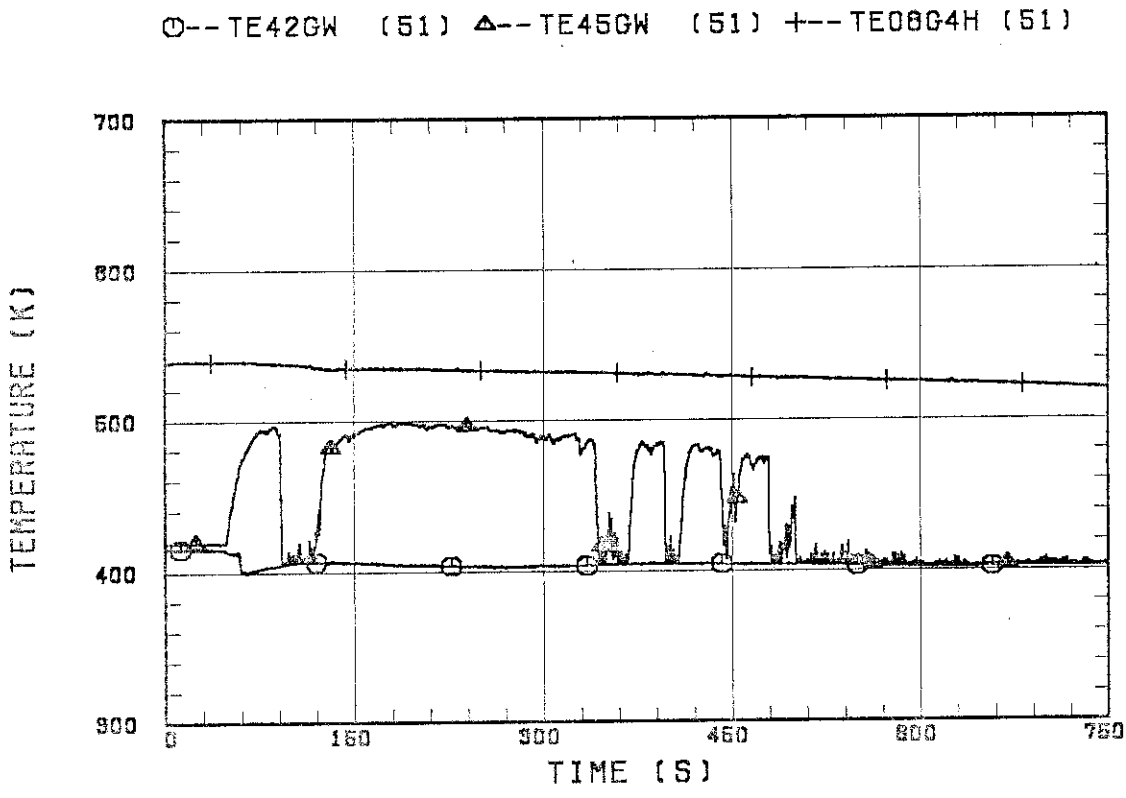

Fig. B.23 Fluid temperature in inlet plenum, outlet plenum, and secondary of steam generator 2.

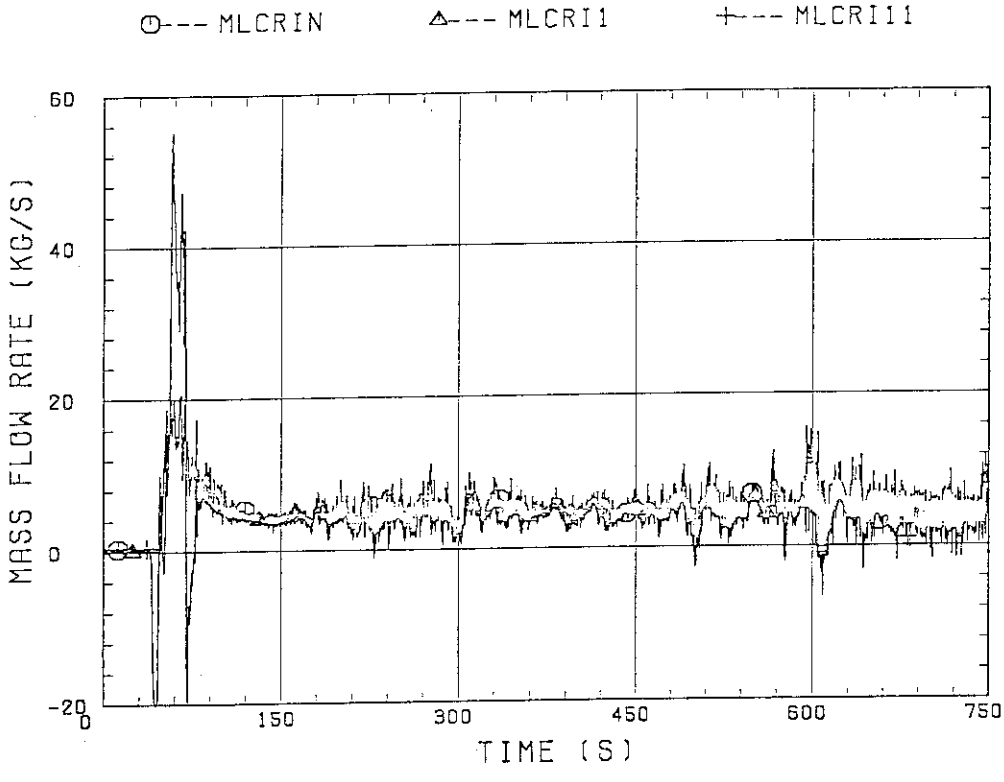

Fig. B.24 Core flooding mass flow rates evaluated with Eqs. (A.1) (A.2)

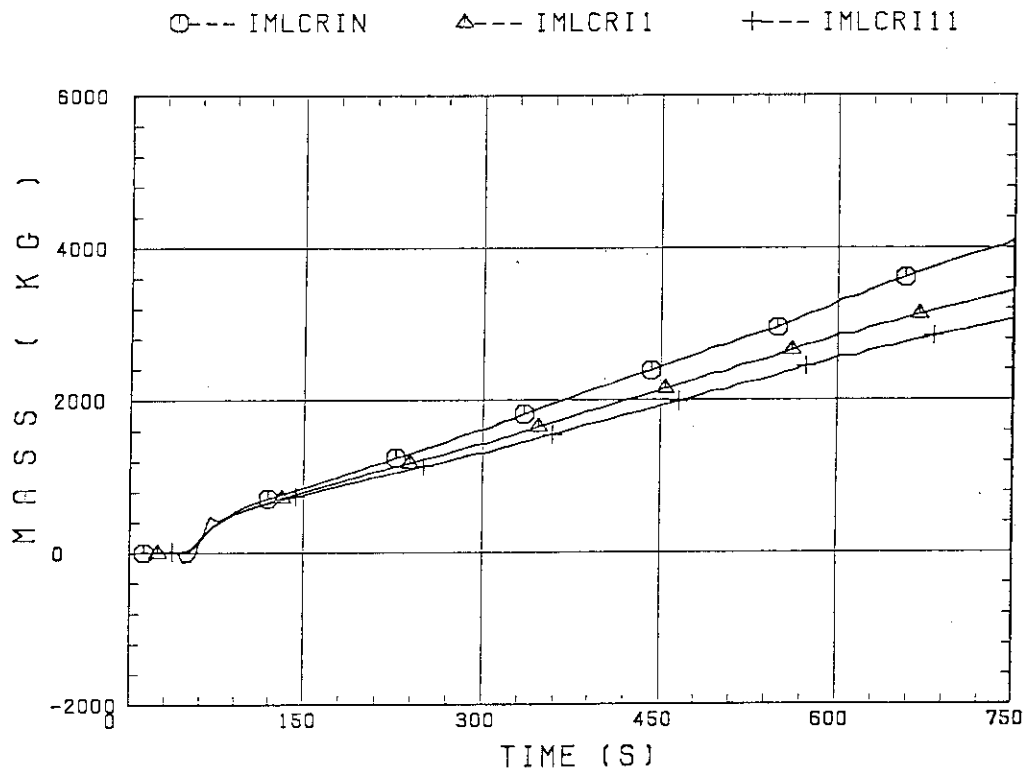

Fig. B.25 Time-integral mass flooded into core evaluated with Eqs. (A.1) and (A.2).

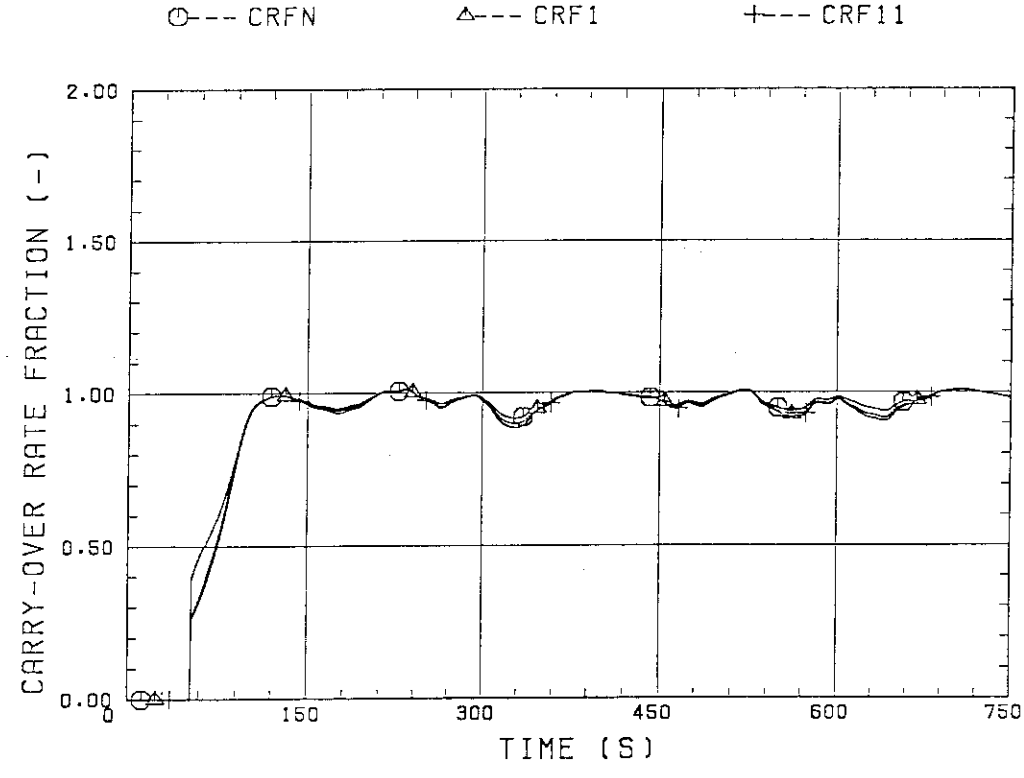

Fig. B.26 Carry-over rate fraction.

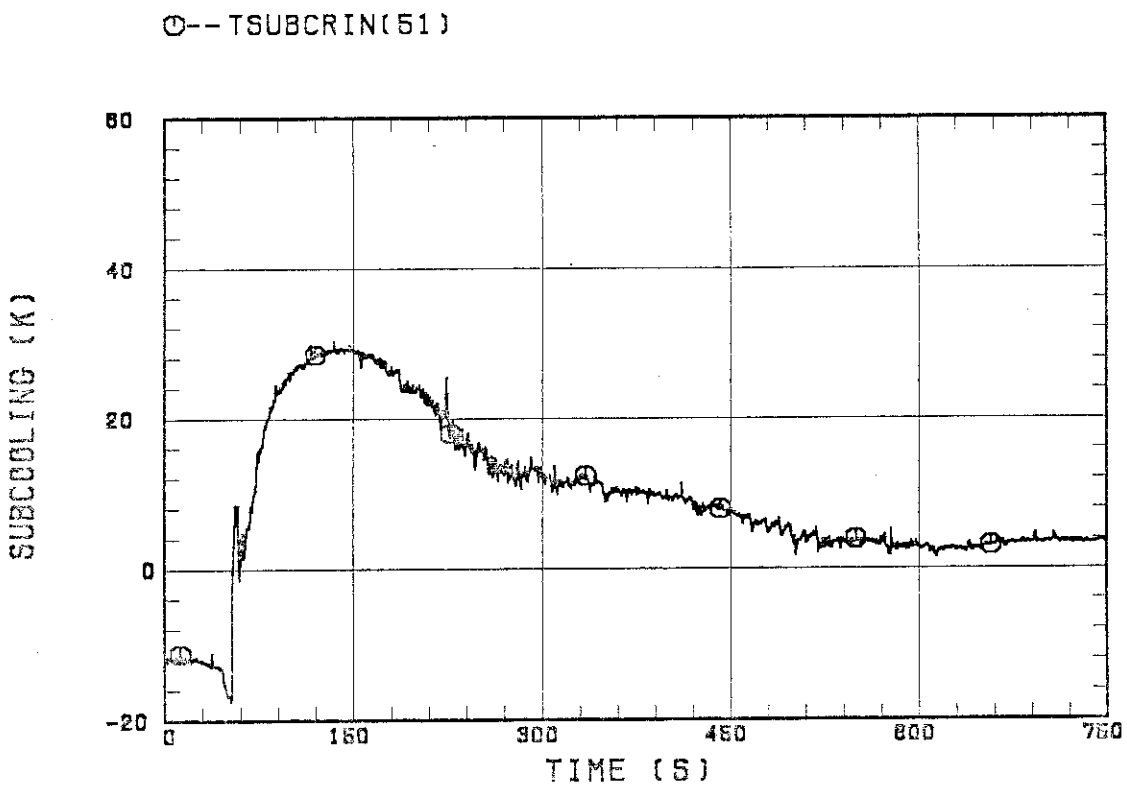

Fig. B.27 Core inlet subcooling.

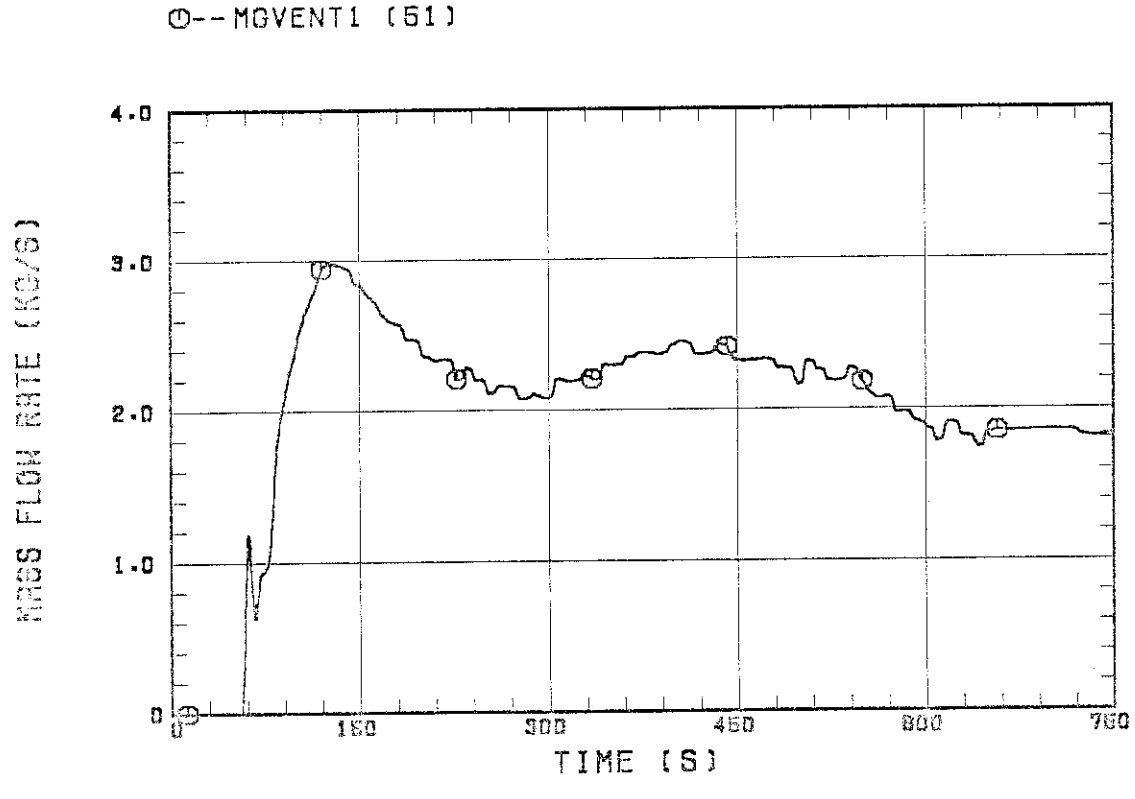

Fig. B.28 Exhausted mass flow rate from containment tank 2.